

Aristovich, E. (2014). Non-invasive Measurement of Cholesterol in Human Blood by Impedance Technique: an Investigation by Finite Element Field Modelling. (Unpublished Doctoral thesis, City University London)



**CITY UNIVERSITY
LONDON**

[City Research Online](#)

Original citation: Aristovich, E. (2014). Non-invasive Measurement of Cholesterol in Human Blood by Impedance Technique: an Investigation by Finite Element Field Modelling. (Unpublished Doctoral thesis, City University London)

Permanent City Research Online URL: <http://openaccess.city.ac.uk/8343/>

Copyright & reuse

City University London has developed City Research Online so that its users may access the research outputs of City University London's staff. Copyright © and Moral Rights for this paper are retained by the individual author(s) and/ or other copyright holders. All material in City Research Online is checked for eligibility for copyright before being made available in the live archive. URLs from City Research Online may be freely distributed and linked to from other web pages.

Versions of research

The version in City Research Online may differ from the final published version. Users are advised to check the Permanent City Research Online URL above for the status of the paper.

Enquiries

If you have any enquiries about any aspect of City Research Online, or if you wish to make contact with the author(s) of this paper, please email the team at publications@city.ac.uk.



CITY UNIVERSITY
LONDON

School of Mathematics, Computer Science and
Engineering

Electrical and Electronic Engineering

Non-invasive Measurement of
Cholesterol in Human Blood by
Impedance Technique: an
Investigation by Finite Element Field
Modelling

Ekaterina Aristovich

Thesis submitted for the fulfilment of the
requirements for the degree of Doctor of Philosophy of the
City University London

December 2014

Table of Contents

Chapter 1. Introduction and background.....	1
1.1 Introduction	1
1.2 Aims and Objectives	4
1.3 Background.....	5
1.3.1 Cholesterol in body.....	5
1.3.2 Methods used for determination of cholesterol levels.....	13
1.3.3 Proposed Non-Invasive Impedance Method	22
Chapter 2. Mathematical Modelling of Electromagnetic Field Distribution in Conductive Suspension	24
2.1 Introduction	24
2.2 Mathematical formulation of electric field distribution in conductive suspension	25
2.2.1 Maxwell's equations	25
2.2.2 Constitutive relations.....	26
2.2.3 Static case.....	28
2.2.4 Alternating current.....	28
2.2.5 Potentials	31
2.2.6 Material Properties	33
2.2.7 Boundary and Interface Conditions	34
2.2.8 Impedance	35
2.3 Finite Element Modelling.....	38

2.3.1	Finite element basics.....	38
2.3.2	FEM application to impedance of conductive suspension	42
Chapter 3.	Realisation of Finite Element Model of Non-invasive Cholesterol Measurement System	45
3.1	Introduction	45
3.2	Model of non-invasive measurement of cholesterol	46
Chapter 4.	Modelling of Non-invasive Cholesterol Measurement System in 2D.....	53
4.1	Building a 2D model.....	53
4.2	Results and discussions on 2D Model	59
4.2.1	Mesh convergence study	59
4.2.2	Frequency analysis	63
4.2.3	Analytical validation of 2D models.....	68
Chapter 5.	Modelling of Non-Invasive Cholesterol Measurement System in 3D.....	78
5.1	Building a 3D model.....	78
5.2	Results of 3D modelling and discussions.....	82
5.2.1	Validation of 3D model from simplistic analytical solution	84
5.2.2	Additional analyses	88
5.2.3	Comparison of impedances for different cholesterol levels in 3D..	95
Chapter 6.	Introduction of Red Blood Cells.....	97
6.1	Modelling investigations with RBC	97
6.1.1	RBC and their electrical properties.....	97
6.1.2	Maximum percentage of RBC	99
6.2	Additional assumptions	100

6.3	3D realisation for earlobe proportions	103
6.4	Combination of RBC and cholesterol	105
6.4.1	Results showing dependence of current on frequency and the orientation of RBC	107
6.4.2	Dependence of the current curve on the number of cholesterol particles	113
6.4.3	Dependence of the current curve on total cholesterol levels	114
Chapter 7.	Validation of some of the FE modelling results against simple experimental data	117
Chapter 8.	Conclusions and further work.....	125
8.1	Conclusions	125
8.2	Contribution to the original work	127
8.3	Further work.....	128
	Bibliography	129
	Appendix 1. Calculation of total volume of cholesterol in a given volume of blood for given total cholesterol level.....	144
	Appendix 2. Software procedures for building 2D finite element models	145
	Appendix 3. Software procedures for building 3D finite element models	150
	Appendix 4. MatLab scripts for random distribution of cholesterol particles in 3D finite element models	160
	Appendix 5. MatLab scripts for random distribution of RBC and cholesterol particles in 3D finite element models	175

List of Tables

Table 1.1.Types of lipoprotein.....	10
Table 1.2. Cholesterol measurements methods.....	22
Table 3.1. Material properties assigned to the domains of the problem.....	49
Table 4.1. Current per unit length in z-direction of electrode in corresponding conducting areas and total current per unit length in z-direction along the cut- line	70
Table 5.1. Current values depending on cylinder/particle positioning	88
Table 5.2. Current through the corresponding conducting volumes and total current through cut-plane	95
Table 6.1. Current values for different RBC orientation (with and without cholesterol)	111

List of Figures

Figure 1.3–1. Chemical structure of cholesterol.....	5
Figure 1.3–2. Plasma membrane.....	6
Figure 1.3–3. Structure of lipoprotein.....	9
Figure 1.3–4. Classification of lipoproteins	10
Figure 1.3–5. Electrophoresis set	18
Figure 1.3–6. PreVu test performance	21
Figure 3.2–1. Particle in electric field, $\sigma_e > \sigma_{part}$	49
Figure 3.2–2. Conduction current I_c and displacement current I_d for a typical tissue [66]	52
Figure 4.1–1. Coagulated cholesterol particles in blood plasma.....	55
Figure 4.1–2. Boundary conditions	56
Figure 4.1–3. 2D custom mesh for 20 particles.....	57
Figure 4.1–4. Custom mesh for 1 particle of coagulated cholesterol	58
Figure 4.2–1. Cut-line for mesh convergence study.....	60
Figure 4.2–2. Electric field distribution for the coarse mesh ($N_{el}=1380$).....	60
Figure 4.2–3. Electric field distribution for the less-course mesh ($N_{el}= 6875$) ...	61
Figure 4.2–4. Electric field distribution for the fine mesh ($N_{el}=11857$).....	61
Figure 4.2–5. Mesh convergence study	62
Figure 4.2–6. Variation of current per unit length with number of particles	62
Figure 4.2–7. Cut-line for frequency analysis.....	64
Figure 4.2–8. Current density along cut-line, area of interest filled with: a) plasma and coagulated cholesterol particles, b) plasma.....	65
Figure 4.2–9. Vectors showing current density distribution for 100 particles	66

Figure 4.2–10. Electric potential plot showing the extension for correct electrical field calculation	67
Figure 4.2–11. Extension of geometry in vertical direction.....	68
Figure 4.2–12. Positioning of the cut-line for estimation of fringe field effects ..	69
Figure 4.2–13. Analytical representation of a system (series)	71
Figure 4.2–14. Practical FEM implementation of a system (series)	71
Figure 4.2–15. Analytical representation of a system (parallel)	72
Figure 4.2–16. Practical FEM implementation of a system (parallel)	72
Figure 4.2–17. Horizontal particles placement	74
Figure 4.2–18 Vertical particle placement.	75
Figure 4.2–19. Values of current per unit length for total cholesterol levels.....	76
Figure 4.2–20. Current per unit length as a function of total cholesterol and number of particles	77
Figure 5.1–1. 3D FE model of the cholesterol measurement system.....	79
Figure 5.1–2. 3D Model with boundary conditions	80
Figure 5.1–3. 3D Model (zoomed in to show details of the electrode-particle assembly)	80
Figure 5.1–4. 3D custom mesh for 8 particles	81
Figure 5.1–5. Quality of the external custom mesh in 3D case	81
Figure 5.1–6 Quality of the external particle custom mesh in 3D case.	82
Figure 5.2–1. Current versus number of particles for 3D case.....	83
Figure 5.2–2. Total current versus frequency for 3D case	84
Figure 5.2–3. Horizontal and vertical lines of cylinders	86
Figure 5.2–4. Horizontal and vertical arrangement of spheres	87
Figure 5.2–5. YZ-Cut plane.....	89

Figure 5.2–6. Electric field distribution on the cut-plane for the case with no particles90

Figure 5.2–7. Position of the central line on the cut-plane90

Figure 5.2–8. Current density for the model with no particles91

Figure 5.2–9. Geometry and central line for the case with 1 particle92

Figure 5.2–10. Electric field distribution for the case with 1 particle92

Figure 5.2–11. Current density plot along the central line93

Figure 5.2–12. Cross-section of the volume with yz-plane95

Figure 5.2–13. Current as a function of total cholesterol and number of particles96

Figure 6.1–1. Frequency dependence of current paths98

Figure 6.1–2. RBC parallel to xy-plane99

Figure 6.2–1. Capillaries in earlobe (Susumu Nishinaga) 102

Figure 6.2–2. Alveoli. Capillary net of an alveola showing the erythrocytes within the blood vessels (Oliver Meckes) 103

Figure 6.3–1. Distribution of RBC 104

Figure 6.3–2. Variation of current with number of RBC, N_r 105

Figure 6.4–1. Distribution of RBC and cholesterol particles 106

Figure 6.4–2 Dependence of total current on the number of RBC N_r at different frequencies (RBC parallel to the electrode surface)..... 107

Figure 6.4–3 Distribution of cholesterol and RBC, tilted by $\theta = -45^\circ$ 108

Figure 6.4–4. Dependence of current on mesh for $\theta= 0^\circ$ 109

Figure 6.4–5. Dependence of current on mesh for $\theta= -45^\circ$ 109

Figure 6.4–6. Dependence of current on the orientation of RBC 110

Figure 6.4–7. Dependence of current on frequency for tilted RBC..... 112

Figure 6.4–8. Dependence of current on number of RBC, N_r ; $N_c = \text{const}$	113
Figure 6.4–9. Dependence of total current for different cholesterol levels	114
Figure 6.4–10. Values of current for total cholesterol concentrations 1, 2, 4, and 8 mmol/l	115
Figure 6.4–11. Average values of current for different cholesterol levels.....	116
Figure 7–1 (a) computational model of the experimental set-up and (b) details of electrode placement.....	117
Figure 7–2 (a) additional 3D model and (b) close-up showing details.....	118
Figure 7–3 Distribution of electric potential lines for electrodes placed facing each other	119
Figure 7–4 Potential distribution along the cut-line ($x=[-5,5]$, $z=0$).	120
Figure 7–5 Current distribution.....	120
Figure 7–6 Potential distribution between the flat electrodes	121
Figure 7–7 Potential distribution along the cut-line for flat electrodes	122
Figure 7–8 Current distribution for flat electrode positioning.	122
Figure 7–9 Cut plane for flat electrode positioning	123
Figure 7–10 Potential distribution for flat electrode positioning, driving electrodes switched off.	123
Figure 7–11 Potential lines for flat electrode positioning with switched off electrodes.	124
Figure A2-8.2–1 Basic model in 2D.	147
Figure A2-8.2–2 Mesh for 2D geometry.....	148
Figure A2-8.2–3 Electric potential in 2D basic model.....	149
Figure A3-8.2–1 Work plane 1.	152
Figure A3-8.2–2 Geometry.....	154

Figure A3-8.2–3. Mesh of main geometry.....	155
Figure A3-8.2–4 Cut-plane 1, $x=0$	156
Figure A3-8.2–5 2D Plot of electric field (cut-plane1).....	157
Figure A3-8.2–6 Cut Line 3D 1	158
Figure A3-8.2–7 Current density along cut line.....	159

Abstract

The main topic of this work is detection of solid particles suspended in conductive medium and development of methodologies for determining cholesterol levels in human blood non-invasively by electrical impedance technique.

The main part of this research is focused on the development of methodologies for numerical finite element (FE) modelling of simplified blood-cholesterol system, representing a real measurement system. This has been done first in 2D, to prove the concept and then in 3D, to take into account all of the effects that would only be present in 3D system as well as taking into account that there is a fully 3D problem in the heart of presented research. The proposed model has been tested in various extreme cases and theoretical and some experimental validations have been carried out to establish a degree of confidence in the modelling methodologies developed.

This included novel way of model simplification by introduction of particle coagulation. This method has been proven to be successful replacement of effective conductivity method, used in the past. It has been tested against variation in physiological parameters, such as particle concentration and distribution, and material properties, such as particle conductivities.

In 3D modelling cases the red blood cells (RBC) have been added to further increase the complexity of the system. Several case studies were used to help analyse which physical parameters of RBC would have the biggest impact on system's impedance. Results were validated against experimental data where possible. This allowed extension of proposed methodology to non-spherical particles modelling.

The other methodology adopted in this work applies to the electrode modelling. All electrodes are modelled as hollows. This tactic has been proven to work. It

was validated both theoretically and by comparing computational model results with experiment results (BERG, City University London).

In Conclusions, it is discussed that both methodologies can be used outside of current research in electromagnetic simulations of less conductive particles in conductive solvent and in cases where electrode material is not known.

Modelling investigations of the simplified blood-cholesterol systems using the 2D and 3D FE modelling methodologies developed in this work have shown that it should be possible to measure cholesterol levels in human blood by impedance technique. Opinion sought from clinical staff highlight that this can potentially improve patient care by minimizing time needed for tests and human error (by shortening the number of people involved in testing). The work also establishes and discusses the need for further work, both theoretical and experimental for development of a measuring device for non-invasive measurement of cholesterol in human blood by impedance technique.

Chapter 1. Introduction and background

1.1 Introduction

The word cholesterol came from the Greek words 'chole' (bile) and 'stereos' (solid), and the suffix 'ol' – from the word alcohol. It was first discovered in solid form in gallstones by the French researcher François Poulletier de la Salle in 1769. Cholesterol ($C_{27}H_{46}O$), 'the most highly decorated small molecule in biology' is a lipid like, waxy alcohol, which is transported in the blood plasma of all animals. It is essential for cellular functions, production of hormones and it plays a key role in many biochemical processes. However, in the last few decades cholesterol has attracted wide publicity because of its association with cardiovascular diseases. While minimum levels of cholesterol are essential for life, high levels in the blood circulation are associated with atherosclerosis. Commonly referred to as a 'hardening' and 'furring' of the arteries, atherosclerosis is a disease of arterial blood vessels manifested in the formation of multiple plaques within the arteries. It is promoted by excessive low-density lipoproteins (proteins that carry cholesterol and triglycerides) circulating in the blood plasma. If not addressed, it can lead to myocardial infarction (commonly known as a heart attack), stroke or peripheral vascular disease.

There are at present a large number of direct and indirect methods that are available in clinical and research laboratories for the quantitative measurement of cholesterol in blood: chemical, electrophoretic, enzymatic [1]–[3]. These measurements are being done increasingly frequently and often for prophylaxis and awareness against cardiovascular diseases. All these methods require a sample of the blood obtained from the body by an invasive procedure. The procedure may carry a risk of bruise, infection and/or haematoma. There are,

however, some indirect methods by which the level of total cholesterol can be estimated using bioelectrical impedance measurements carried out elsewhere in the body [4]. As these methods are indirect and based on inference of cholesterol level from statistical data obtained by multiple impedance measurements of substances other than blood, they are complicated, time consuming and often lack accuracy and reproducibility.

Thus, there is a growing need to develop a simple, non-invasive method for measuring total blood cholesterol. It is proposed to do this by using an electrical impedance technique in which the conductivity distribution of objects (e.g. cholesterol particles carried by lipoproteins) within a test volume (e.g. blood plasma) is measured in the form of impedance (Z) or admittance ($Y=1/Z$) by measuring the voltage (V) induced on electrodes attached to the surface when a small current (I) is passed between them. For example, in a tetrapolar impedance measurement the impedance is obtained by measuring the voltage drop between a pair of suitably placed electrodes (measuring or passive electrodes) when a small current flows between two separate driving or active electrodes placed on the body surface ($Z=V/I$). For cholesterol measurement, the measured impedance is a function, among others factors of the size, concentration and distribution of lipoproteins carrying cholesterol particles.

The electrical impedance technique has been used successfully for many biological measurements, especially for measuring characteristics of blood. These include measurement of body fluid volume [5], fat [6], [7], glucose[8]–[10], blood coagulation [11], haematocrit (erythrocyte volume fraction, EVF) [12], white blood cell count and other blood measurements [13]. All these blood measurement methods involve an invasive procedure for obtaining blood from the body.

As mentioned earlier, in the impedance technique the conductivity distribution of objects (e.g. cholesterol particles carried by lipoproteins) within a test volume (e.g. blood plasma) is measured in the form of impedance by measuring the voltage induced on electrodes attached to the surface. The impedance is

calculated from measured voltage and current ($Z=V/I$). The mathematical modelling of the living tissue can theoretically establish the feasibility of the impedance technique for direct, non-invasive measurement of cholesterol level in the blood. One of the main challenges is to establish by simulation various design parameters of the measurement circuit (electrode material, size, shape, number, alignment and placement, current level, frequency, etc.) that ensures adequate distribution of current (electric field) and an induced electric potential between electrodes. Although the mathematical physics of conduction is well understood, the mathematics of describing the current and potential fields between and around impedance electrodes, particularly those attached to tissue, is more challenging (e.g. skin-electrode impedance, capacitance effect of skin, skin layers - epidermal, dermal, subcutaneous layers, etc.).

Finite element (FE) models are used to investigate the effects of various parameters on the distribution of alternating currents and electric potential (hence voltage drops) in the problem domain. These parameters include various physiological (e.g. level and distribution of lipoproteins, other blood components), material (e.g. dielectric permittivities and conductivities of blood components) and electrical variables (e.g. measurement circuitry, excitation frequency, electrode geometry and their placement). Since the unknown potential distribution is a function of many of the physiological components in blood and tissue, the modelling challenge here is to, by simulation, establish an adequate and identifiable functional relationship between this distribution and the level of cholesterol in the blood.

By advanced biomedical signal analyses the impedance data obtained in the methods outlined above from FE simulation and from subsequent investigation conducted on experimental prototypes discussed below, it should be possible to establish a functional relationship between calculated voltage drops across measuring electrodes (hence impedance values) and concentration of lipoproteins in the blood.

This leads to the main aims and objectives of the research.

1.2 Aims and Objectives

Considering the above, the main aims and objectives of the proposed research were formulated:

Aim 1 Justify necessity of new method for cholesterol level measurement. This will be done by:

- a) Analysis of all existing methods, including highlighting their advantages and disadvantages
- b) In depth understanding of current routine test process
- c) Sought clinician's opinion on proposed method

Aim 2 Development of appropriate methodologies for mathematical modelling and simulation of penetration of electric field and distribution of electric current and potential in living tissues. This leads to further objectives:

- a) Develop 2D realistic finite element (FE) models
- b) Develop 3D realistic finite element (FE) models

Aim 3 Investigate the distribution of alternating currents and electric potential in developed FE models. This will be achieved through the following objectives:

- a) Use various physiological properties (e.g. level and distribution of lipoproteins, other blood components) in FE models developed in Aim1 (a) and Aim1 (b)
- b) Change of material properties (e.g. dielectric permittivities and conductivities of blood components including lipoproteins carrying cholesterol particles)
- c) Change of electrical parameters (e.g. measurement circuitry, excitation frequency, electrode geometry and their placement)

Aim 4 Establish functional relationship between calculated currents on measuring electrodes (hence impedance values) and concentration of cholesterol in the blood. Objective related to this aim is:

- a) For a given voltage drop, this is done by advanced biomedical signal processing of potential signals calculated by FE modelling.

1.3 Background

1.3.1 Cholesterol in body

Role and function

Cholesterol (see Figure 1.3–1 for chemical structure) is a waxy steroid, which is synthesized in many types of tissue, but particularly in liver and intestinal wall. It is used for hormone and cell membrane production and is transported in the blood plasma [14]. It is an essential structural component of cell membranes. One of its functions is to establish proper membrane permeability and fluidity. It also is one of the key components for production of bile acids, steroid hormones, and Vitamin D. On one hand small quantities of cholesterol are important and necessary, on the other hand high levels of cholesterol can damage arteries and are potentially linked to diseases such as those associated with the cardiovascular system (heart disease) [15]. At the end of its life cycle cholesterol is recycled; excreted by the liver into the digestive tract. Typically about 50% of the excreted cholesterol is reabsorbed by the small bowel back into the bloodstream [16].

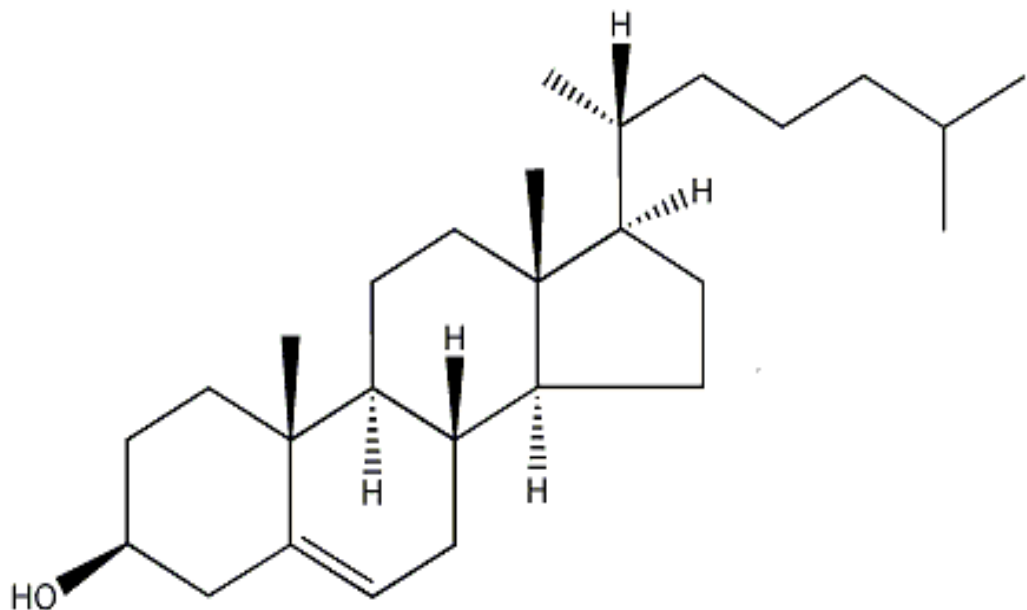


Figure 1.3–1. Chemical structure of cholesterol

Cholesterol is a unique building block for membranes; it also influences membrane fluidity. Cholesterol's hydroxyl group interacts with the polar head groups of the membrane phospholipids, while the steroid and the hydrocarbon chain are sitting inside the membrane. Basically cholesterol reduces the permeability of the plasma membrane to protons (positive hydrogen ions) and sodium ions [17]. Figure 1.3–2 illustrates this mechanism.

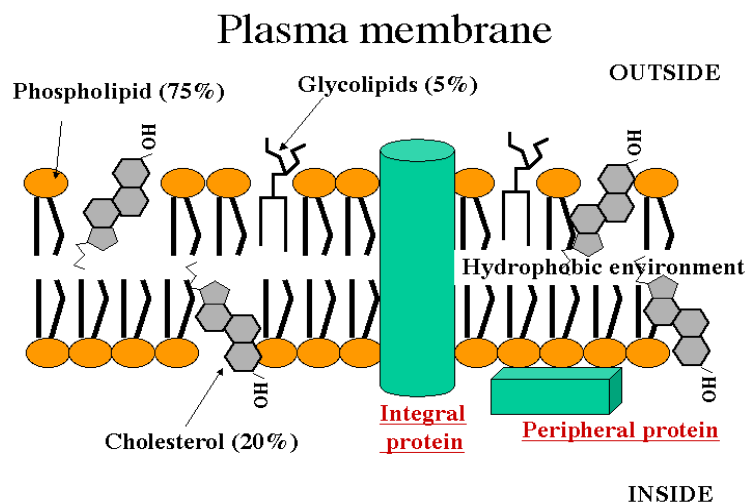


Figure 1.3–2. Plasma membrane

Within the cell membrane, cholesterol also functions in intracellular transport, cell signalling and nerve conduction. Recently, cholesterol has also been implicated in cell signalling processes, assisting in the formation of lipid rafts in the plasma membrane. For example, a myelin sheath, rich in cholesterol, in neurons provides insulation for more efficient impulse conduction [18].

Cholesterol is also known as a predecessor in several biochemical processes. It is converted to bile in liver, which is then stored in the gallbladder. Bile salts are initial component in the intestinal absorption of fat molecules as well as the fat-soluble vitamins, such as Vitamin A, D, E and K. Which makes cholesterol is an important precursor molecule for the synthesis of Vitamin D and the steroid hormones (including cortisol, aldosterone, progesterone, oestrogens, and

testosterone, and their derivatives). Some research indicates that cholesterol may act as an antioxidant [19]. Moreover, in its unoxidized form it eliminates risk of diseases induced by free-radicals and cancer, by functioning as a membrane protector [20].

Sources

Food

Approximately three quarters of cholesterol is newly synthesized and a quarter originates from dietary intake. Animal fats are complex mixtures of triglycerides, with phospholipids and cholesterol. This means that all foods containing animal fat contain cholesterol [21]. Major cholesterol sources are cheese, egg yolks, beef, pork, poultry, and shrimp [22]. Human breast milk also contains significant quantities of cholesterol [23].

The amount of cholesterol present in plant-based food sources is generally much lower than animal based sources [22], [24]. Total fat intake, especially saturated fat and trans fat [25], plays a larger role in blood cholesterol than direct cholesterol intake. Sources of saturated fat are full fat dairy products, animal fats, some types of oil and chocolate. Trans fats are found in the partial hydrogenation of unsaturated fats. Products having trans fat are margarine and hydrogenated vegetable fat, as well as fast foods, packed snacks, fried and baked goods.

It is believed that a change in dietary fat and cholesterol intake can lower blood cholesterol levels [15], (and thus reduce the likelihood of development of coronary artery disease). But results are equivocal as there were experiments showing that reduction of dietary cholesterol intake is counteracted by the organs trying to compensate it and trying to keep blood cholesterol levels constant [26]. Also it was shown that ingested animal protein can raise blood cholesterol more than the ingested saturated fat or any cholesterol [27].

Body synthesis

Animal cells can produce cholesterol; the amount of it depends on cell type and function. About 20–25% of total daily cholesterol production occurs in the liver; other sources of synthesized cholesterol include the intestines, adrenal glands, as well as reproductive organs. For cholesterol synthesis one molecule of acetyl CoA and one molecule of acetoacetyl-CoA are needed. As a result of a chain of chemical reactions with enzymes, reactions with presents of adenosine-5'-triphosphate (ATP) lanosterol is produced, which is then converted into cholesterol [28].

Biosynthesis of cholesterol is directly regulated by the cholesterol levels present. A higher intake from food decreases its endogenous production, lower intake from food leads to opposite. The main regulatory mechanism is the registration of intracellular cholesterol in the endoplasmic reticulum by the protein SREBP (sterol regulatory element-binding protein 1 and 2) [29]. In the presence of cholesterol, it is bound to two other proteins: SCAP (SREBP cleavage activating protein) and Insig-1. When cholesterol levels fall, second one dissociates from the complex SREBP-SCAP, allowing the complex to migrate to the Golgi apparatus, leading to a chain of reactions that stimulates the transcription of many genes. Among these is the low-density lipoprotein (LDL) receptor. The former scavenges circulating LDL from the bloodstream, whereas there are other processes leading to an increase of endogenous production of cholesterol [30].

Cholesterol synthesis can be turned off when cholesterol levels are high, as well. Increasing concentrations of cholesterol (and other sterols) cause some changes, which makes it more susceptible to destruction by the proteosome, which activity can also be reduced by phosphorylation by an AMP-activated protein kinase. Because this last one is activated by adenosine monophosphate (AMP), which is produced when ATP is hydrolysed, it follows that cholesterol synthesis is halted when ATP levels are low [31].

Transportation

Cholesterol is almost insoluble in water (0.095 mg/L at 30 °C) and that is why it can dissolve and travel in the water-based bloodstream at exceedingly small concentrations. This property also leads to the fact that it is transported in the blood stream by means of bigger particles called lipoproteins, which are complex particles that have an exterior composed of amphiphilic proteins and lipids whose outward-facing surfaces are water-soluble and inward-facing surfaces are lipid-soluble; triglycerides and cholesterol esters are carried inside. Phospholipids and cholesterol, being amphipathic, are placed in the surface monolayer of the lipoprotein (Figure 1.3–3).

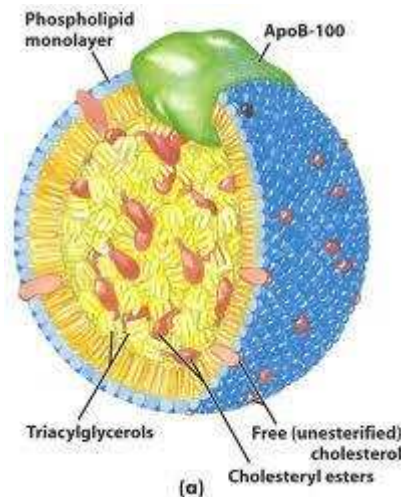


Figure 1.3–3. Structure of lipoprotein

In addition to that, lipoproteins have their own 'signature' in a form of apolipoprotein that direct the lipids they carry to certain tissues. Because of that, there are several types of lipoproteins within blood called, in order of increasing density and decreasing size, very low density lipoprotein (VLDL), intermediate density lipoprotein (IDL), low density lipoprotein (LDL) and high density lipoprotein (HDL) (Table 1-1).

Table 1.1.Types of lipoprotein

Lipoprotein type	Diameter, nm	Density, g/ml	Cholesterol/triglycerides
chylomicrons	100-1000	<0.95	8%/84%
VLDL	30-80	0.95-1.006	22%/50%
IDL	25-50	1.006-1.019	29%/31%
LDL	18-28	1.019-1.063	50%/4%
HDL	5 - 15	>1.063	20%/8%

The density of lipoprotein depends on cholesterol/protein concentration. The more cholesterol/less protein there is the lower its density is. The cholesterol within all types of lipoproteins is identical, although some of it is carried as the 'free' alcohol and some as fatty acyl esters called cholesterol esters. However, the different apolipoproteins, which serve as markers for cell membrane receptors, determine the start- and endpoints for cholesterol transport (Figure 1.3–4).

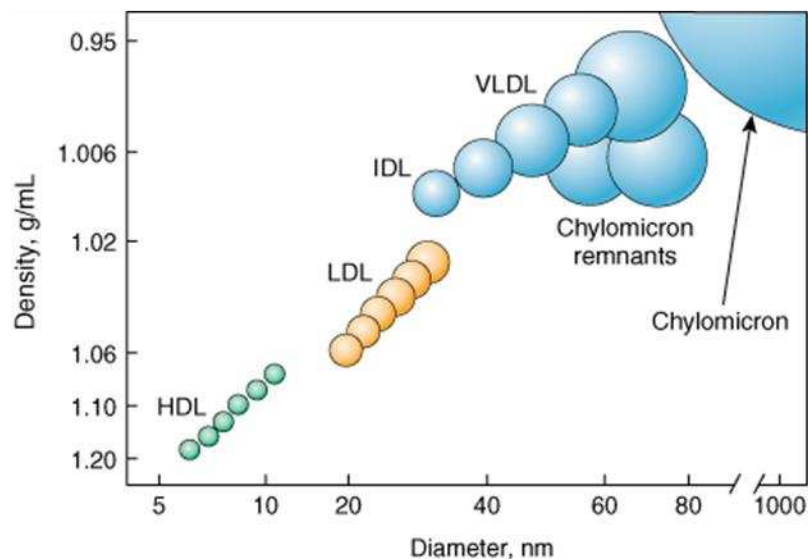


Figure 1.3–4. Classification of lipoproteins

Chylomicrons, the least dense type of cholesterol carrying molecules, contain apolipoprotein B-48, apolipoprotein C, and apolipoprotein E. They transport fats from the intestine to muscle and other tissues that need fatty acids to produce

energy or fat. Chylomicron remnants are taken up from the bloodstream by the liver and are cholesterol-rich because of not used cholesterol.

VLDL are produced by the liver and contain excess triacylglycerol and cholesterol. They have apolipoprotein B100 and apolipoprotein E in their shells. During transport in the bloodstream, triacylglycerol is partially absorbed from IDL molecules, which leads to even higher percentage of cholesterol. The IDL molecules are either taken up by the LDL receptor on the liver cell surfaces or continue to lose triacylglycerols in the bloodstream until they become LDL molecules, having the highest percentage of cholesterol present within.

This means that LDL molecules are the major carriers of cholesterol in the blood. Each molecule of LDL has about 1,500 molecules of cholesterol ester. Apolipoprotein B100 set on a shell of LDL molecule is recognized by the LDL receptor in tissues. Once it happens many LDL receptors become trapped and after several chemo-physical processes its cholesterol is hydrolyzed (becoming cholesterol esters). After that cholesterol can be used within the cell for membrane biosynthesis or esterified and stored within the cell.

Synthesis of the LDL receptor and control of cholesterol synthesis in response to its presence in the cell are regulated by the same protein. When the cell has more cholesterol than needed, LDL receptor synthesis is blocked so that no more cholesterol (LDL molecules) can get in. In the opposite case, more LDL receptors are made when the cell has lack of cholesterol [32]. When this system is not balanced, there will be LDL molecules in the blood having no receptors. They are oxidized and taken up by macrophages, which become foam cells. They can then get trapped in blood vessel walls and contribute to atherosclerotic plaque formation. Differences in cholesterol homeostasis effects the development of early atherosclerosis (carotid intima-media thickness) [33]. This is known to lead to heart attack, stroke, and other medical problems. That is why LDL cholesterol is often referred being a 'bad' cholesterol [31].

HDL particles are thought to play a key part in transporting cholesterol back to the liver for excretion or to other tissues that use cholesterol to synthesize

hormones in a process known as reverse cholesterol transport (RCT) [34]. Having large numbers of large HDL particles correlates with better health outcomes [35]. In contrast, having small numbers of large HDL particles is independently associated with atheromatous disease progression within the arteries.

Metabolism, recycling and excretion

Liver oxidizes cholesterol into different bile acids [36]. These in turn are conjugated with glycine, taurine, glucuronic acid and sulphates. A mixture of bile acids, including cholesterol, is excreted into the bile from the liver. Approximately 95% of the bile acids are reabsorbed from the intestines and the remainder are lost in the faeces [37]. The excretion and reabsorption of bile plays a major part in the digestion and absorption of dietary fats. In some situations, in places with higher concentration e.g. the gallbladder, cholesterol crystallises and is the major constituent of most gallstones [38]. Cholesterol is mainly converted into coprostanol, a non-absorbable sterol which is excreted in the faeces [39].

Cholesterol disorders

Hypercholesterolaemia

Having high concentrations of LDL in combination with low concentrations of functional HDL (hypercholesterolaemia) are strongly associated with cardiovascular disease because these causes development of atheroma in arteries (atherosclerosis). This leads to myocardial infarction (heart attack), stroke, as well as peripheral vascular disease. Because higher LDL particle concentrations and its smaller size, contribute to this process more than the cholesterol content of the HDL particles [40], LDL is often called 'bad cholesterol'. On the other hand, if concentrations of functional HDL, which is responsible for cholesterol removal from cells and atheroma, are high, this is termed to as 'good cholesterol'. The balance of these two is determined genetically but changes can be made by medications, food choices, and other

factors [41]. Increased levels of the lipoprotein fractions as well as LDL, IDL and VLDL are called *atherogenic* ('helping' to develop atherosclerosis) [42]. These fractions, and not the total cholesterol level, are known to correlate with the extent and progress of atherosclerosis. That means that although the total cholesterol can be within normal limits, if it is made up mostly of small LDL and small HDL particles, the atheroma growth rates would be high. But if LDL particle number is low and a large portion of the HDL particles are large, then atheroma growth rates are low for any given total cholesterol concentration [43]. In case of increased cholesterol levels a strict diet (low-saturated fat, trans-fat free) is recommended as well as low cholesterol foods [44], [45], and is often followed by one of various hypolipidaemic agents, cholesterol absorption inhibitors, nicotinic acid derivatives or bile acid sequestrates [46]. Extreme cases of atheroma have previously been treated by means of partial ileal bypass surgery, which has now been replaced by medication. Although the role of cholesterol in cardiovascular disease is well known, some studies have suggested an inverse correlation between cholesterol levels and mortality. One of them, performed in 2009, shows that for patients with acute coronary syndromes there is an association of hypercholesterolemia with better mortality outcomes [47].

Hypocholesterolemia

Abnormally low levels of cholesterol are known as hypocholesterolemia. Some studies suggest that this condition has a link with depression, cancer, and cerebral haemorrhage. In general, the low cholesterol levels seem to be a consequence of an underlying illness, rather than a cause [48].

1.3.2 Methods used for determination of cholesterol levels

There is a whole variety of methods available to determine serum cholesterol, such as ultracentrifugation, electrophoresis, high-performance liquid chromatography (HPLC), precipitation-based methods and direct methods. The direct methods are used routinely. The most common method for determination of Total, HDL-, LDL- cholesterol and triglycerides nowadays is enzymatic

colorimetric test. It is an automated method for direct determination of cholesterol in serum and plasma. There were also some attempts to perform non-invasive cholesterol measurements. The short review of those methods is given below.

Invasive methods

Reference method

There is a reference method for cholesterol measurements. The process starts with serum cholesterol esters being hydrolysed by alcoholic KOH (potassium hydroxide). Then cholesterol is extracted by hexane, and is dried. After the dry residue is treated with acetic acid, acetic acid anhydride, and sulphuric acid (Liebermann-Burchard reagent), that develops a colour reaction that is measured at 620 nm. This method has minimum positive bias compared with the definitive method for cholesterol, which is mass spectrometry [49]. The results can be presented either in molar c_i or mass concentration ρ_i :

$$\rho_i \text{ (mg/dL)} = 38.7^* c_i \text{ (mmol/L)} \quad (1.3-1)$$

This method is very accurate, but its downside is that it is time-consuming and not suitable for automation. For routine screenings enzymatic methods have been developed.

Ultracentrifugation

The ultracentrifugation is a method used in biochemistry for determination of blood/serum/plasma components and their analysis. The ultracentrifuge is optimized for spinning a rotor at very high speeds, generating an acceleration as high as 1,000,000 g (9,800 km/s²). The two major kinds of ultracentrifuges are preparative and analytical. Both classes of instruments find important uses in molecular biology, biochemistry and polymer science. In analytical type of ultracentrifuge operator can observe a sample that is being spun in real time

through an optical detection system. The phenomena being monitored is ultraviolet light absorption and/or interference optical refractive index. The operator can see sample concentration evolution the axis of rotation profile as a result of the applied centrifugal field. Then the observed data are digitalized and stored for further analysis.

The aim of the process is to distinguish between the shape and molar mass of different macromolecules dissolved in analysed solution [50].

The huge rotational kinetic energy of the rotor in an operating ultracentrifuge makes the failure of a spinning rotor a serious concern. As the analyser is being used under stress of routine and is exposed to chemical solutions, its rotor can deteriorate with time. Proper use of the instrument and rotors within recommended limits and careful maintenance of rotors to prevent corrosion and to detect deterioration is necessary to avoid this hazard. In addition, maximum capacity is six samples, which in a hospital setting is not enough. For total cholesterol, one needs just one rotating cycle, for HDL/LDL separation 2 or more.

Enzymatic colorimetric test

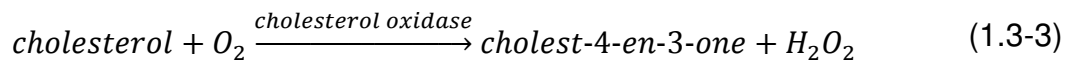
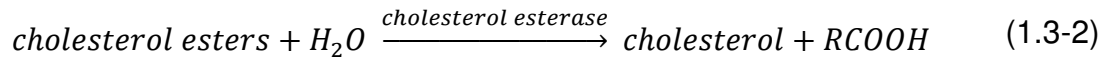
The whole process starts when blood is withdrawn from a patient. It is put in a labelled sample holder and transferred from laboratory to biochemistry lab. Then on the first stage the blood is centrifuged adding a buffer solution, as a result blood plasma is separated from the blood cells. The blood plasma then is placed in a different holder and put into automated clinical chemistry analyser. There the chain of chemical reactions takes place with different reagents and catalysts.

For cost reasons, LDL values have long been estimated using the Friedewald formula (or a variant):

TC [total cholesterol] $-$ HDL [total HDL] $-$ $0.2TG$ [20% of the triglyceride value] = estimated LDL.

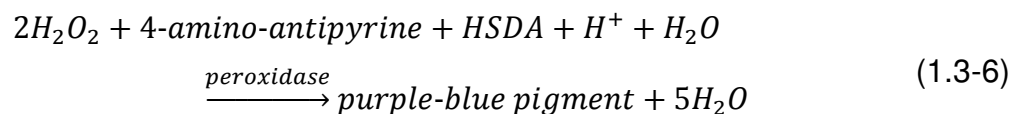
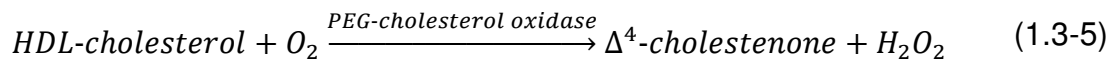
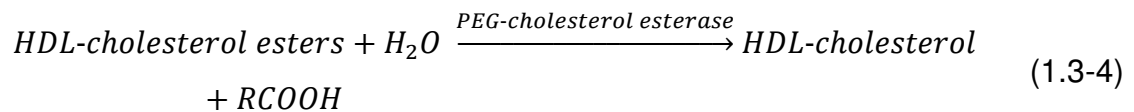
The main idea is that TC is defined as the sum of HDL, LDL, and VLDL. Usually just the total, HDL, and triglycerides are measured. The VLDL is calculated as one-fifth of the triglycerides.

Below, there is a list of chemical reactions to obtain TC.



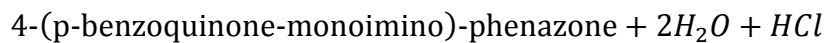
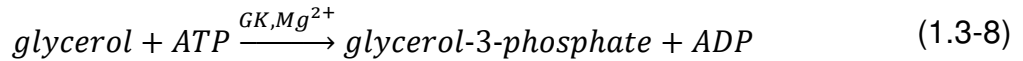
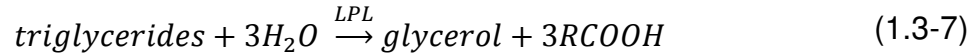
The hydrogen peroxide created forms a red dyestuff by reacting with 4-aminophenazone and phenol under the catalytic action of peroxidase. The colour intensity is directly proportional to the concentration of cholesterol and can be determined photometrically [51].

For HDL-cholesterol direct method with PEG-modified enzymes is used [52]:



The method used for determination of triglycerides is based on work by Wahlefeld getting a lipoprotein lipase from microorganisms for the rapid and complete hydrolysis of triglycerides to glycerol that is then oxidised to dihydroxyacetone phosphate and hydrogen peroxide. This product then reacts with 4-aminophenazone and 4-chlorophenol under the catalytic action of

peroxidase to form a red dyestuff (Trinder endpoint reaction). The colour intensity is directly proportional to the triglyceride concentration [53].



On average these tests take about 10-15 minutes each, but there is a lot of room for human factor errors (such as labelling and transferring of the blood samples to the lab, changing the samples and getting correct results in the relevant files). Serum cholesterol tests are not the first priority in the biochemistry lab, which is why it takes up to one week to get the results of the test (information obtained from Biochemistry lab, Whittington Health, London).

Electrophoresis

Electrophoresis (cataphoresis) is the motion of charged particles in a solid or liquid matrix under the influence of an electric field [54], [55]. For this type of analysis blood plasma samples are used. Rate of movement for particles in suspension depends on its mass and size: larger particles move slower because of friction and highly charged particles move quicker. Lipoproteins are separated through a gel matrix with varying pore size, for that purpose polyacrylamide is commonly used. Those gels can be cast as columns or slabs. For analysis slabs are widely used, because it allows the separation and comparison of multiple samples. A 'stacking' gel is placed on the top of the

separating ('running') gel to sharpen the bands before they enter the gel (Figure 1.3–5).

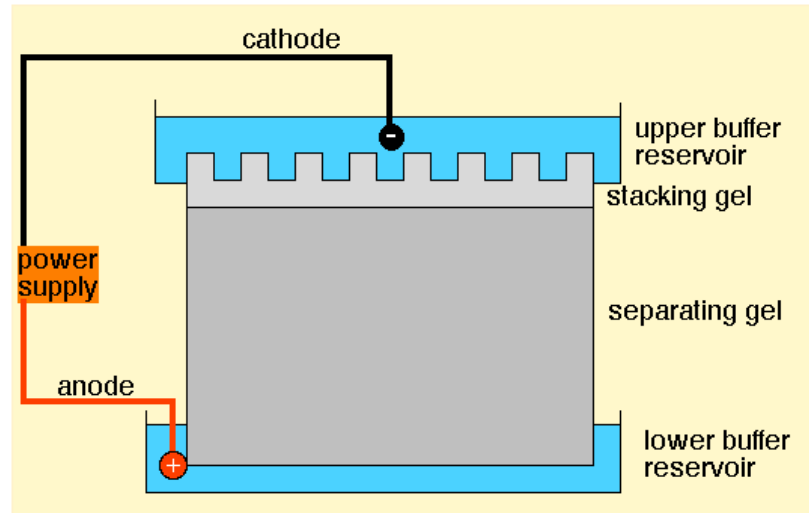


Figure 1.3–5. Electrophoresis set

The electrophoresis buffer and the buffer in the separating gel have a high pH (8.9) and contain glycine. In contrast, the stacking gel buffer has a low pH (6.8) and contains Cl^- . At the low pH of the stacking gel, the Cl^- ions in the stacking gel are negatively charged and start moving towards the anode, but the glycine entering from the gel buffer has only a very small negative charge. Because Cl^- moves faster than glycinate, a low conductivity zone within the gel is formed. Higher electric field appears and accelerates the proteins so that they come to the separating gel as a narrow band at the boundary between the leading Cl^- and the trailing glycinate ions. The glycine becomes completely dissociated once the protein complexes reach the running gel, and it migrates at the same speed as Cl^- . For visible results the membrane is stained. After electrophoresis the cellulose acetate strips are stained overnight at room temperature and then rinsed in solution containing industrial spirit, water and glacial acetic acid. Colour and intensity of the stripes obtained are analysed [56].

This method is one of the oldest used for lipoprotein separation and one of the most reliable but it is time-consuming and not suitable for automation. There is

also plenty of room for human mistakes as any changes in sample preparation can lead to the sample being destroyed.

High-Performance Liquid Chromatography

The main principle of high-performance liquid chromatography (HPLC) is that solution moved through the column is slowed by specific chemical or physical interactions with the stationary phase present within the column. The velocity of this solution movement depends on the nature of the sample and on the compositions of the stationary (column) phase. The time at which a specific sample comes out of the end of the column is called the retention time; the retention time under particular conditions is considered an identifying characteristic of a given sample.

The analysed sample is put, in small volumes, into the stream of mobile phase. Lipoprotein samples are isolated by ultracentrifugation and separated by chromatography on Bio-Gel agarose. Total lipid extracts of the lipoprotein samples are prepared by extraction with chloroform-methanol. Cholesteryl heptadecanoate added to aliquots of lipoprotein total lipid extracts. The lipoprotein extracts are prepared for HPLC analysis by evaporating the extraction solvent and re-dissolving the lipid in tetrahydrofuran-acetonitrile. This volume is injected into the liquid chromatograph. Cholesterol and cholesteryl esters are eluted from the column using a linear water gradient. The water concentration in acetonitrile-tetrahydrofuran is reduced from 3% to 0% over a 20-min period at 37°C with a solvent flow rate of 2.0 ml/min. Cholesterol and cholesteryl esters eluting from the column are detected by their ultraviolet absorption at 123 nm [57]. The mass of cholesterol are calculated from standard curves of mass versus peak area by the following formula:

$$\text{Sample mass} = \left(\frac{\text{Mass of standard}}{\text{Peak of standard}} \times \text{Peak area of standard} \right) \div \quad (1.3-11)$$
$$\div (\% \text{ Recovery of standard})/100$$

Reversed phase columns are quite difficult to damage compared with normal silica columns. They can be used with aqueous acid, but the column should not be in contact with the acid for too long, as it can damage the metal parts of the HPLC equipment. The metal content of columns must be kept low if the best possible ability to separate substances is to be retained. The main down side of this method is that there is a need for ultracentrifugation prior to chromatographic analysis.

Accutrend® Plus Dual Testing System

The lipoprotein complexes are dissolved by the detergent DONS so that the cholesterol esterase can split the cholesterol ester into cholesterol and the corresponding fatty acid. Cholesterol then is oxidized to 4-cholesten-3-one plus H₂O₂ by cholesterol oxidase. The hydrogen peroxide converts an indicator dye (TMB) to a blue colour by means of peroxidase [58].

On a plus side this system is portable and gives results within minutes.

But test strips have to be stored in tight capped vial, they have expiration date and the test result coming out on the screen as either high or low (higher than 7.76 mmol/L or lower than 3.88 mmol/L).

Non-invasive methods

Classification of Total Cholesterol Level Using Bioelectrical Impedance

A rule based expert system has been developed for total cholesterol (TC) level classification using bioelectrical impedance analysis (BIA). Parameters that are being used as predictors are body capacitance (BC), basal metabolic rate (BMR), extracellular mass (ECM), and lean body mass (LBM). This method can classify subjects' TC level between normal (≤ 5.2 mmol/L) and abnormal (>5.2 mmol/L).

The first tests show that the system total accuracy for classifying TC level at 0.6 probability cut-off prediction was only 70%. The sensitivity was 67%, and

specificity of 74%. From the validation data, this system can classify 6 from 10 subjects correctly [59].

PreVu Non-Invasive Cholesterol Test

This method is used to predict skin cholesterol levels. Skin cholesterol does not correlate with those of serum, but have been proven to give valid prediction of coronary artery disease (CAD) possibility. A foam pad with 3 wells is placed on the palm of the patient's hand and adheres with special medical adhesive (Figure 1.3–6). Then a drop of detector solution is added. A one minute wait is needed for the co-polymer (Digitonin & HRP) to bond with skin cholesterol. A drop of indicator solution (TMB) is added. Cholesterol changes solution colour in the foam pad well. After a two minute wait the resulting blue colour can be read and quantified using handheld spectrophotometer. This is then translated into a risk number [60], [61].



Figure 1.3–6. PreVu test performance

Even though this method is non-invasive and does give information on cholesterol level and CAD possibility, there is no link between those levels and cholesterol levels measured during routine screening. This does not create any difficulties in case of low cholesterol levels. For increased cholesterol levels dosage of statins is directly linked to blood cholesterol levels. Which means that there is a need for regular blood test.

1.3.3 Proposed Non-Invasive Impedance Method

The review of all existing methods (Table 1-2) shows that there is an urgent need for creation of portable non-invasive speedy reliable method that measures some parameter strongly linked with serum cholesterol levels. It will be proven in the presented research that impedance of blood is such quantity.

Table 1.2. Cholesterol measurements methods

	Method	Principle	Advantages	Disadvantages
Invasive	Reference method	Chain of chemical reactions followed by colour intensity measurement	Very accurate	Time-consuming, not suitable for automation
	Ultracentrifugation	Ultraviolet light absorption test after high-speed centrifugation	Accurate	Low capacity, time-consuming
	Enzymatic colorimetric test	Chain of chemical reactions followed by colour intensity measurement	Accurate	Is a low priority test performed in hospitals
	Electrophoresis	Electrophoretic separation followed by	Reliable, accurate	Time-consuming, not suitable for automation

		product staining and colour intensity analysis		
	HPLC	Lipoproteins are separated in accordance with their mass, then ultraviolet absorption measured	Reliable	Needs ultracentrifugation prior to chromatography
	Accutrend Plus	Chemical reaction producing colour on a test strip	Portable system, quick results	Indicates cholesterol level as “high” or “low”
Non-invasive	Classification BIA	Rule based system	Non-invasive	Low accuracy
	PreVu	Chemical reaction results are measured with portable spectrometer	Non-invasive	Measured cholesterol levels do not correlate with serum cholesterol

Chapter 2. Mathematical Modelling of Electromagnetic Field Distribution in Conductive Suspension

2.1 Introduction

This chapter reviews finite element method and mathematical formulation of electric field distribution in 2D/3D model. The aim is to discuss direct current (DC) and high-frequency cases and explain the way they are simulated.

Non-invasive electrical measurement of cholesterol is an alternative to existing methods for determination of cholesterol levels. The suggested method is based on impedance measurement. To find the impedance of a biological object one needs to know current flowing through it. And to find current it is necessary to know field and its distribution inside the object being studied. For better problem understanding and setting up a correct mathematical model of a set-up its physics background needs to be reviewed.

For 2D modelling COMSOL 4.0 has been used on a machine with Intel Core 2 duo CPU GHz, 4GHz RAM, 64-bit operating system.

For 3D modelling COMSOL 4.2 has been used on a machine with Intel Xeon CPU 3.1Ghz processor, 16GB RAM, 64-bit operating system and Intel Xeon CPU 3.6Ghz processor, 32GB RAM, 64-bit operating system.

2.2 Mathematical formulation of electric field distribution in conductive suspension

2.2.1 Maxwell's equations

All electromagnetic problems are described by four basic Maxwell's equations. To solve an electromagnetic problem on a macroscopic level means to solve those equations when certain boundary conditions are known. Maxwell's equations describe the relationships between the fundamental electromagnetic quantities. In this work the differential form is being used as it leads to partial differential equations that the finite element method can handle. Maxwell's equations for general time-varying fields can be presented as:

$$\nabla \times \mathbf{H} = \mathbf{J} + \frac{\partial \mathbf{D}}{\partial t} \quad (2.2-1)$$

$$\nabla \times \mathbf{E} = -\frac{\partial \mathbf{B}}{\partial t} \quad (2.2-2)$$

$$\nabla \cdot \mathbf{D} = \rho \quad (2.2-3)$$

$$\nabla \cdot \mathbf{B} = 0 \quad (2.2-4)$$

1

Where \mathbf{E} - the electric field intensity, V/m; \mathbf{D} - the electric displacement or electric flux density, C/m²; \mathbf{H} - the magnetic field intensity, A/m; \mathbf{B} - the magnetic flux density, V*s/m²; \mathbf{J} - the current density, A/m²; ρ - the electric charge density, C/m³.

The first two equations are known as the *Maxwell-Ampère's law* and *Faraday's law* respectively. The third and fourth equations are electric and magnetic forms of *Gauss' law*.

Another fundamental equation is called the *equation of continuity* and can be written as

$$\nabla \cdot \mathbf{J} = -\frac{\partial \rho}{\partial t} \quad (2.2-5)$$

Three out of these five equations are independent. The first two combined with either the electric form of Gauss' law or the equation of continuity form an independent system.

2.2.2 Constitutive relations

To achieve a closed system, we should include constitutive relations in the equations. These describe the macroscopic properties of the medium:

$$\mathbf{D} = \varepsilon_0 \mathbf{E} + \mathbf{P} \quad (2.2-6)$$

$$\mathbf{B} = \mu_0 (\mathbf{H} + \mathbf{M}) \quad (2.2-7)$$

$$\mathbf{J} = \sigma \mathbf{E} \quad (2.2-8)$$

Here ε_0 is the *permittivity of vacuum*, μ_0 is the *permeability of vacuum*, and σ the *electric conductivity*. In the SI system, the permeability of vacuum is chosen to be $4\pi \cdot 10^{-7}$ H/m. The velocity of an electromagnetic wave in a vacuum is given as c_0 and the permittivity of vacuum can be found from the relation

$$\varepsilon_0 = \frac{1}{c_0^2 \mu_0} = 8.854 \cdot 10^{-12} \text{ F/m} \approx \frac{1}{36\pi} \cdot 10^{-9} \text{ F/m} \quad (2.2-9)$$

The *electric polarization vector* \mathbf{P} shows how the material is polarized in the presence of an electric field. It can be interpreted as the volume density of electric dipole moments and it is generally a function of \mathbf{E} . Some materials can have a non-zero \mathbf{P} even when there is no electric field.

The *magnetization vector* \mathbf{M} describes how the material is magnetized when a magnetic field \mathbf{H} is present. It can be interpreted as the volume density of magnetic dipole moments and is generally a function of \mathbf{H} . For permanent magnets \mathbf{M} is not equal to zero also when there is no magnetic field present.

We consider all the materials modelled in our study being as linear, which means that the polarization is proportional to the electric field, $\mathbf{P} = \epsilon_0 \chi_e \mathbf{E}$, where χ_e is the *electric susceptibility*. That also means that magnetization is proportional to the magnetic field, $\mathbf{M} = \chi_m \mathbf{H}$, where χ_m is the *magnetic susceptibility*. The constitutive relations for this type of materials are changed to:

$$\mathbf{D} = \epsilon_0(1 + \chi_e)\mathbf{E} = \epsilon_0\epsilon_r\mathbf{E} = \epsilon\mathbf{E} \quad (2.2-10)$$

$$\mathbf{B} = \mu_0(1 + \chi_m)\mathbf{H} = \mu_0\mu_r\mathbf{H} \quad (2.2-11)$$

The parameter ϵ_r is the *relative permittivity*, and μ_r is the *relative permeability* of the material. The properties ϵ and μ are the *permittivity* and *permeability* of the material. For isotropic materials as in our study these are scalar properties.

After setting the general equations we can proceed to our particular case. For impedance measurements the following two cases are most common. First one is when the direct current (DC) is applied to the system under study. In the second case the sinusoidal voltage or current is applied. It is a well known fact that in most biological systems such periodic input will induce periodic output.

2.2.3 Static case

When the field quantities do not vary with time, the field is called static. In this case, (2.2-1), (2.2-2) and (2.2-5) can be re-written respectively as

$$\nabla \times \mathbf{E} = 0 \quad (2.2-12)$$

$$\nabla \times \mathbf{H} = \mathbf{J} \quad (2.2-13)$$

$$\nabla \cdot \mathbf{J} = 0 \quad (2.2-14)$$

whereas (2.2-3), (2.2-4), and (2.2-5) remain the same. It is evident that in this case there is no interaction between electric and magnetic fields; therefore, we can either have a separate electrostatic case described by (2.2-3) and (2.2-12) or a separate magnetostatic case described by (2.2-4) and (2.2-13), with (2.2-14) being a natural consequence of (2.2-13).

2.2.4 Alternating current

Eddy-current

The range of frequencies, which is normally used for measuring living tissue impedance, is between 50Hz and 100MHz. With higher frequencies all electromagnetic properties of tissue becomes very close to the properties of water, so no useful information can be obtained . Thus for considered frequency range and average properties of biological matter the average depth of penetration [62] can be calculated:

$$\delta = \frac{1}{\sqrt{f\pi\mu\sigma}} \quad (2.2-15)$$

where f is the frequency, μ is the magnetic permeability, and σ is the electric conductivity of materials. The lowest skin depth value is 30mm (for blood plasma and 100MHz), which is significantly higher than the characteristic size of analysed object (normally finger, or ear). Therefore there is no eddy current effect presented in all related problems.

Time-harmonic fields

When field quantities in Maxwell's equations are harmonically oscillating functions with a single frequency, the field is referred to as time-harmonic. Using the complex phasor notation [62], (2.2-1), (2.2-2), and (2.2-5) can be written in a simplified form as

$$\nabla \times \mathbf{E} = -j\omega\mathbf{B} \quad (2.2-16)$$

$$\nabla \times \mathbf{H} = j\omega\mathbf{D} + \mathbf{J} \quad (2.2-17)$$

$$\nabla \cdot \mathbf{J} = j\omega\rho \quad (2.2-18)$$

where the time convention $e^{j\omega t}$ is used and suppressed and ω is angular frequency. It is evident that in this case, the electric and magnetic fields must exist simultaneously and they interact with each other, and it is also evident that the static case is the limiting case of the harmonic fields as the frequency ω approaches zero. The use of time-harmonic fields is not as restrictive as it first appears. Using Fourier analysis, any time-varying field can be expressed in terms of time-harmonic components via the Fourier transforms

$$\mathbf{E}(t) = \int_{-\infty}^{+\infty} \mathbf{E}(\omega)e^{j\omega t}d\omega \quad (2.2-19)$$

$$\mathbf{E}(\omega) = \frac{1}{2\pi} \int_{-\infty}^{+\infty} \mathbf{E}(t)e^{-j\omega t}dt \quad (2.2-20)$$

Therefore, if a time-harmonic field is known for any ω , its counterpart in the time domain can be obtained by evaluating (2.2-19).

The Quasistatic Approximation

A consequence of Maxwell's equations is that changes in time of currents and charges are not synchronized with changes of the electromagnetic fields. The changes of the fields are always delayed relative to the changes of the sources, reflecting the finite speed of propagation of electromagnetic waves. Under the assumption that you can ignore this effect, it is possible to obtain the electromagnetic fields by considering stationary currents at every instant. This is called the *quasistatic approximation* and is usually used in impedance tomography [63], [64].

The quasistatic approximation implies that the equation of continuity can be written as

$$\nabla \cdot \mathbf{J} = 0 \quad (2.2-21)$$

and that the time derivative of the electric displacement $\partial \mathbf{D} / \partial t$ can be disregarded in Maxwell-Ampère's law. Whereas Faraday's law remains unchanged.

In application to time-harmonic problem, the system of equations becomes

$$\nabla \times \mathbf{E} = -j\omega \mathbf{B} \quad (2.2-22)$$

$$\nabla \times \mathbf{H} = \mathbf{J} \quad (2.2-23)$$

$$\nabla \cdot \mathbf{J} = 0 \quad (2.2-24)$$

The quasi-static approximation is to assume that

$$\omega \mathbf{B} = \omega \mu \mathbf{H} \quad (2.2-25)$$

is negligible, so that

$$\nabla \times \mathbf{E} = 0 \quad (2.2-26)$$

2.2.5 Potentials

The Finite element method works with potential distribution. That means there is a need for formulation of an electromagnetic problem in terms of the *electric scalar potential* V and the *magnetic vector potential* \mathbf{A} .

$$\mathbf{B} = \nabla \times \mathbf{A} \quad (2.2-27)$$

$$\mathbf{E} = -\nabla V - \frac{\partial \mathbf{A}}{\partial t} \quad (2.2-28)$$

The magnetic vector potential equation comes from the magnetic Gauss' law (2.2-3). The electric potential one is a result of Faraday's law (2.2-2). The general Maxwell equations for each specific case can be simplified to the domain equations combined with boundary conditions equations. Let us specify the domain equations for the cases which are used throughout this thesis.

In static formulations, the induced current is zero. Maxwell-Faraday's law reduces to Laplace's equation [63]

$$\nabla^2 \varphi = 0 \tag{2.2-29}$$

For time-harmonic quasi-static systems solving for scalar potential, the formulation results in the following PDE obtained from (2.2-22), (2.2-23), and (2.2-24) with the substitution of (2.2-28):

$$-\nabla \cdot (\epsilon \nabla V) + \frac{j}{\omega} \nabla \cdot (\sigma \nabla V) = 0 \tag{2.2-30}$$

which is normally solved with respect to electric scalar potential V by application of variational principle and spatial discretization. In this work, this equation is solved via Finite Element Method described below under assumptions also listed below.

EM field assumptions:

- Built model is linear (as none of the domain properties depend on field).
- Material properties are isotropic as electrical properties of cholesterol, plasma and red blood cells (RBC) are independent of direction.
- Permeability μ is set being constant and equal to this of vacuum. It is quite a common assumption for modelling of biological tissues [65], [66] as we consider no magnetic effects influencing impedance are presented in biological tissues under study.
- The material properties are piecewise-homogeneous as there are cholesterol particles and RBC in blood plasma, material properties in domains are different.
- The total volume of cholesterol is modelled as a number of spherical particles of relevant radius (calculated below) giving the same total volume. Further assumptions for modelling of cholesterol particles are given in the next Chapter.

- RBC are modelled as cylinders; radius to height ratio is taken from experimental data [67].

Following the numerical solution of the field equation, the current density is calculated by using the following equation

$$\mathbf{J} = \sigma \mathbf{E} = -\sigma \nabla V \quad (2.2-31)$$

2.2.6 Material Properties

Until now, there has only been a formal introduction of the constitutive relations. These seemingly simple relations can give rise to complicated behaviour at times. There are three main groups of materials where they require some consideration. A given material can belong to one or more of these groups. The groups are:

- Homogeneous and inhomogeneous materials
- Isotropic and anisotropic materials
- Linear and nonlinear materials

The least complicated of the groups above is that of the inhomogeneous materials. An inhomogeneous medium is one where the constitutive parameters vary with the space coordinates, so that different field properties prevail at different parts of the material structure.

For anisotropic materials, the field relations at any point are different for different directions of propagation. This means that a 3-by-3 tensor is required to properly define the constitutive relations. If this tensor is symmetric, the material is often referred to as *reciprocal*. In these cases, the coordinate system can be rotated in such a way that a diagonal matrix is obtained. If two of the diagonal entries are equal, the material is *uniaxially anisotropic*. If none of the

elements have the same value, the material is *biaxially anisotropic* [68]. An example where anisotropic parameters are used is the conductivity when modelling solenoids.

Nonlinearity is the effect of variations in permittivity or permeability with the intensity of the electromagnetic field. This also includes hysteresis effects, where not only the current field intensities influence the physical properties of the material, but also the history of the field distribution.

Finally, dispersion describes changes in the velocity of the wave with wavelength. In the frequency domain, dispersion is expressed by frequency dependence in the constitutive laws.

As for our system it has been considered inhomogeneous (heterogeneous), isotropic and linear (see Chapter Model Assumptions).

2.2.7 Boundary and Interface Conditions

To get a full description of an electromagnetics problem, boundary conditions at material interfaces and physical boundaries are needed. At interfaces between two media, the boundary conditions can be expressed mathematically as

$$\mathbf{n}_2 \times (\mathbf{E}_1 - \mathbf{E}_2) = \mathbf{0} \quad (2.2-32)$$

$$\mathbf{n}_2 \cdot (\mathbf{D}_1 - \mathbf{D}_2) = \rho_s \quad (2.2-33)$$

$$\mathbf{n}_2 \times (\mathbf{H}_1 - \mathbf{H}_2) = \mathbf{J}_s \quad (2.2-34)$$

$$\mathbf{n}_2 \cdot (\mathbf{B}_1 - \mathbf{B}_2) = 0 \quad (2.2-35)$$

where ρ_s and \mathbf{J}_s denote *surface charge density* and *surface current density*, respectively, and \mathbf{n}_2 is the outward normal from medium 2. Of these four conditions, only two are independent. One of the first and the fourth equations,

together with one of the second and third equations, form a set of two independent conditions.

A consequence of the above is the interface condition for the current density,

$$\mathbf{n}_2 \cdot (\mathbf{J}_1 - \mathbf{J}_2) = -\frac{\partial \rho_s}{\partial t} \quad (2.2-36)$$

In case of our bioimpedance studies boundary conditions on the interface are:

$$E_{1\tau} = E_{2\tau} \quad (2.2-37)$$

$$D_{1n} = D_{2n} \quad (2.2-38)$$

$$\varepsilon_1 E_{1n} = \varepsilon_2 E_{2n} \quad (2.2-39)$$

We assume that a homogeneous electric field E is applied along the z -axis.

When conductors are involved, the source term representing charge density vanishes and it is replaced by boundary conditions of the Dirichlet type, modelling a constant-voltage surface (perpendicular to the electric field).

2.2.8 Impedance

The impedance technique has been successfully used in many areas (industry, chemical production, pharmacy, medicine, biosciences) and it has allowed to create reliable qualitative tools for imaging (EIT, ERT) [6], [64], [69] and for quantitative analyses (BMI, fuel purity, food quality, impedance spectroscopy) [65], [70]–[78].

Bioimpedance is something that deals with passive electrical properties of bio-tissues, it shows tissue ability to oppose (impede) electric current. The biological tissues can be seen as a volume conductor or a dielectric. With frequencies lower than 100 kHz most of the tissues are assumed being electrolytic conductors. At higher frequencies (e.g. 50 MHz), the dielectric

properties of bio-tissue may dominate. The higher the frequency the closer tissue properties come to those of water [65], [79]. The impedance of blood is purely resistive for the range of frequencies up to 100 kHz [80].

Impedance is a ratio between voltage and current. The following equation can be used in both direct and alternating current cases:

$$Z = \frac{V}{I} \quad (2.2-40)$$

Although it is a very simple ratio, it cannot be calculated analytically for most of the biological systems. So for both direct current and alternating current it is more important to link these quantities with properties of materials.

Direct current case (DC)

When the direct current is applied the impedance of our system contains only resistivity and can be calculated using following equations:

$$R = \frac{V}{I} = \frac{El}{\sigma ES} = \frac{l}{\sigma S} \quad (2.2-41)$$

where l is current path length, σ – material conductivity, S – cross-section.

This is valid only for a situation when no particles are present in between electrodes and the full volume is filled with blood plasma and it is also being assumed a homogeneous and isotropic medium (current density and E-field directions are coinciding) [65] .

In case of particles being present in the solution the system can be modelled as a superposition of series and parallel resistances and the effective impedance will be calculated using well-known equations. Some of the extreme cases are being looked at in Chapter 4.

Alternating current case (AC)

In case of alternating current the impedance will consist of two parts:

$$Z = \frac{V}{I} \tag{2.2-42}$$

$$Z = R + jX \tag{2.2-43}$$

$$X = \omega L - \frac{1}{\omega C} \tag{2.2-44}$$

$$Z = R + \frac{1}{j\omega C} \tag{2.2-45}$$

As we do not consider blood components to have inductance it can be seen from (2.2-43) that at high frequencies impedance becomes purely resistive. If properties of the medium are known than (2.2-45) can be evaluated into intrinsic impedance of the conductive medium[46]:

$$Z_0 = \sqrt{\frac{j\omega\mu}{\sigma + j\omega\epsilon}} \tag{2.2-46}$$

It is more convenient to work with tissue properties, such as conductivity, permittivity and permeability rather than with resistance, capacitance and inductance. Replacing J in (2.2-1) with (2.2-31), will get [62]:

$$\nabla \times \mathbf{H} = \sigma\mathbf{E} + \frac{\partial \mathbf{D}}{\partial t} \tag{2.2-47}$$

In case of current flowing in x direction:

$$-\frac{\partial H_z}{\partial x} = \sigma E_y + j\omega\epsilon E_y \quad (2.2-48)$$

According to the ratio

$$\frac{\sigma}{\omega\epsilon} \quad (2.2-49)$$

media can be classified as being a conductor or a dielectric ($\omega = 2\pi f$, radian frequency) [62].

Dielectrics:	$\frac{\sigma}{\omega\epsilon} < \frac{1}{100}$
Quasiconductors:	$\frac{1}{100} < \frac{\sigma}{\omega\epsilon} < 100$
Conductors:	$100 < \frac{\sigma}{\omega\epsilon}$

Calculations of (2.2-49) ratio for biological tissues are presented in the next chapter.

2.3 Finite Element Modelling

2.3.1 Finite element basics

In a case of homogeneous or composite materials for a known set of excitation parameters and material properties any problem can be solved in terms of

current or electrical field distribution using Maxwell's equations. There are only two types of problems that are solved in differential equation, boundary value or initial value problems. If the values of the unknown parameter is given at a point (e.g. at particular time) and the task is to find values for all other time points, it is called initial value problem. When parameter values are given on the material boundaries and the values on the inside are to be found, this is called a boundary value problem. For most bioimpedance problems boundary value problems are solved (e.g. known current or voltage drop on electrodes and unknown field distribution within the volume of interest).

Maxwell's equations in their differential form describe behaviour of our system. The problem is that this way they describe an infinite-dimensional object. To overcome this issue, finite-dimensional approximation must be used. It can be done by means of two main approximations: finite difference or finite element method. The core of finite difference method is replacement of the differential equations (DE), describing the continuous change of parameter values, with approximations that describe the slope of change between the finite number of discrete points (mesh points). For FEM it is division of the domains into smaller volumes - elements and expression of unknown solutions in the form of the weighted sum of basis functions, which are polynomials in each element [65].

The main function of the finite element method is to proceed from the form of DE to a system of joint equations, which can be solved by a computer. That is made by minimization of energy functional. Non-linear equations are then linearized using different methods (that depends on software). The set of solution is then connected directly or by means of simple computations to unknown quantities of interest.

The first step in finite element analysis is a creation of mathematical FE model, which geometrically represents the physical structures under investigation. The starting point for the finite element method is a mesh, a partition of the geometry into small units of a simple shape, mesh elements, and then the values of the

unknown variables under study are calculated in selected points of those elements. These points are called “nodes”. Division of the body into elements is called discretisation and the whole solution of the problem depends on the way it is made. As build mathematical model represents the actual physical one, the actual physical properties should be assigned to model parts that are ‘made’ of that material.

The idea of the method is described in detail in [81]. According to the mathematical formulation, the considered unknown field variable u in the equation like (2.2-29) and (2.2-30) can be approximated throughout a set of functions χ_i . Each of these functions has simple structure and most commonly it is the polynomial function of second order. Subdividing the entire space Ω onto the number of simple volumes, it is possible to calculate the distribution of the unknown in the space and approximate each volume as a uniform subspace which has the internal distribution of unknown as χ_i . Considering the shearing boundary conditions of two neighbour elements and providing the conditions for external surface, the linear system of equations could be written and then solved. More formally, in the simple case for 3D problem we can write an equation for our unknown u :

$$u(x, y, z) = \sum_{k=1}^N u_k \chi_k(x, y, z) \quad (2.3-1)$$

For the external loading function $f(x, y, z)$ we achieve the same structure as:

$$f(x, y, z) = \sum_{k=1}^N f_k \chi_k(x, y, z) \quad (2.3-2)$$

Then, using substitution for our first order differential problem we have the following system of linear first order equations:

$$-\sum_{k=1}^N u_k \int_{\Omega} \nabla \chi_k \cdot \nabla \chi_j dV = \sum_{k=1}^N f_k \int_{\Omega} \chi_k \chi_j dV \quad (2.3-3)$$

for $j = 1, \dots, N$

Using the matrix-vector form we obtain:

$$-\mathbf{L}\mathbf{u} = \mathbf{M}\mathbf{f} \quad (2.3-4)$$

where matrixes \mathbf{L} and \mathbf{M} are calculated from the equation (2.3-3):

$$L_{kj} = \int_{\Omega} \nabla \chi_k \cdot \nabla \chi_j dV$$

$$M_{kj} = \int_{\Omega} \chi_k \chi_j dV \quad (2.3-5)$$

for $j, k = 1, \dots, N$

Considering the electromagnetic quasistatic simulations (\mathbf{f} is constant and fully determined), the problem can be described in following form in terms of unknown magnetic potential $\varphi(x, y, z)$:

$$\mathbf{K}\varphi = \mathbf{S} \quad (2.3-6)$$

Where \mathbf{K} and \mathbf{S} are the coefficient matrix and boundary condition vector respectively [82].

2.3.2 FEM application to impedance of conductive suspension

If a potential distribution φ on the electrodes is known (Figure 4.1–2, Figure 5.1–2) then the electric field distribution between these electrodes in the 2D ($\Omega(x,y)$) or 3D ($\Omega(x,y,z)$) problem domains is given by equation (2.2-29) and is solved by means of finite element method (FEM) in Ω . It is solved in terms of potential φ with appropriate boundary conditions and using conductivity (σ) and permittivity (ε) values distribution for problem domain Ω . It is all done under assumptions summed up in 2.2.5 and 2.2.6. Following the solution of equation (2.2-29), field intensity and flux density vectors $\mathbf{E} = -\text{grad}V$ (V is the potential difference) and $\mathbf{D} = \varepsilon\mathbf{E}$ are calculated. From these the current $\mathbf{I} = \mathbf{J}A$ (A is the cross-sectional area) is calculated using current density (2.2-31).

In COMSOL [83] the set of equations is solved using generalized minimum residual (GMRES) method described in [84]. This is an iterative method for general linear systems of the form $\mathbf{Ax} = \mathbf{b}$. For fast convergence it is important to use an appropriate preconditioner, which conditions a given problem into a form that is more suitable for numerical solution. This means that the condition number decreases and changes the problem from ill-conditioned to well-conditioned. GMRES method uses the left preconditioned system:

$$\mathbf{P}^{-1}(\mathbf{Ax} - \mathbf{b}) = 0 \quad (2.3-7)$$

which gives the same solution as the original system so long as the preconditioner matrix \mathbf{P} is non-singular.

The goal of this preconditioned system is to reduce the condition number of the left preconditioned system matrix $\mathbf{P}^{-1}\mathbf{A}$.

There is a trade-off in the choice of \mathbf{P} . Since the operator \mathbf{P}^{-1} must be applied at each step of the iterative linear solver, it should have a small cost (computing time) of applying the \mathbf{P}^{-1} operation. \mathbf{P} is usually chosen as somewhere between $\mathbf{P}=\mathbf{I}$ and $\mathbf{P}=\mathbf{A}$, in an attempt to achieve a minimal number of linear iterations while keeping the operator \mathbf{P}^{-1} as simple as possible.

Each element calculation introduces a small error to the overall solution, but ideally it is supposed to diminish as a number of nodes and respectively elements increases. However in a case of ill-posed problem there is no certainty that the overall sum of diminishing errors will not have a large impact on overall solution. This is why several verifications are supposed to be used for every computational model. This included mesh convergence study and test with simple analytical solution, where possible.

When an iterative solver in COMSOL Multiphysics is used, it estimates the error of the solution while solving. Once the error estimate is small enough, as determined by the convergence criterion

$$\rho|\mathbf{P}^{-1}(\mathbf{Ax} - \mathbf{b})| < tol \cdot |\mathbf{P}^{-1}\mathbf{b}|, \quad (2.3-8)$$

the software terminates the computations and returns a solution. When a direct solver COMSOL Multiphysics is used it can optionally make a check (**Error check**), to determine if the above convergence criterion is fulfilled after the solution step. If the error criterion is not met, the solution process is stopped an error message is given. In (2.3-8) \mathbf{P} is a preconditioner matrix. The convergence criterion (2.3-8) states that the iterations terminate when the relative (preconditioned) residual times the factor ρ called stability constant is less than

a tolerance tol . The factor ρ in the **Factor in error estimate** field (default = 400). For solvers where \mathbf{P} is equal to the identity matrix, the iterations can sometimes terminate too early with an incorrect solution if the system matrix \mathbf{A} is ill-conditioned. For solvers where \mathbf{P} is not equal to the identity matrix, the iterations can sometimes terminate too early if \mathbf{P} is a poor preconditioner. If the iterations terminate too early due to an ill-conditioned system matrix or a poor preconditioner, the ρ factor should be increased to a number of the order of the condition number for the matrix $\mathbf{P}^{-1}\mathbf{A}$. If ρ is greater than the condition number for the matrix $\mathbf{P}^{-1}\mathbf{A}$, the convergence criterion implies that the relative error is less than tol :

$$|x - \mathbf{A}^{-1}\mathbf{b}| < tol \cdot |\mathbf{A}^{-1}\mathbf{b}| \quad (2.3-9)$$

In general larger value of ρ increases the number of iterations, but decrease the chance that the iteration is terminated too early [83].

In the presented COMSOL solution, accuracy due to discretization was controlled by the relative tolerance value. For all of the simulations it has been kept at a value of 0.001, which sets estimated error maximum at 0.1%. Once the error estimate is small enough the software terminates the computations and returns a solution. If the error criterion is not met, the solution process is stopped and an error message is given. The real global error $LinErr$ can be found from convergence graph that is plotted along the solution or in custom generated report file.

Chapter 3. Realisation of Finite Element Model of Non-invasive Cholesterol Measurement System

3.1 Introduction

Mathematical model is a representation of a real system made using mathematical concepts and language. For that, several assumptions have to be made. The first step is to select the area of the body where electrodes are going to be placed.

Blood for cholesterol tests is withdrawn from the vein, usually on left arm. So it is suggested that a vein model should be built. But as the method is non-invasive this means that electrodes are placed at the skin surface, the simplest model will involve arm modelling. On the other hand, it highlights several problems. The most important is the electrode positioning and placement. It is necessary to look at all possible situations to find the most suitable for modelling.

If the arm is chosen as a place for electrodes: it gives a choice of number of electrodes to be used. Due to some effects stated in [65] (e.g. arising complexity of field distribution and interference) the best system for our purpose is a 2-electrode system. Two positions for electrodes are possible: on the same side of the arm along the vein or on opposite sides. In the first case it is hard to predict the path current will take and the portion of current that will reach the electrode. In the second case, again current path is not easy to predict, it also raises such problems as eddy-current, and complexity of the mathematical model, representing skin-vein-bone-skin system.

Taking all of that into account the other place of interest was picked: the earlobe. It does not have a bone inside; its average thickness is less than skin-depth for frequency ranging from 1Hz up to 100 MHz. There are several assumptions that are to be made to reduce the complexity of the system for modelling purposes. First, is capillary blood content the same as venous? It has been proven in [85], [86] that there is no significant difference between samples taken from vein and finger-tip, which means that ear capillaries are suitable for modelling and representing total cholesterol measurement system. Electrodes are placed on opposite sides of earlobe. Two electrodes system also helps to eliminate (or at least reduce) the effect of parasitic capacitances in setup in the frequency range over 12 kHz up to 100 MHz [65], [87].

3.2 Model of non-invasive measurement of cholesterol

So earlobe has been selected as a most suitable place for performing non-invasive impedance cholesterol measurements.

Capillary fulfil the whole volume of earlobe this gives a possibility to model the earlobe as a volume filled with blood. Average earlobe thickness has been selected equal to 5 mm.

Earlobe size varies, so the electrodes should be selected to suit all people. This led to electrode size being selected at 5mm. The next step is to choose electrode material.

There is a whole variety of materials used for electrode production: silver-silver chloride, platinum metals, gold, titanium, stainless steel, tin, lead, nickel, silver, zinc, iron, aluminium, carbon, polymers. And even though some of them are not biocompatible and some are noisy or polarizable, it still leaves us with a lot of choice. As no choice has been made and no particular electrode material has been selected, a decision has been made to model electrodes as two hollows. It also allows overcoming problem of some software to model metals, as for most

of existing programs the usage of real properties of metals will not lead to obtaining correct results. However there is a method of overcoming this issue by assigning metal domains a very high value for permittivity [88]. One of the test runs performed have shown that this technique does not work in COMSOL. Voltage values are put on all of the surfaces that 'build' the electrode. It is assumed that skin does not influence impedance of the system, which in practice means that there is a conductive gel in between electrode and skin surface that moisturizes skin, making its conductivity higher and takes care of the air gap between the electrode and the skin.

The last step is to decide what assumptions should be made for blood modelling. Human blood is a complex suspension that is composed of cells of different size and shape (red blood cells, platelets, etc.) distributed in an aqueous solution called the plasma, which means that in reality it is highly inhomogeneous material. But for modelling purposes spherical particles suspended in a solvent is a first iteration in building a blood model. Volume content is as following: 55 % of volume is blood plasma, 45 % are formed elements (blood cells). Blood plasma contains 91.5% of water and has lipids, salts, glucose, amino acids, vitamins, hormones, and waste products of metabolism presented in [67]. For simplification of the model it is proposed to investigate the impedance impact of pure cholesterol, excluding all the blood cells and other particles as a first iteration.

The electrical properties (e.g. electrical conductivity, σ and dielectric permittivity, ϵ) of whole blood are very different from those of blood plasma, which contains no cells [89], [90]. In addition, as the idea is to find how total cholesterol (TC) number is transformed into impedance signal. This means that usage of total blood characteristics is not correct in that case. Therefore, for the basic mathematical model blood has been modelled as a suspension, containing only blood plasma and cholesterol. As all the constituents of blood plasma are presented in small quantities it is displaced within the model with

0.9% physiological saline solution that is commonly used in blood transfusion because of being isotonic with blood plasma [91].

Finally yet importantly is a blood flow assumption. It is well known that frequency of a heart beat and therefore of blood pulsation leading to blood movement is about 1 Hz. In comparison with frequency of current (50 kHz) it is low enough to consider blood and hence blood particles stationary objects.

The next iteration is to calculate volume proportion of blood plasma occupied by cholesterol using TC level value. In most of the cases once the results of the blood tests come in, there is a number characterizing level of cholesterol presented in blood. In the UK the unit for cholesterol levels is mmol / L (millimoles per litre). But what does it mean if someone is told to aim for a total cholesterol level equal to 5 mmol/L?

The percentage of given volume occupied by cholesterol molecules using information on HDL and LDL is calculated (Appendix 1). It has been done in two different ways to ensure that results obtained with one methods correlate well with those calculated differently.

Clearly, it is not possible to model separate cholesterol molecules as firstly, they are too small in comparison with selected model size and secondly there are hardly any free cholesterol particles presented in blood stream. Moreover even single HDL or LDL particles are not modelled as their size is still too small and taking each and every of them into account would dramatically increase the time of solution. As it is going to be proven it is not necessary to model all of them. Cholesterol molecules will be joined into bigger particles, which are going to be modelled. This can be proven by the review of the ways biological tissues have been modelled in past decades.

An effective conductivity of dilute suspension in aqueous media of spherical particles (that do not have a permanent electric moment) has been derived by Maxwell [92]. First let us take a spherical particle of radius R and conductivity

σ_{part} and place it into a homogeneous solvent with conductivity σ_e and apply a uniform electric field E_0 (see Figure 3.2–1)

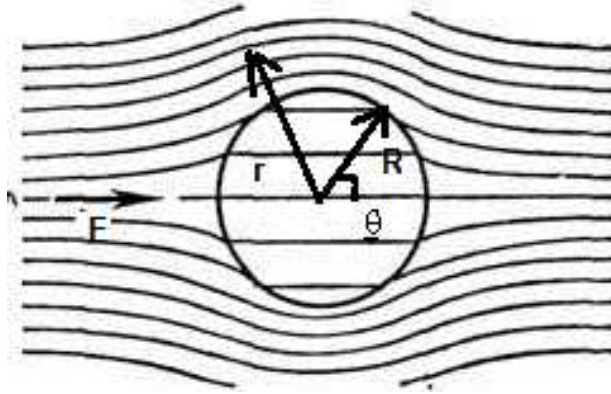


Figure 3.2–1. Particle in electric field, $\sigma_e > \sigma_{part}$

In case of our study the conductivity contrast is equal to 70 (Table 3.1).

Table 3.1. Material properties assigned to the domains of the problem

		Frequency	1 kHz	50 kHz	1 MHz	10 MHz	100 MHz
		Material					
σ , S/m	Blood base	1.76	1.76	1.9	2	2	
	Cholesterol	0.025	0.025	0.03	0.04	0.06	
	Whole blood	0.7	0.7	0.7	0.8	1	
ϵ_r	Blood base	10^6	79	0.001	0.0001	0.0001	
	Cholesterol	$2 \cdot 10^4$	10000	50	30	12	
	Whole blood	$4 \cdot 10^3$	$4 \cdot 10^3$	$2 \cdot 10^3$	100	40	

This table shows that blood plasma is a much better conductor than cholesterol particles. This contrast is a quality that is used in our research as a main instrument for cholesterol level measurement.

An equation for the potential outside the particle is found from the Laplace equation with the proper boundary conditions using spherical co-ordinates. The centre of coordinates (r, θ, ϕ) is in the middle of the sphere. In that case the potential is [93]:

$$V(r, \theta) = - \left(1 + \frac{\sigma_e - \sigma_{part} R^3}{2\sigma_e + \sigma_{part} r^3} \right) E_0 r \cos \theta \quad (3.2-1)$$

$$V(r, \theta) = - \left(1 + N \frac{\sigma_e - \sigma_{part} R^3}{2\sigma_e + \sigma_{part} r^3} \right) E_0 r \cos \theta \quad (3.2-2)$$

If we look at that model from macroscopic point of view, we see a spherical shaped medium with an aqueous solution of spherical particles inside it. A potential outside the big sphere is given by the expression (1.2-25), where σ_{part} is replaced by the effective conductivity and at a distance $r > R'$:

$$V(r, \theta) = - \left(1 + \frac{\sigma_e - \sigma_{eff} R'^3}{2\sigma_e + \sigma_{eff} r^3} \right) E_0 r \cos \theta \quad (3.2-3)$$

where σ_{eff} is the effective conductivity of a sphere that contains N particles.

Volume fraction occupied by particles:

$$p = NR^3/R'^3 \quad (3.2-4)$$

gives a possibility to find effective conductivity σ_{eff} from the Maxwell's mixture equation:

$$\frac{\sigma_e - \sigma_{eff}}{2\sigma_e + \sigma_{eff}} = p \frac{\sigma_e - \sigma_{part}}{2\sigma_e + \sigma_{part}} \quad (3.2-5)$$

As mentioned above biological cells have complex geometry, so the Maxwell's mixture equation has been modified for ellipsoidal particles that are orientated in parallel by Sillars [94]. When p is very low and the field is applied along the a -axis it gives:

$$\sigma_{eff} = \sigma_e \left[1 + \frac{p(\sigma_{part} - \sigma_e)}{\sigma_e + (2\sigma_{part} - \sigma_e)L_a} \right] \quad (3.2-6)$$

Where L_a is the depolarization factor of the ellipsoid in the a -axis direction [95]:

$$L_a = \frac{abc}{2} \int_0^\infty \frac{ds}{(a^2 + s)\sqrt{(a^2 + s)(b^2 + s)(c^2 + s)}} \quad (3.2-7)$$

$$L_a + L_b + L_c = 1 \quad (3.2-8)$$

Where a , b and c are the semi-axis of the ellipsoid. In case of spherical particles $a = b = c$ the depolarization factor $L_a = 1/3$ [96]. That gives:

$$\sigma_{eff} = \sigma_e \left[1 + \frac{3p(\sigma_{part} - \sigma_e)}{3\sigma_e + (2\sigma_{part} - \sigma_e)} \right] \quad (3.2-9)$$

These calculations show that blood plasma and cholesterol system can be represented by conductive solution with cholesterol particles combined into particles of relevant radius.

Taking into account the atherosclerotic plaque structure and suggestions made by Stiles and Oakley in [97] we can use those conductivity and permittivity values in our simulation. Material properties assigned to domains are presented in Table 3.1. There are several values for physiological saline (blood base) conductivity at the given frequency band ranging from 2 S/m [65] down to 1.4 S/m [98]. The decision has been made to take conductivity value that lies in between the two and has been found in [99]–[101].

Although real conductivity and permittivity values for various tissue vary significantly, Figure 3.2–2 shows typical curves for displacement and conduction components of the total current. In the used range of frequencies there is a visible domination of conduction current over displacement.

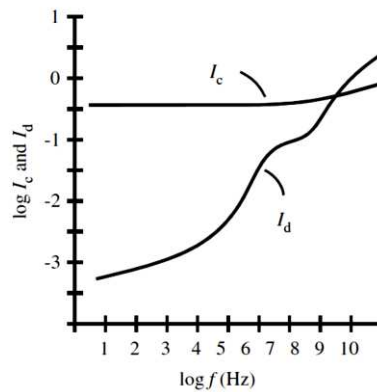


Figure 3.2–2. Conduction current I_c and displacement current I_d for a typical tissue [66]

A set of simulations have been performed to recreate some of the possible situations and investigate what parameters are putting an impact on impedance of system under study. Results are presented in next two chapters.

Chapter 4. Modelling of Non-invasive Cholesterol Measurement System in 2D

4.1 Building a 2D model

In 2D the basic model comprises of six air domains, three blood plasma domains and two hollow domains representing electrodes. The whole model measures 35×20 mm². This model is shown in Figure 4.1–1. The size of upper and lower blood-base domains is selected because in reality earlobe size is bigger than the size of an electrode and as distance between electrodes is comparable with their size we should consider that a fringe effect will have significant influence on impedance of the system. Manual 2D model set up file can be found in Appendix 2.

It is simply not possible to model separate cholesterol molecules. So, as it has been previously mentioned, the equivalent cholesterol volume has been calculated and the whole amount of cholesterol is divided into smaller particles for modelling purposes [102].

Knowing the total volume of cholesterol in 1 mm³ of blood plasma, we can calculate amount of cholesterol in the volume being modelled. In 2D area of interest is a square 5×5 mm². Now we can calculate the volume of cholesterol in blood plasma cube.

The volume occupied by cholesterol in 125 mm³ is:

$$V_{125mm^3} = V_{chol\ in\ 1\ mm^3} * V = 1.87 * 10^{-2} * 125 = 2.34\ mm^3 \quad (4.1-1)$$

If it is assumed that all the cholesterol particles form a sphere shape, then the radius of that sphere is:

$$r = \sqrt[3]{3 * V / (4 * \pi)} = \sqrt[3]{0.559} = 0.824 \text{ mm} \quad (4.1-2)$$

That means that area of the great circle (Riemannian circle) for that sphere is:

$$S = \pi * r^2 = 2.133 \text{ mm}^2 \quad (4.1-3)$$

The fraction will be:

$$\gamma_s = \frac{S}{S_0} = \frac{2.133 \text{ mm}^2}{25 \text{ mm}^2} = 0.085 \quad (4.1-4)$$

Therefore, this means that in the plane of great circle the cholesterol particle will take 8.5% of the whole volume of blood.

It is obvious that there will be dependence between number of particles that cholesterol is divided into and impedance of the system. To calculate radius of each particle we need, in case of 2D modelling, to divide the whole area by number of particles and then radius of one sphere will be equal to:

$$r_N = \sqrt{\frac{S}{N \cdot \pi}} \quad (4.1-5)$$

For greater feasibility, those N particles should be distributed randomly. It is being taken care of by introducing following method. The number of particles is divided so that it gives equal (where possible) number of rows and columns.

Therefore, it is a good idea to set N equal to the square of some number. Radius of one sphere is calculated. Then the whole area is divided into N small squares, a particle is set in the middle of each square and then using random number generator the particle is shifted from that position. As COMSOL can work with MathLab files as input, such file has been made to facilitate the model creation. An example of such file is presented in Appendix 4.

The random particle distribution realisation is presented in Figure 4.1–1. The algorithm of random particle generation is demonstrated in detail in Appendix 4.

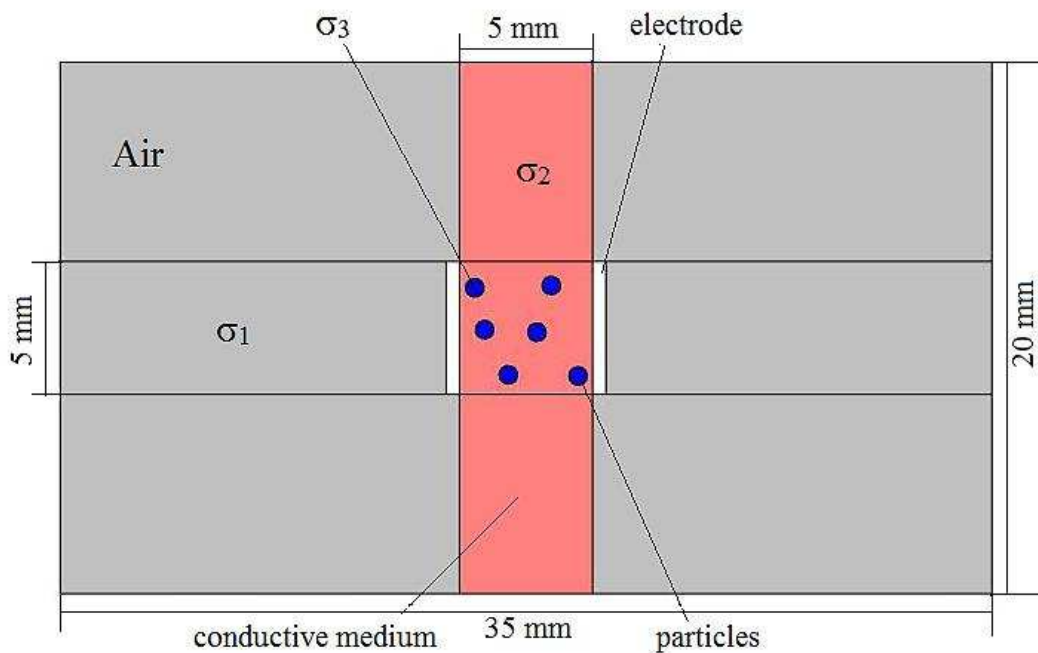


Figure 4.1–1. Coagulated cholesterol particles in blood plasma

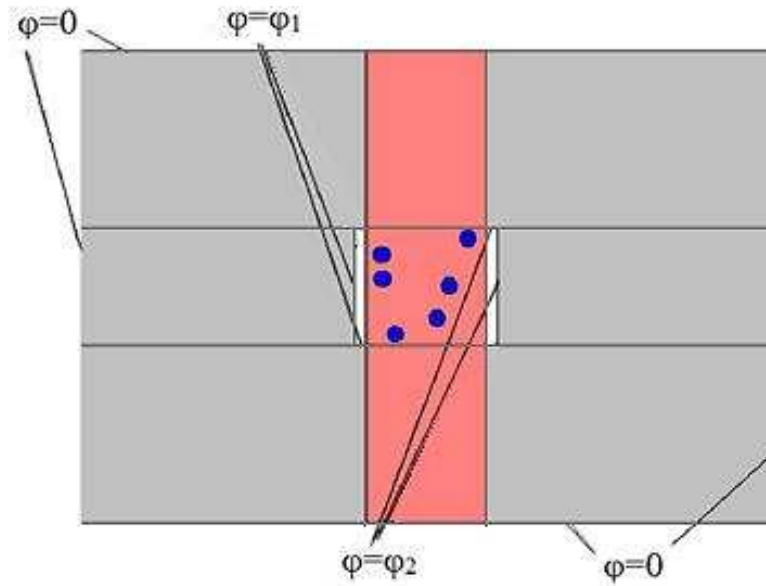


Figure 4.1–2. Boundary conditions

Outside geometry edges have ground as a boundary condition. Voltage is applied to all the boundaries surrounding hollows. Voltage values have been decided on using next set of assumptions: maximum current should not be more than 30 mA as it is an average pain threshold in human; voltage is divided in by two and applied symmetrically on both electrodes as this helps to simplify theoretical validation using field lines and voltage and current distribution graphs. We assume that current passing through is of 10mA and use whole blood conductivity to find relative voltage [65]. From that statement, voltage values can be calculated from set of simple equations:

$$I = \frac{V}{R} = \frac{\sigma SV}{l} \quad (4.1-6)$$

$$V = \frac{Il}{\sigma S} \quad (4.1-7)$$

This gives $V_{el} = \pm 1.428V$.

Boundary conditions are put on the outer edges (as in FE modelling all conditions inside the volume simulated are resolved automatically):

$$V = 0 \quad (4.1-8)$$

Mesh analysis was performed and its results are presented in 4.2. Fragment of custom mesh has been selected and the mesh of model with 100 particles in is displayed in Figure 4.1–3

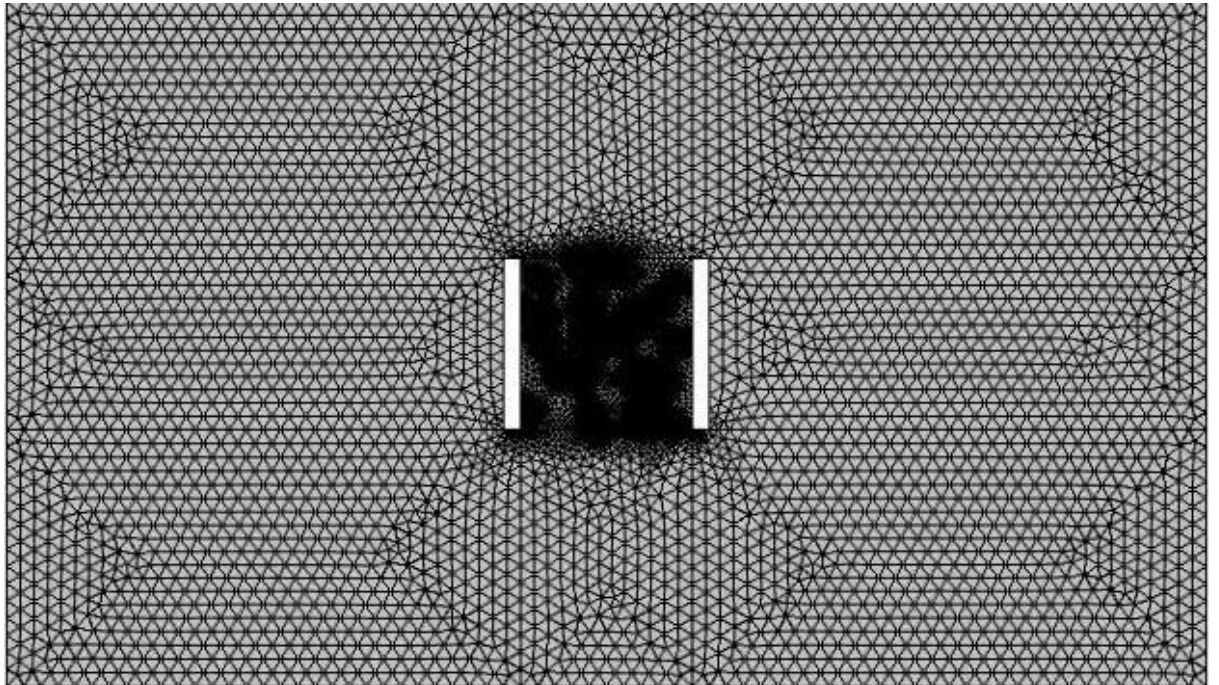


Figure 4.1–3. 2D custom mesh for 20 particles

A quantity that characterizes mesh in COMSOL is called mesh element quality and is calculated from:

$$q = \frac{4\sqrt{3}A}{h_1^2 + h_2^2 + h_3^2} \quad (4.1-9)$$

where A is area and h_1, h_2, h_3 – sidelights. Value of q lies between 0 and 1 and the closer it gets to 1 the closer element shape comes to an equilateral triangle. This criterion is stronger than used in most of the other software products. Everything above value of 0.3 is considered a good mesh, which means that the mesh quality does not affect the solution quality. Also extra care should be taken if any warnings come up regarding possible inverted elements, as this may significantly affect local solution. Our goal for 2D was to keep average element quality above 0.9 and minimum element quality above 0.3 [83]. Maximum element growth rate is 1.3, which means that difference in size between two adjacent elements cannot exceed 30 %.

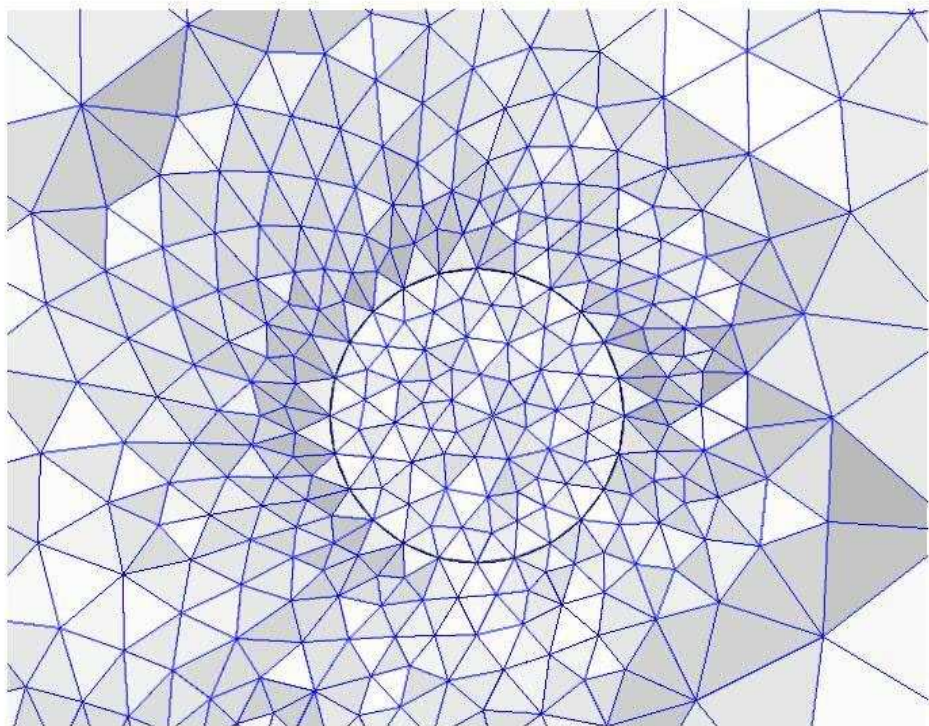


Figure 4.1–4. Custom mesh for 1 particle of coagulated cholesterol

4.2 Results and discussions on 2D Model

4.2.1 Mesh convergence study

As it was suggested in the previous Chapter, current values will vary according to the size of the particle selected. So it was suggested for the first simulation set to find dependence of current per unit length (as we are solving a 2D problem) from number of particles. In parallel for each step a mesh convergence study has been performed. The aim of that study is to find such optimal size of mesh elements that further decrease in element sizing will not make a difference in solution (the only difference will be time consumption).

None of the build-in meshes was considered appropriate and a custom made mesh has been created. The difference between 'good' and 'bad' mesh (its influence on solution) is shown on following Figures (Figure 4.2–2, Figure 4.2–3, Figure 4.2–4). The cut-line for those graphs is shown in Figure 4.2–1. The drop in current value on graphs shows cholesterol particles position, for example the square shaped one is a particle that is crossed by a cut-line right in the middle. From those graphs it is obvious that the fine mesh presented in Figure 4.2–4 gives smooth solution and further refinement will only lead to increase in computation time of the problem.

One of the mesh convergence study curves is shown below to describe the way the number of elements influences solution (Figure 4.2–5). This figure shows that after certain point ($N_e=6000$) curve comes to plateau and further refinement does not have any sufficient impact on quantity of interest. Resulting number of particles–electric field dependence has been traced and related curve can be seen in Figure 4.2–6.

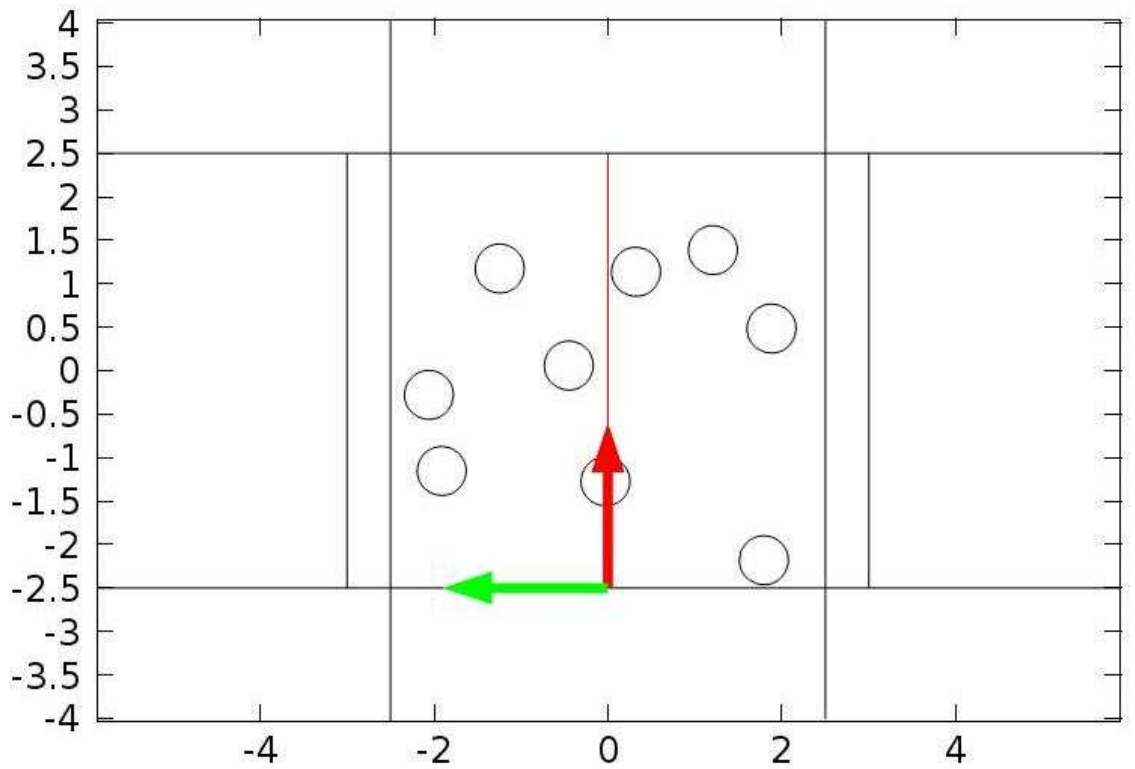


Figure 4.2–1. Cut-line for mesh convergence study

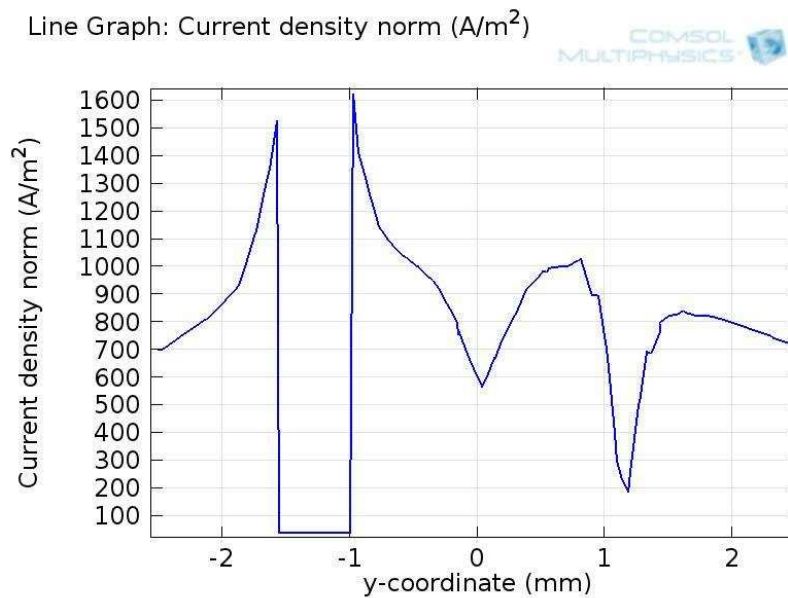


Figure 4.2–2. Electric field distribution for the coarse mesh ($N_{el}=1380$)

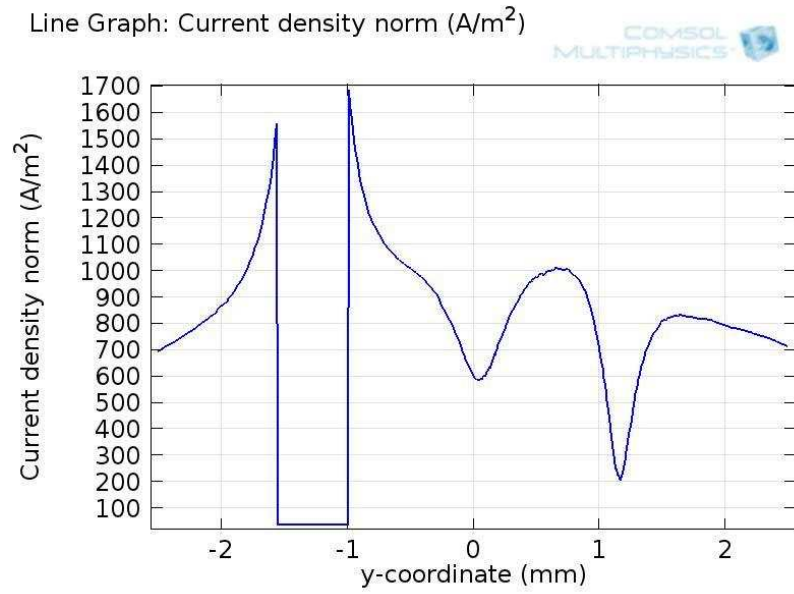


Figure 4.2–3. Electric field distribution for the less-course mesh ($N_{el}= 6875$)

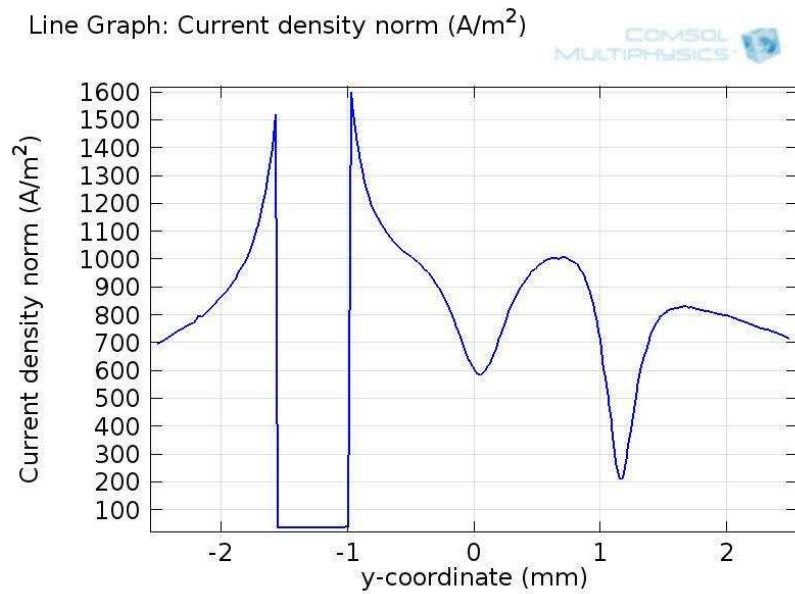


Figure 4.2–4. Electric field distribution for the fine mesh ($N_{el}=11857$)

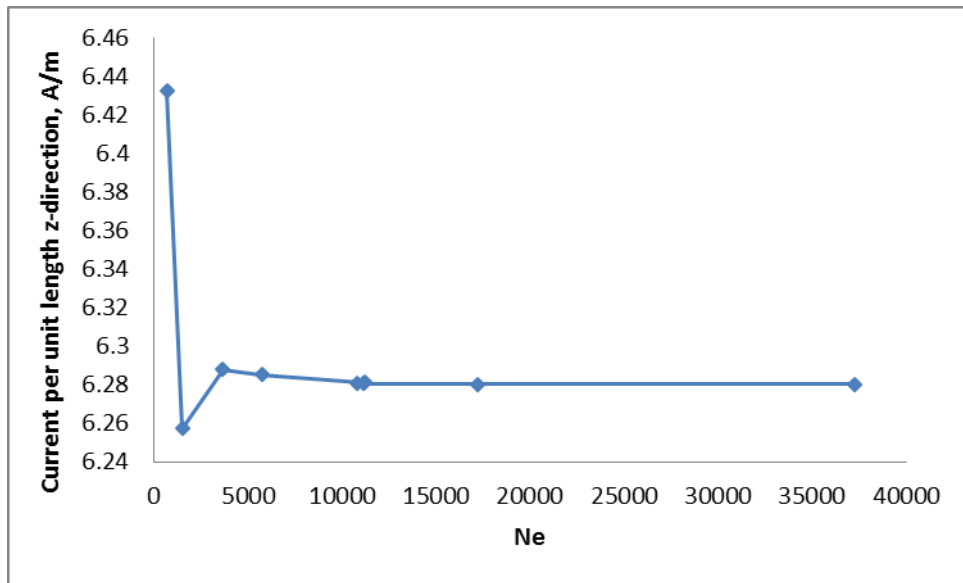


Figure 4.2-5. Mesh convergence study

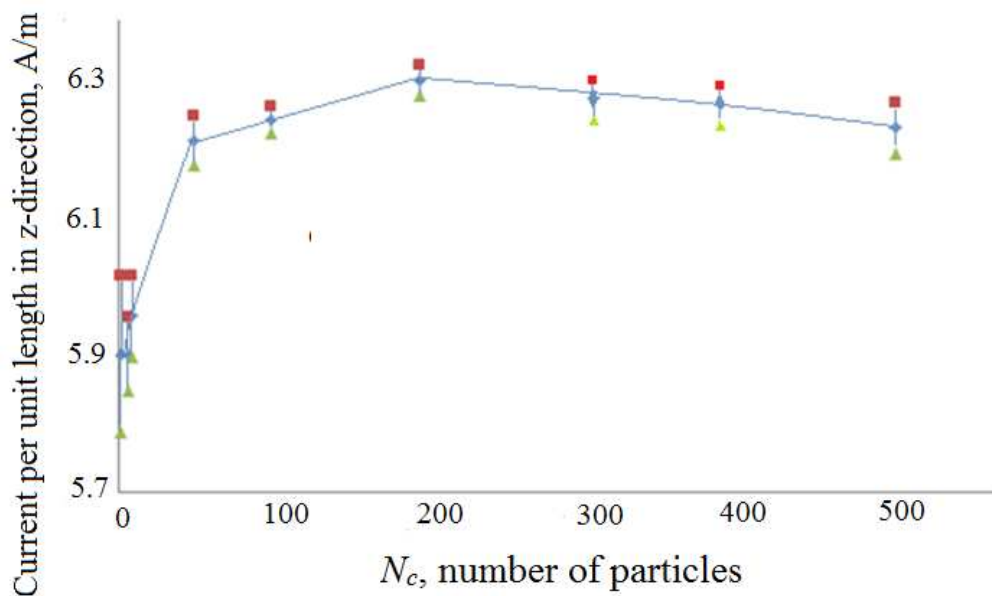


Figure 4.2-6. Variation of current per unit length with number of particles

As it was predicted, after reaching certain $N_{\text{particles}}$ curves reaches the plateau region and stops changing. That means that one of the assignments proves to be right and that cholesterol in such case can be modelled as separate particles being united in bigger particles without significant solution change. It also can

be noticed that the dispersion decreases when we increase number of elements. This is again something that is expected and is a basic property of FEM.

This graph gives a possibility to say that 100 particles in 2D case are enough to represent cholesterol particle distribution in blood plasma.

Even though DC analysis highlights difference in impedance for cholesterol-blood plasma system, once other particles are introduced to the suspension the only way to distinguish which particle type produced the impedance change is frequency analysis. So the next step is to perform frequency analysis of our model.

Frequency analysis has been performed for a fixed number of particles equal to 100.

4.2.2 Frequency analysis

Frequency analysis gives set of curves: with and without cholesterol (Figure 4.2–8). These results show that in case of our model the preferable frequency lies between 50 kHz and 100 MHz. That means that more factors should be taken into account. To choose the right frequency we should consider:

- The frequency of voltage/current should be higher than frequency of heart beat, so that we can ignore the movement of blood particles (and relevant magnetic field effects), which means that DC cannot be used.
- At high frequency (500-700 kHz - MHz-range) current will get through blood cells [65].

So taking all of those facts into account 50 kHz frequency has been selected. As it is also shown by several publications it is of the typical range for impedance measurements [103], [104] .

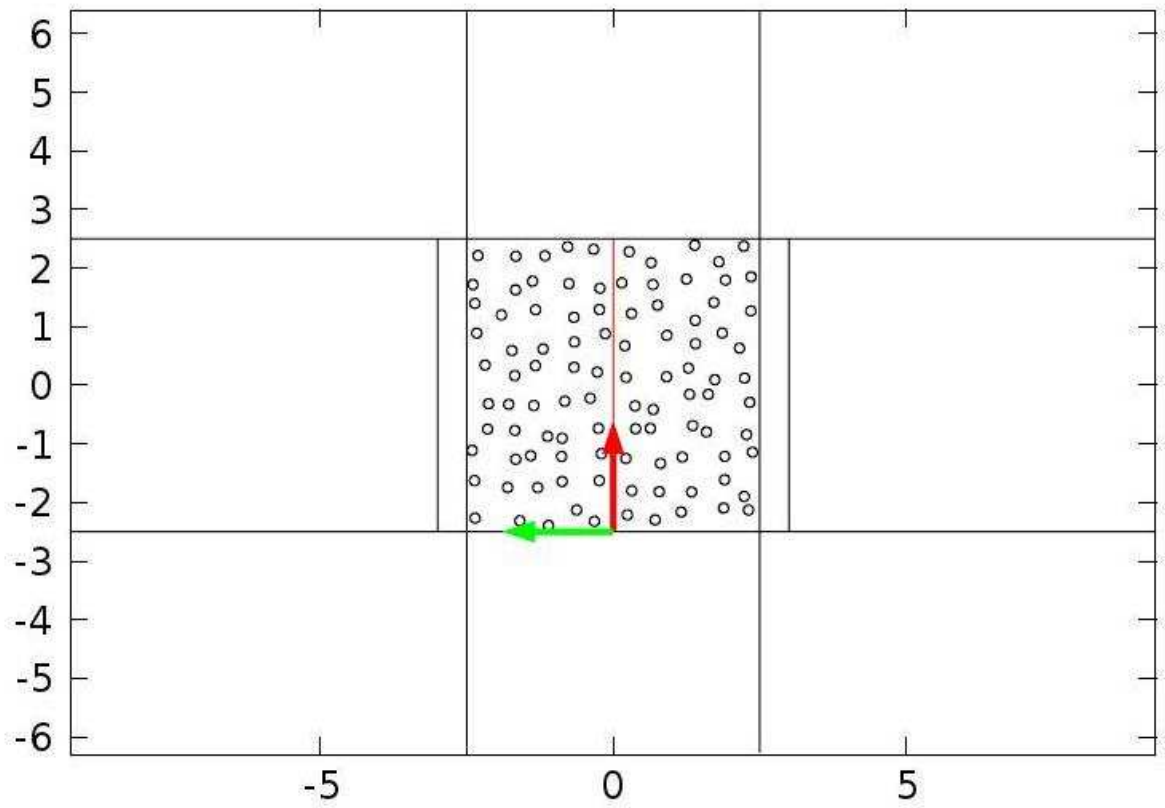


Figure 4.2–7. Cut-line for frequency analysis

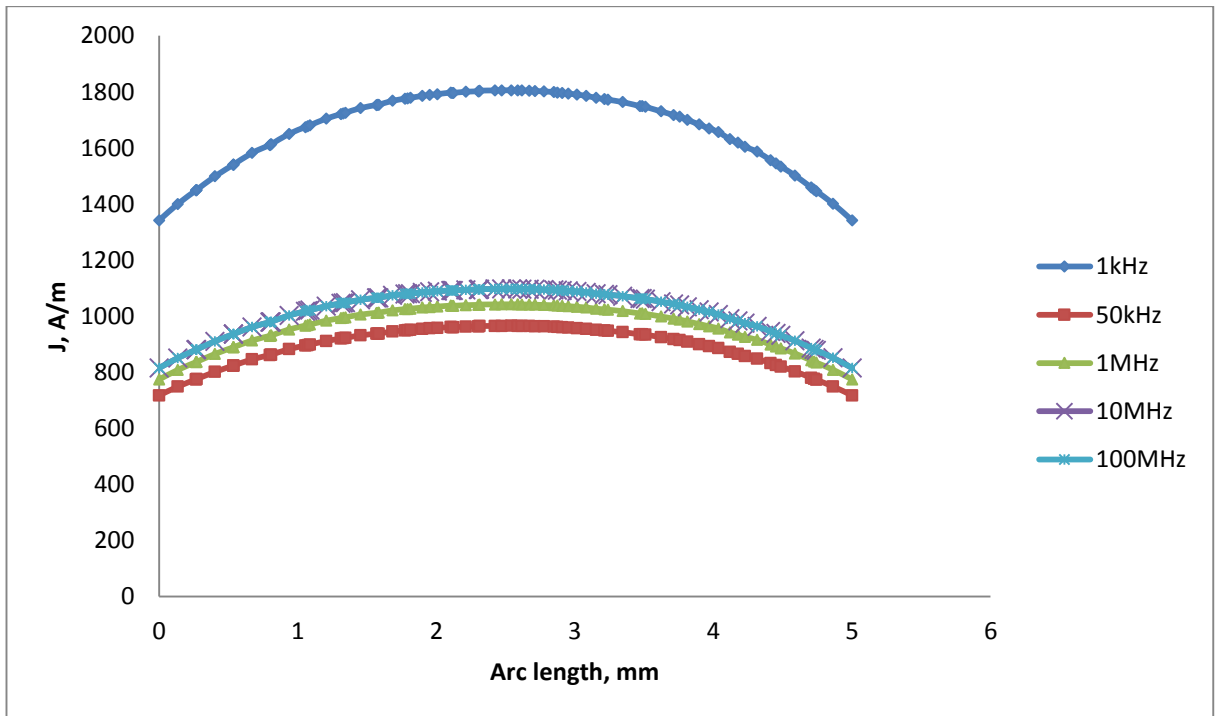
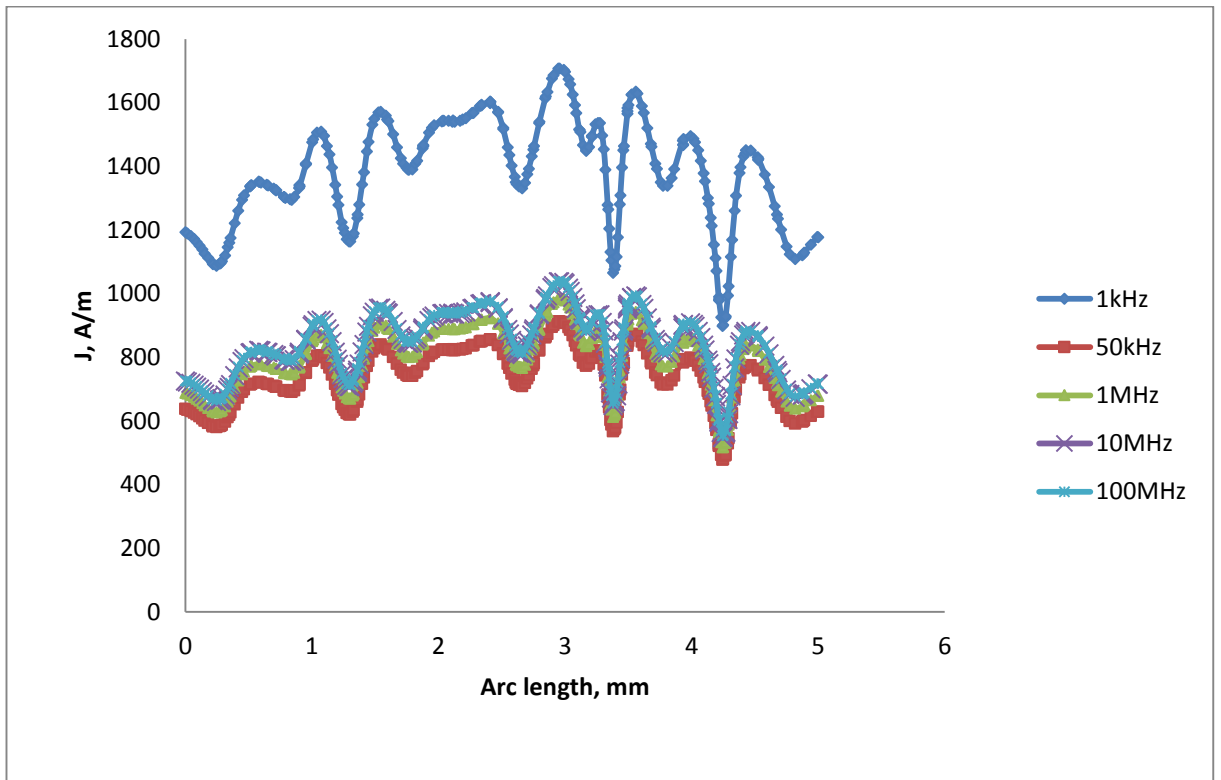


Figure 4.2–8. Current density along cut-line, area of interest filled with: a) plasma and coagulated cholesterol particles, b) plasma

The last effect to be checked for building a valid model is fringe field effects. There is a well-known effect that electric field of capacitor does not end abruptly at the edge of capacitor plates, but tend to bulge (extend) on both sides. The fringing can be taken care of by increasing the volume of the model in vertical direction, so that is why it has been extended by 7.5 cm at both ends from the volume of interest. The fringe field effect is illustrated in the figures below (Figure 4.2–9 and Figure 4.2–11).

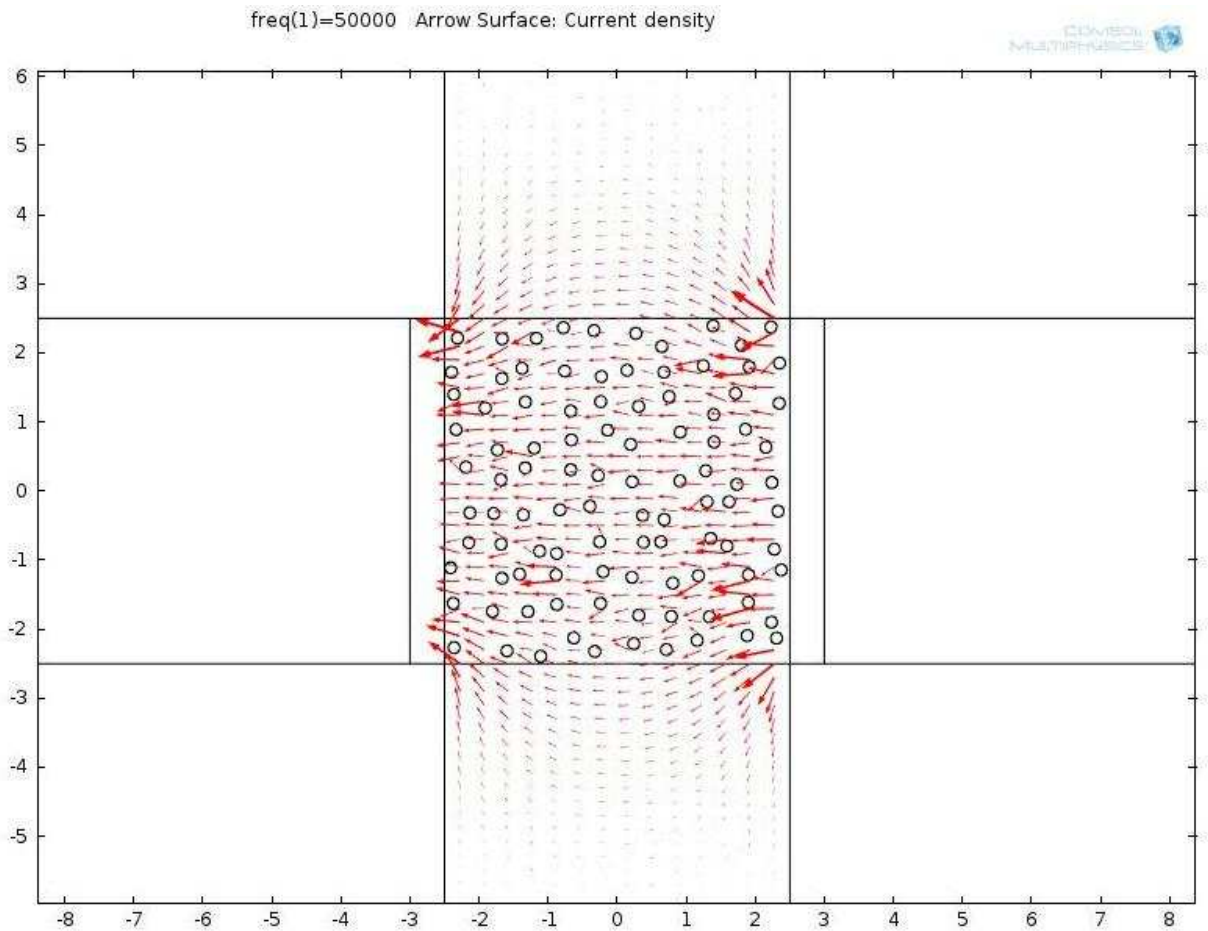


Figure 4.2–9. Vectors showing current density distribution for 100 particles

The other phenomenon that should be monitored closely is potential lines in regards to the boundary position. It is known that putting boundaries too close to the area of interest can lead to potential lines deformation, which would lead to

incorrect solution. Because of that geometry had to be extended both vertically and horizontally (Figure 4.2–10).

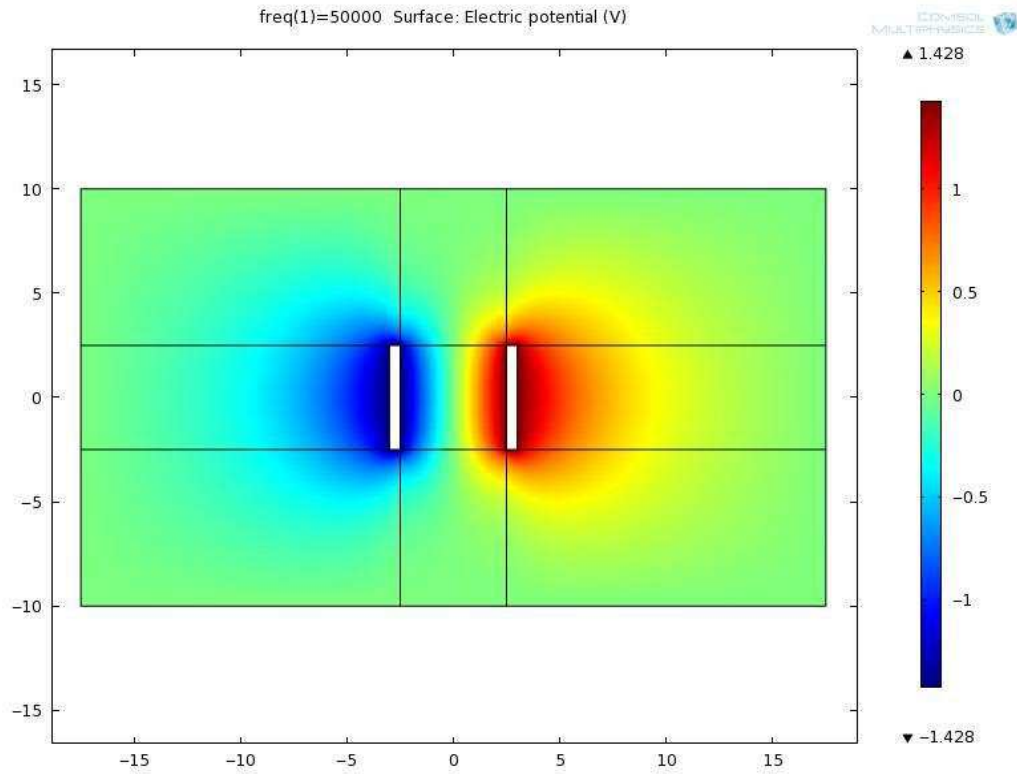


Figure 4.2–10. Electric potential plot showing the extension for correct electrical field calculation

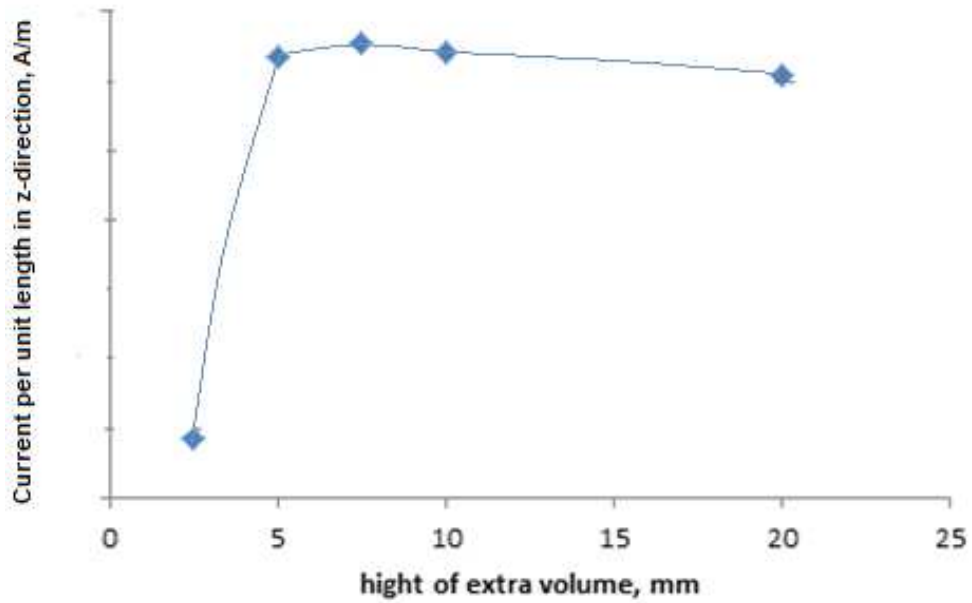


Figure 4.2-11. Extension of geometry in vertical direction

The positioning of particles can play a huge role in resulting current. Several extreme cases have been modelled. Some of them can be approximately simulated by the series or parallel impedances. Size of each particle has been calculated in such way that the line of particles blocks the whole volume. These studies and results are presented above in Figure 4.2-11. This study is linked with theoretical validation of the model below.

4.2.3 Analytical validation of 2D models

First step is to calculate current per unit length using model where only the volume between electrodes is filled with blood plasma, all the other domains are assigned air properties, no cholesterol presented. That way no current leaves the volume of interest, making it easier to calculate current per unit length using equation:

$$\frac{I}{d} = \frac{V\sigma b}{l} = 5.03 \text{ A/m} \quad (4.2-1)$$

COMSOL result is $\frac{I}{d} = 5.03 \text{ A/m}$. This shows that at this stage modelling agrees well with theoretical results.

We can also estimate fringe effect using current per unit length in z-direction along the cut-line going through the middle of geometry.

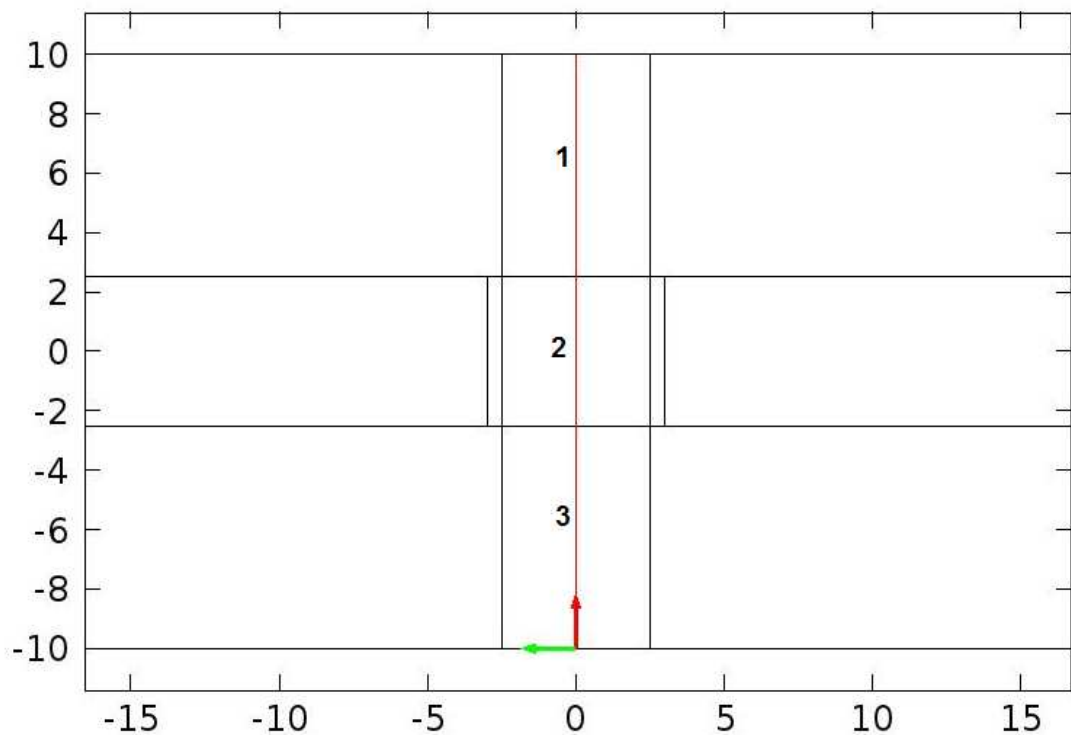


Figure 4.2–12. Positioning of the cut-line for estimation of fringe field effects

From data presented in Table 4.1 it can easily be seen that fringing gives about 40% of the total current. In reality, there is cholesterol present above and below the area of electrode placement, which will reduce the fringe effect, but it will also mean that somehow this cholesterol will affect impedance of our system.

However, for the moment we assume that major change in impedance is only due to the cholesterol present in the region of interest.

Table 4.1. Current per unit length in z-direction of electrode in corresponding conducting areas and total current per unit length in z-direction along the cut-line

Domain	Current per unit length in z-direction, A/m
1	1.41
2	4.45
3	1.41
Along the cut -line	7.27

The extreme cases of this research are: all cholesterol particles are arranged in parallel with current lines or perpendicular to it. As it is hard to calculate those cases manually, when cholesterol is arranged in particles, further simplifications are made. Cholesterol total area is recalculated in such way that it forms a rectangle one side of which is equal to 5mm.

For all the cases frequency is chosen to be zero as it is in good agreement with model assumptions made and impedance turns into resistance.

Rectangle blocks. Connection in series

In case of perpendicular placement, the system can be represented by 3 impedance elements connected in series (Figure 4.2–13). The FEM geometry for numerical simulation on this case can be observed in Figure 4.2–14.

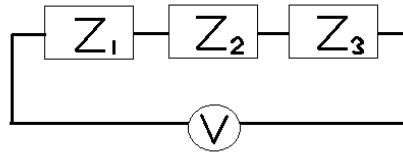


Figure 4.2–13. Analytical representation of a system (series)

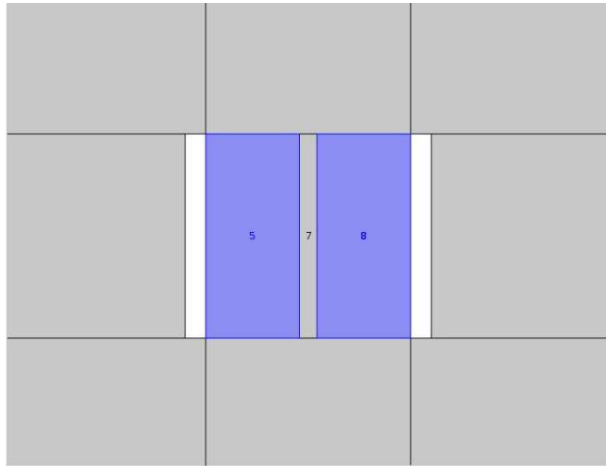


Figure 4.2–14. Practical FEM implementation of a system (series)

In that situation equivalent resistance is calculated analytically as a sum of three.

$$\frac{R_{eq}}{d} = \frac{2R_2 + R_1}{d} \quad (4.2-2)$$

$$\frac{I}{d} = \frac{Vd}{R_{eq}} = 0.7 \text{ A/m} \quad (4.2-3)$$

Value of current calculated with FEM in this situation was $I_{FEM}=0.79 \text{ A/m}$. Calculated value exceeds theoretical value by 12%.

Rectangle blocks. Parallel connection

Analytical and FEM formulation for this case are presented in Figure 4.2–15
Figure 4.2–16 respectively.

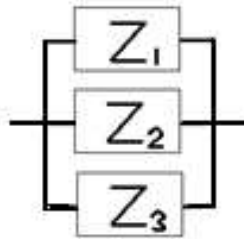


Figure 4.2–15. Analytical representation of a system (parallel)

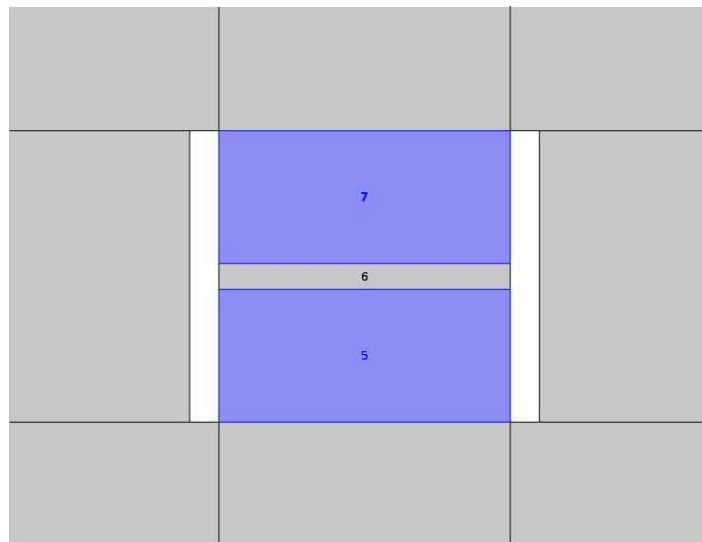


Figure 4.2–16. Practical FEM implementation of a system (parallel)

For parallel resistance case, the equation for equivalent resistance will be
(taking into account that in our case $R_1 = R_3$):

$$\frac{R_{eq}}{d} = \left(\frac{R_1 R_2}{2R_2 + R_1} \right) \frac{1}{d} \quad (4.2-4)$$

$$\frac{I}{d} = \frac{Vd}{R_{eq}} = 4.58 \text{ A/m} \quad (4.2-5)$$

$I_{FEM}=4.59 \text{ A/m}$. For this case, simulation result exceeds theoretical value by 0.2%. This study shows then in both cases, the simulation is in good agreement with theoretical results. In case of vertical cholesterol positioning it blocks a major part of current flowing through the system. This is why, even the small current that flows along the edge of geometry (simulation), results in difference between theoretical and FEM simulation results. Horizontal positioning blocks just a small portion of current lines.

Circular particles positioned in a line

This simulation test shows the comparison of two extreme cases with similar conditions where rectangle is replaced with cholesterol particles set demonstrates decrease in current per unit length value in horizontal placement. This is believed to be related to the fact that current faces have bigger cross-sectional area in that case than that of rectangular. The result for particles line positioned horizontally is shown in Figure 4.2–17. Picture represents geometry (above) and final computed current density plot (below).

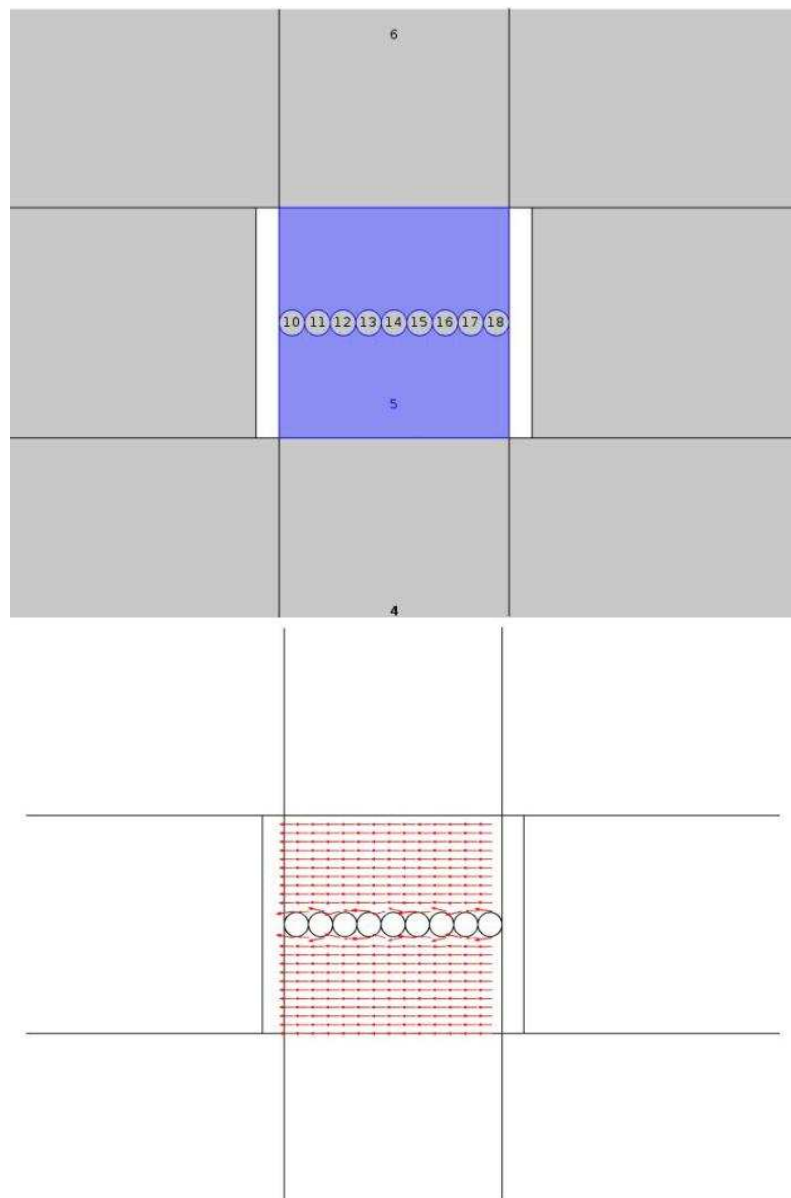


Figure 4.2-17. Horizontal particles placement

In case of vertical particle line, the value of current per unit length goes up as there is a possibility of current passing in between the particles. This is illustrated in Figure 4.2-18.

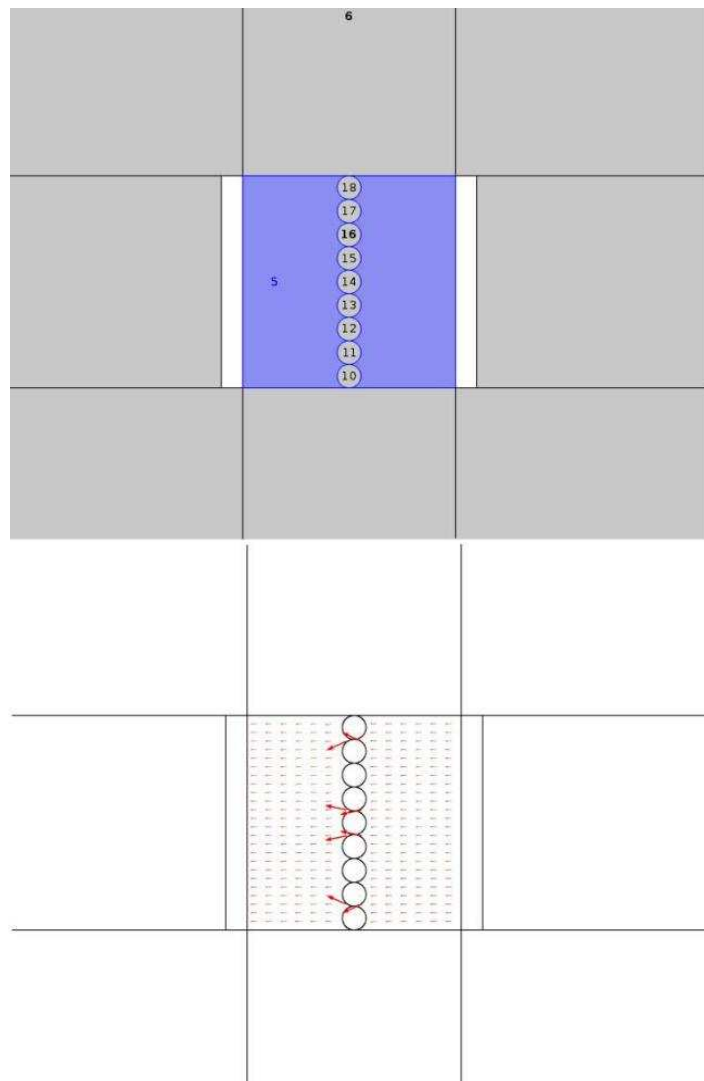


Figure 4.2-18 Vertical particle placement.

This means that particle positioning will play the most important role in case of small number of particles in the area of interest.

Comparison impedances for various cholesterol levels

Assuming that all possible for now validations have been passed the new set of simulations has been performed. For total cholesterol values equal to 5 mmol/L and 3 mmol/L 500 files have been generated in attempt to represent real statistics of cholesterol distribution in blood plasma. Resulting histograms are presented in Figure 4.2-19.

Blue histogram is related to total cholesterol value of 3 mmol/L, orange represents total cholesterol of 5 mmol/L. Vertical axis reflects number of models with values (frequency) of results falling in related interval. Even though the difference between mean values does not exceed 3.2 % this graph gives clear evidence that impedance method (at least its 2D mathematical representation) can be used for cholesterol measurement. This graph has been created in first attempts to understand the whole idea of blood-cholesterol impedance.

Further simulations led to a more efficient set of curves representing a dependence of the current density per unit length from total cholesterol level and number of cholesterol particles. The upper line is equivalent to total cholesterol of 3 mmol/L, middle one is 5 mmol/L, and the lower represents 7mmol/L case (Figure 4.2–20).

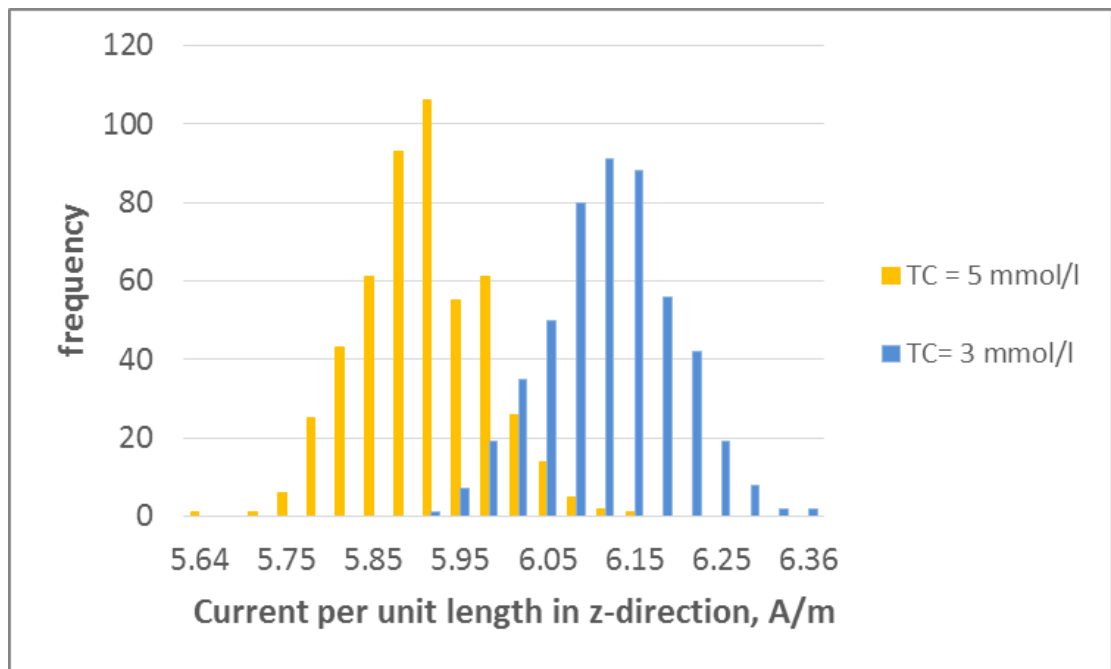


Figure 4.2–19. Values of current per unit length for total cholesterol levels at 3 mmol/L and 5 mmol/L

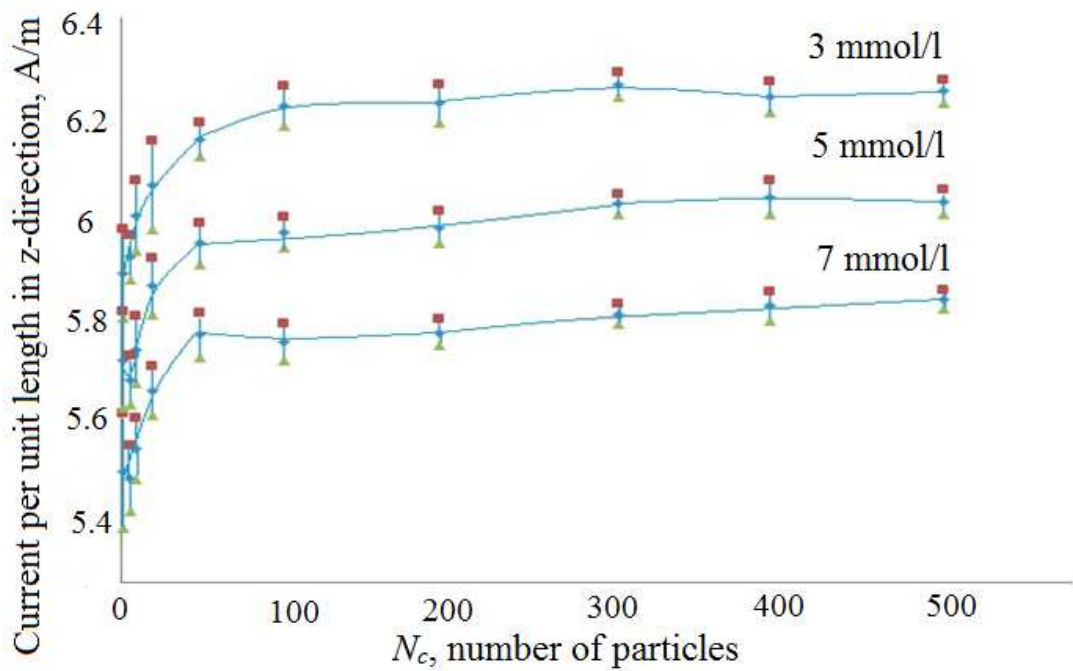


Figure 4.2–20. Current per unit length as a function of total cholesterol and number of particles

From the modelling point of view, strictly speaking the problem under investigation in this study is a truly 3D problem since a 2D problem domain cannot take into account the realistic geometry and material properties, the distribution of field and electrical parameters in the third dimension. This justifies the need for 3D FE modelling of the problem.

Chapter 5. Modelling of Non-Invasive Cholesterol Measurement System in 3D

5.1 Building a 3D model

All assumptions used for 2D modelling are used in 3D. The first 3D model tested is similar to that of 2D being extended by 5 mm in third direction. Two more air domains added: one in front and one behind the central bit of the model (Figure 5.1–1). Material properties and boundary conditions for 3D case are present in Figure 5.1–2.

The only difference is that in 3D case the fraction will be:

$$\gamma_V = \frac{V}{V_0} = \frac{2.34 \text{ mm}^3}{125 \text{ mm}^3} = 0.019 \quad (5.1-1)$$

This means that in the volume of interest the cholesterol particle will take only 1.9% of the total volume of blood. Zoomed in central volume can be seen in Figure 5.1–3. The radius of that particle has already been calculated in (4.1-2). If that volume is divided between N small particles radius of each of them can be found as:

$$r_N = \sqrt[3]{\frac{3 \cdot V_0}{4 \cdot N \cdot \pi}} \quad (5.1-2)$$

Mesh quality in 3D:

$$q = \frac{72\sqrt{3}V}{(h_1^2 + h_2^2 + h_3^2 + h_4^2 + h_5^2 + h_6^2)^{3/2}}$$

Again the criteria for 3D mesh is that element quality should be kept no less than 0.015. Average quality is kept above 0.8 (Figure 5.1–4, Figure 5.1–5, Figure 5.1–6) and, although they might not have a massive influence on overall solution, no inverted elements should be found within geometry [83]. The procedure of model building can be found presented in details in Appendix 3.

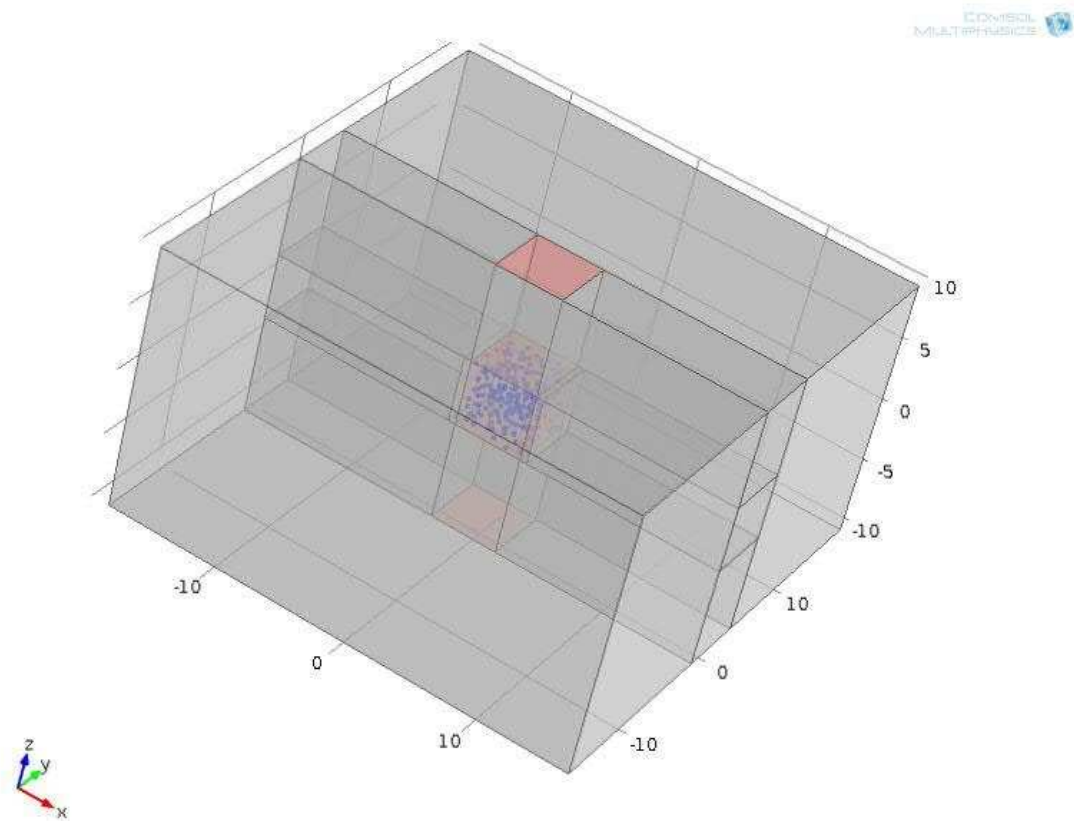


Figure 5.1–1. 3D FE model of the cholesterol measurement system

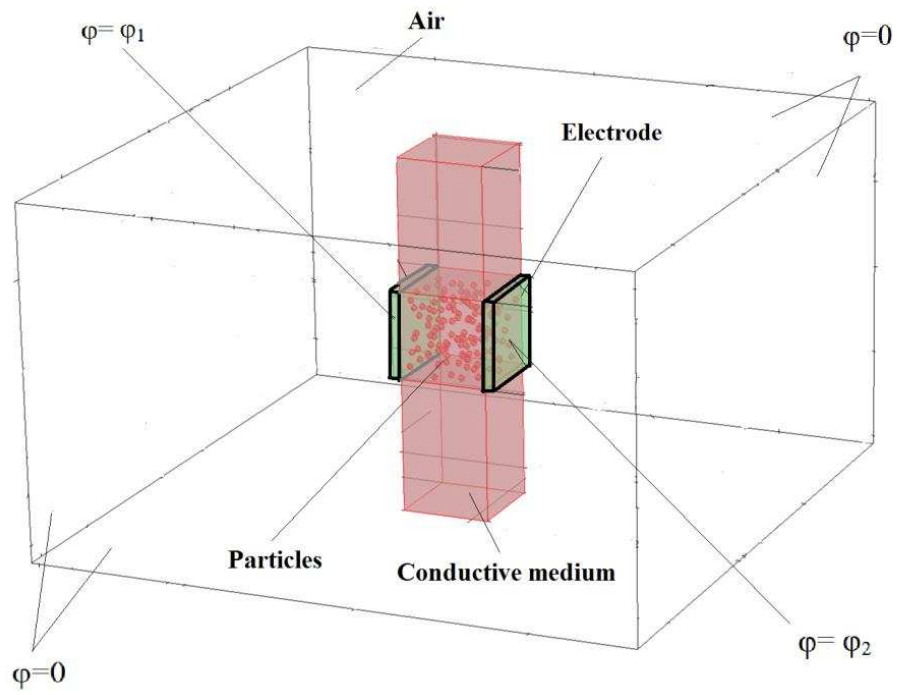


Figure 5.1–2. 3D Model with boundary conditions

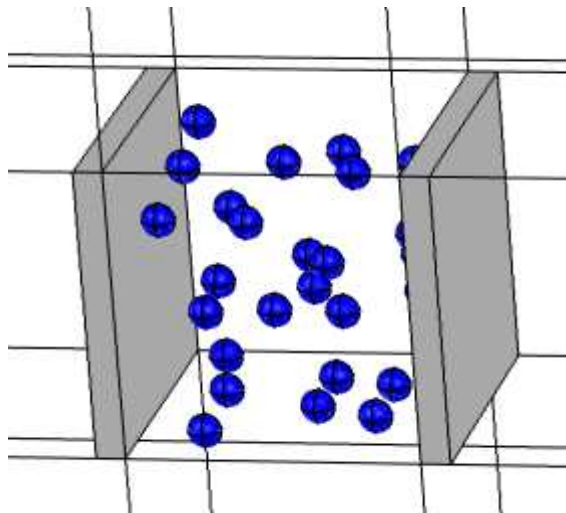


Figure 5.1–3. 3D Model (zoomed in to show details of the electrode-particle assembly)

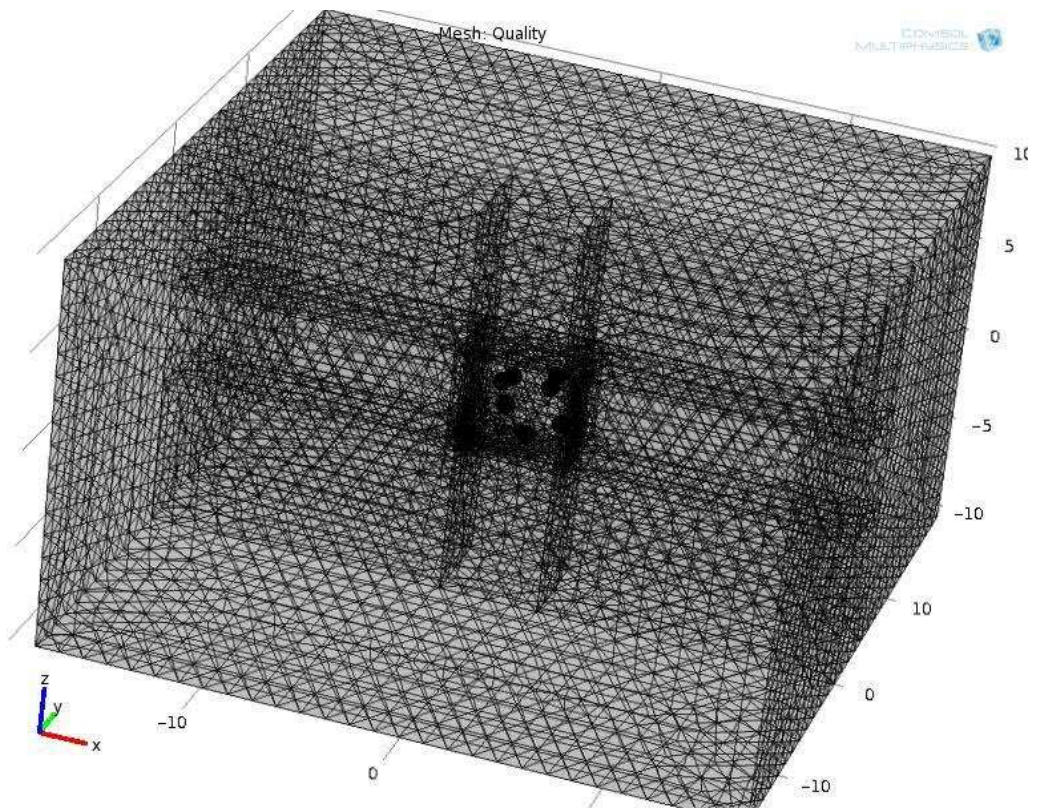


Figure 5.1–4. 3D custom mesh for 8 particles

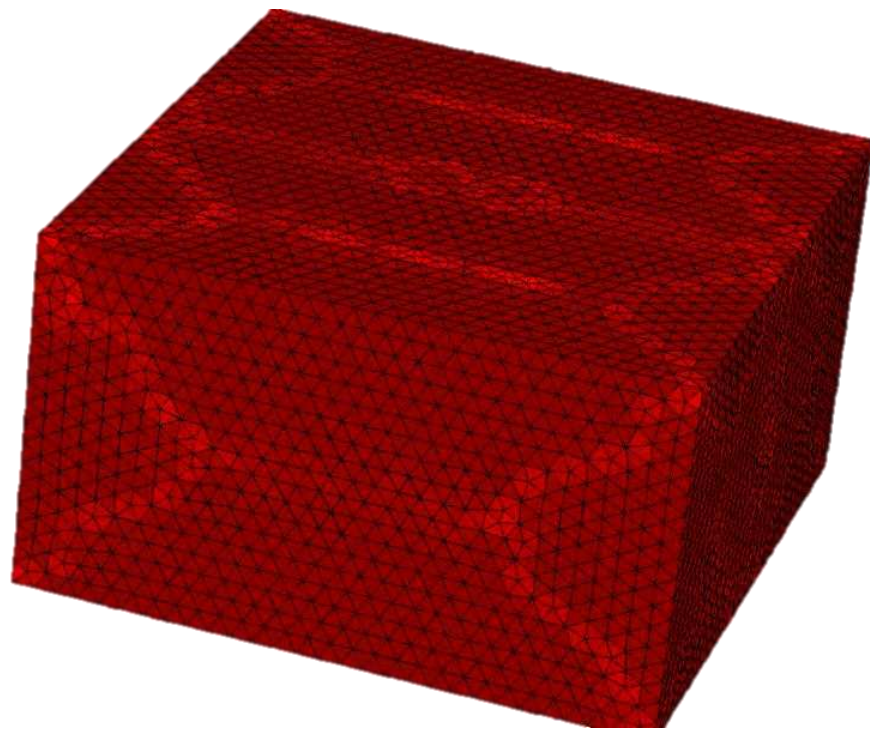


Figure 5.1–5. Quality of the external custom mesh in 3D case

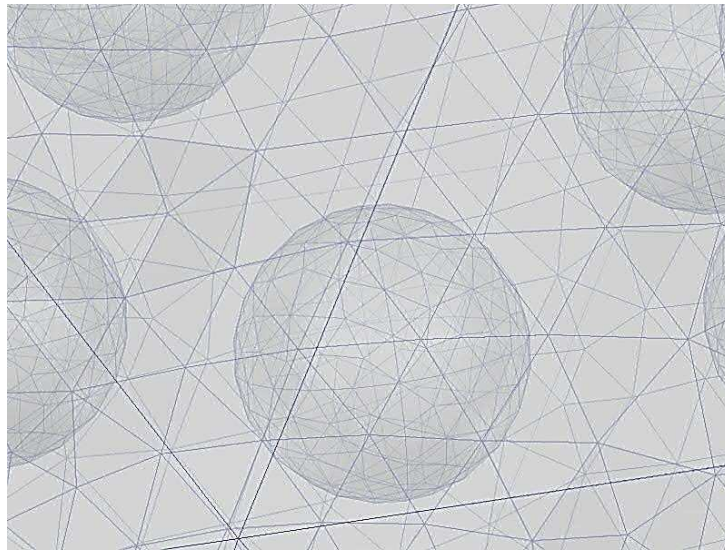


Figure 5.1–6 Quality of the external particle custom mesh in 3D case.

Mesh convergence study has been done, as well as two more types of meshing. Adaptive mesh study only led to significant increase in the time of solution (from 20 minutes to 2 days). Quadratic mesh also did not influence the solution by more than 0.1%.

5.2 Results of 3D modelling and discussions

In this section the complete set of analysis described above has been performed for a 3D case. Predefined extra fine mesh has been selected as a most appropriate according to mesh convergence analysis.

The analysis of a total current as a function of number of particles was performed and results are displayed in Figure 5.2–1.

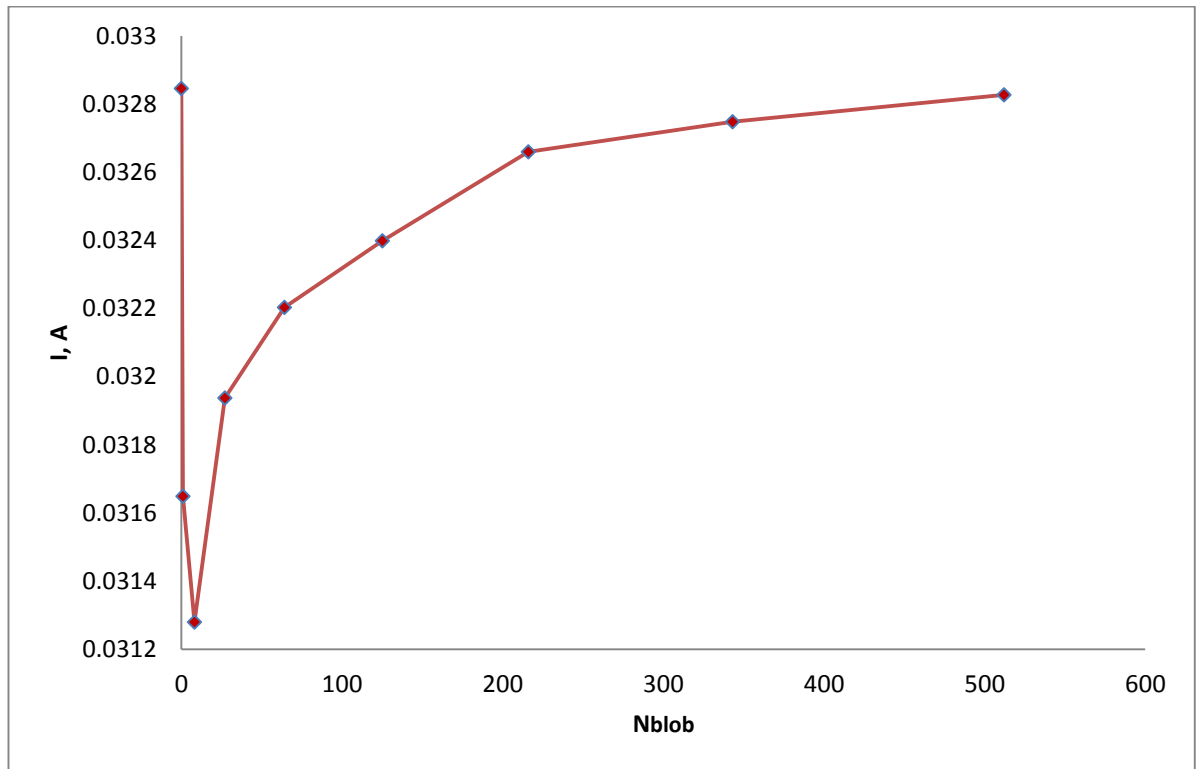


Figure 5.2–1. Current versus number of particles for 3D case

This graph shows that increase in the number of particles does lead current curve to a plateau.

The following investigation has been performed and the graph, representing current as a function of frequency has been evaluated (Figure 5.2–2). This graph highlights the problem that we are facing in 3D. The difference between current values without particles and current values with cholesterol presented is smaller than methods error.

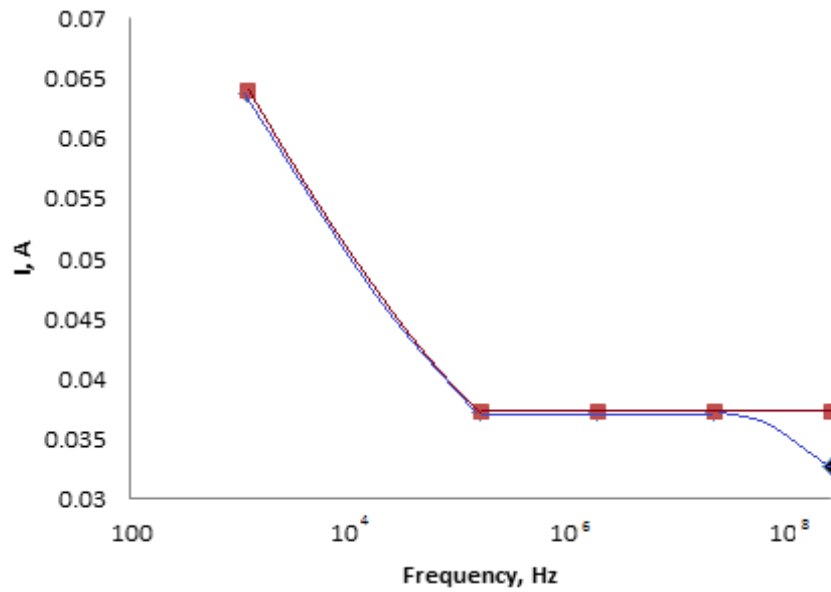


Figure 5.2-2. Total current versus frequency for 3D case

This highlights a doubt whether this is a result of incorrect modelling or the problem connected with a model of a system itself. Again a theoretical validation of obtained numerical results has been performed.

5.2.1 Validation of 3D model from simplistic analytical solution

One cubic volume conductor

First result to be checked is a current when all of the volume but a central cube is assigned with air properties and central cube has got saline solution properties. In this case, total current can be calculated via:

$$I = \frac{V}{R} = \frac{V\sigma A}{l} = 25.1mA \quad (5.2-1)$$

This is in agreement with that obtained by FE modelling from COMSOL solution, $I_{\text{COMSOL}} = 25.13 \text{ mA}$. Results difference is 0.1%. This is because that is a model of ideal capacitor and field lines are not leaving volume of interest. This also gives a brief view on how fringe field effects (see below) influence the current and hence the impedance of our system.

Parallel cylinders

Any of 2D model results can be simulated in 3D by extrusion of a 2D model in third direction. So that for example current values in 3D are supposed to be equal to those in 2D multiplied by size of the volume of interest in third direction:

$$I_{3D} = \left(\frac{I}{d}\right)_{2D} d \quad (5.2-2)$$

So the 2D model with particles positioned vertically/ horizontally converts into 3D model with cylinders positioned the same way. The geometrical representation is demonstrated in Figure 5.2–3. The current values are presented in Table 5.1. As expected, vertical line of cylinders blocks certain amount of current lines.

Spherical particles arranged in a line

In case of spheres, current has an additional possibility to go around the particles in third dimension, that fact explains increase in current values. Spheres arrangement is shown in Figure 5.2–4. The values of the current for those cases are presented in Table 5.1.

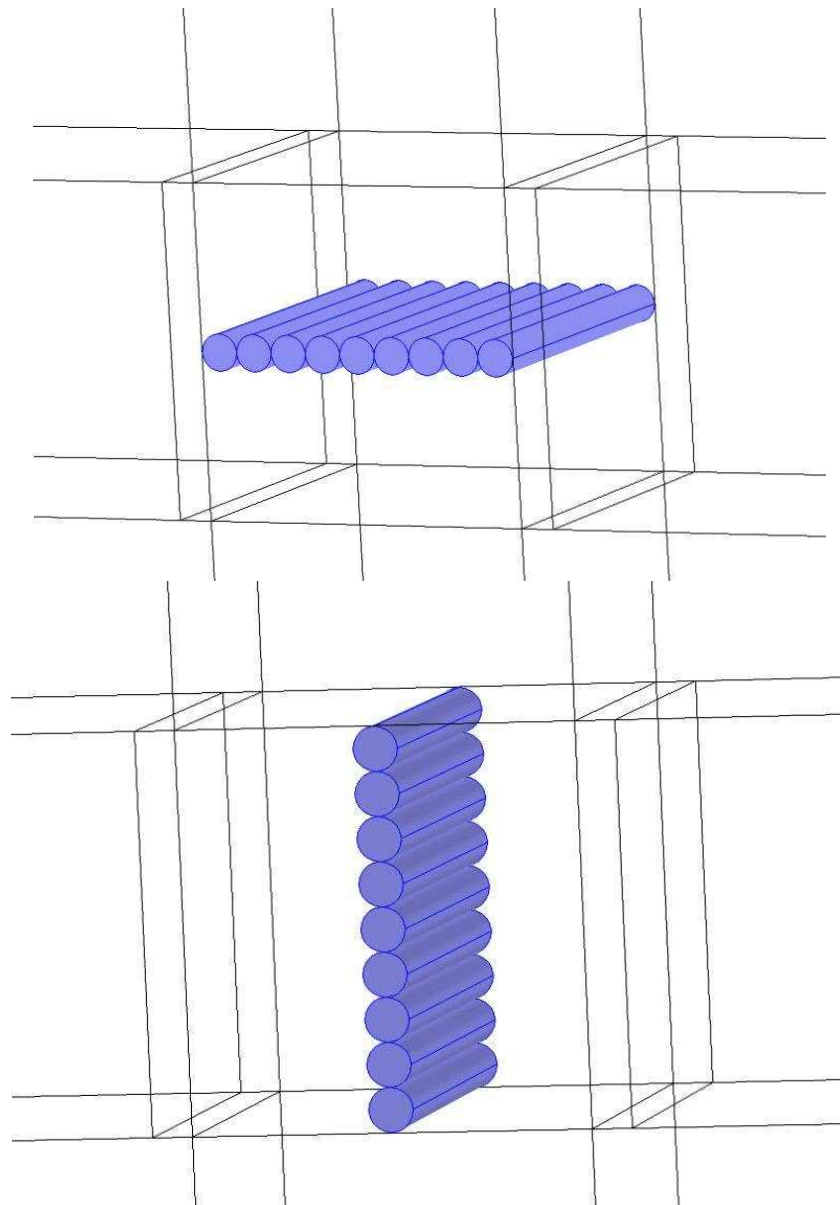


Figure 5.2–3. Horizontal and vertical lines of cylinders

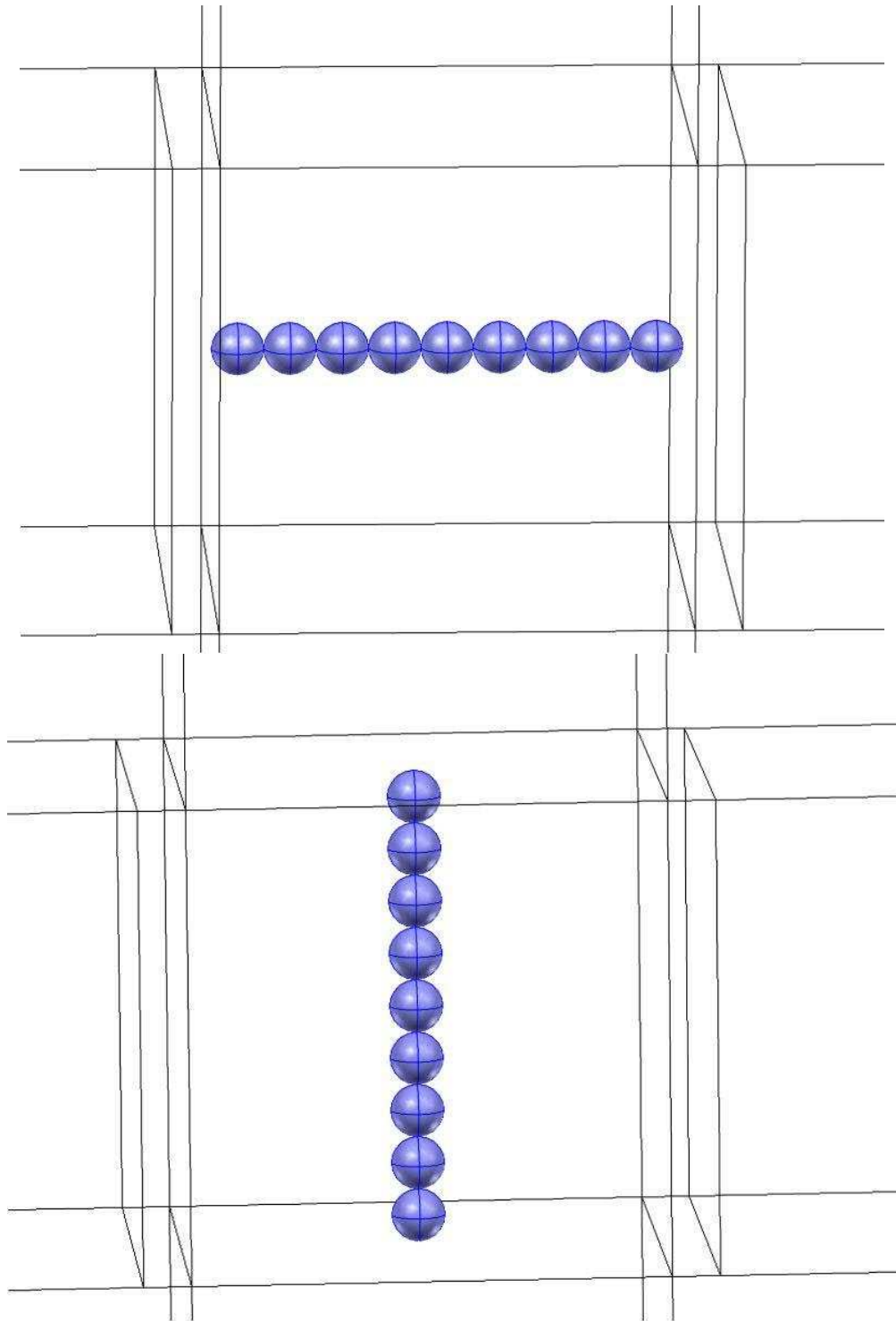


Figure 5.2–4. Horizontal and vertical arrangement of spheres

Table 5.1. Current values depending on cylinder/particle positioning

I, mA	2D->3D cylinders	3D cylinders	3D spheres
Horizontal line	30.7	29.6	32.0
Vertical line	23.0	22.8	32.4

The first column of current values was recalculated from 2D results. For line of circles current value per unit length in z-direction were multiplied by length of z-direction of the model, giving 5 mm cylinders as on Figure 5.2–3. Values for second and third column were obtained directly from 3D simulations of particle arrangements illustrated on Figure 5.2–3 and Figure 5.2–4. Values for 3D simulation of cylinders sets are lower than recalculated from 2D simulations (3.5% for horizontal orientation and 1% for vertical). As expected for set of spheres they are significantly higher (8% for horizontal and 42% for vertical orientation). This can be attributed to excessive current paths that appear when cylinders are swapped for spheres.

5.2.2 Additional analyses

As results show there is no evidence that computation has calculated incorrect solution.

More analyses have been performed, such as establishing the link between current and electric field.

Case without particles

When there is no particle in the volume the electric field on the plane, which crosses the total volume approximately in centre (cut-plane going through the centre is shown in Figure 5.2–5) should be uniform in the electrode area and its value is proportional to current value. Results are demonstrating the correct behaviour (Figure 5.2–6)

The current density, which is calculated along cut line (the position of the line is shown in Figure 5.2–7) is demonstrated in Figure 5.2–8. The total agreement with theory can be observed as the current density forms almost perfect step with the computed value to be exactly equal to analytical one calculated with Ohm's law:

$$j = \sigma E = 976.8 \text{ A/m}^2 \quad (5.2-3)$$

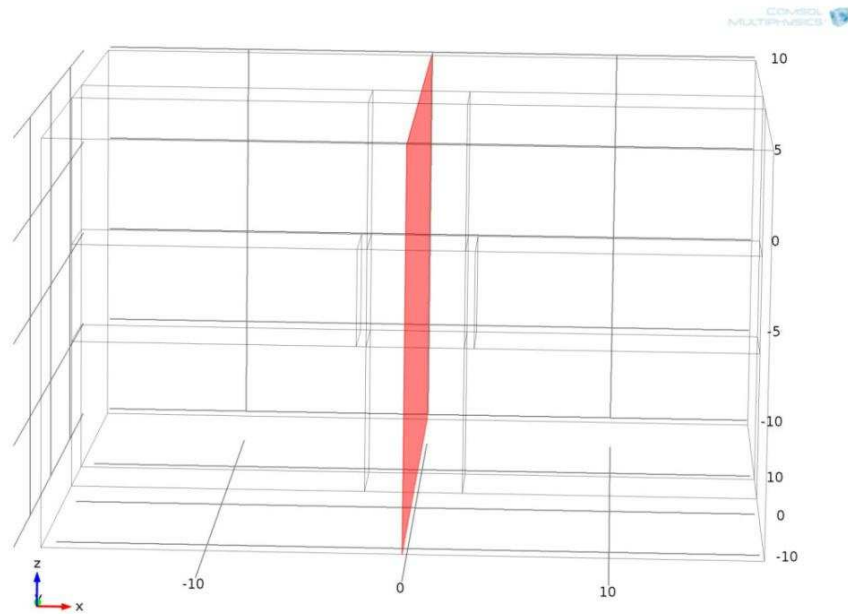


Figure 5.2–5. YZ-Cut plane

Modelling of Non-Invasive Cholesterol Measurement System in 3D

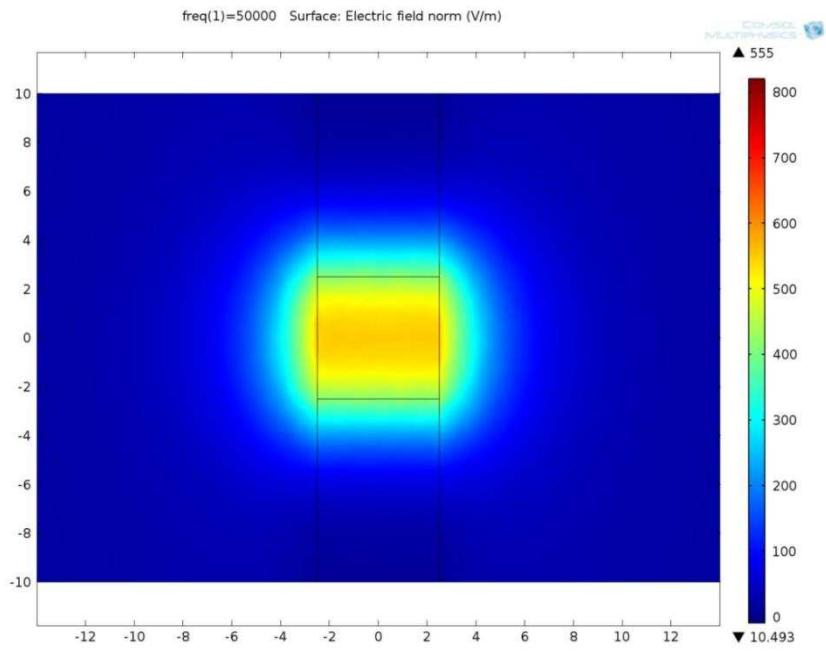


Figure 5.2–6. Electric field distribution on the cut-plane for the case with no particles

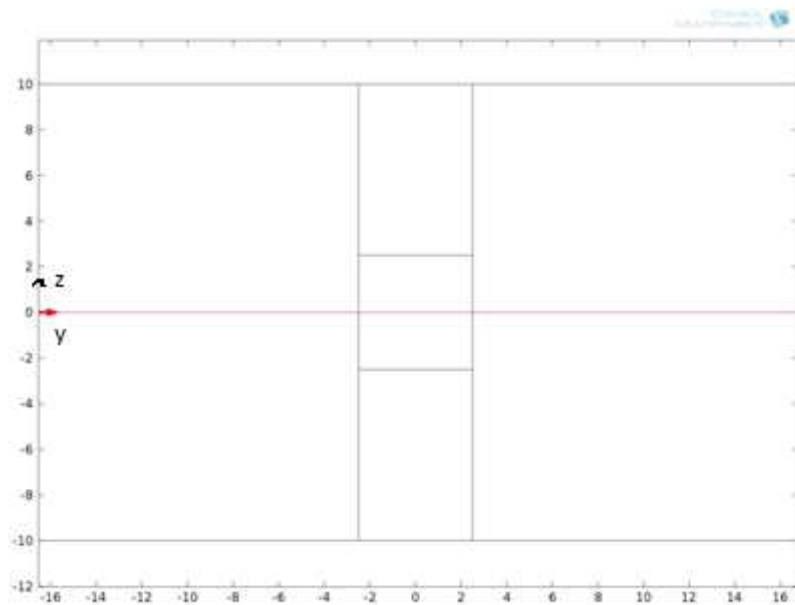


Figure 5.2–7. Position of the central line on the cut-plane

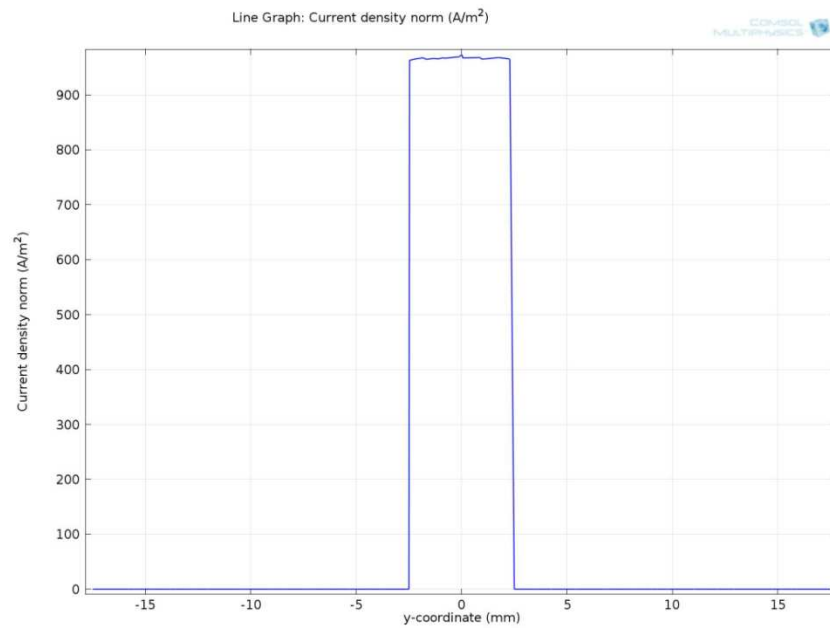


Figure 5.2–8. Current density for the model with no particles

Case with 1 particle in the middle

The geometry and cut-plane together with the central line where the current density is evaluated is presented in Figure 5.2–9.

Electric field distribution plot for this case is demonstrated in Figure 5.2–10, and current density plot along the central line is plotted in Figure 5.2–11

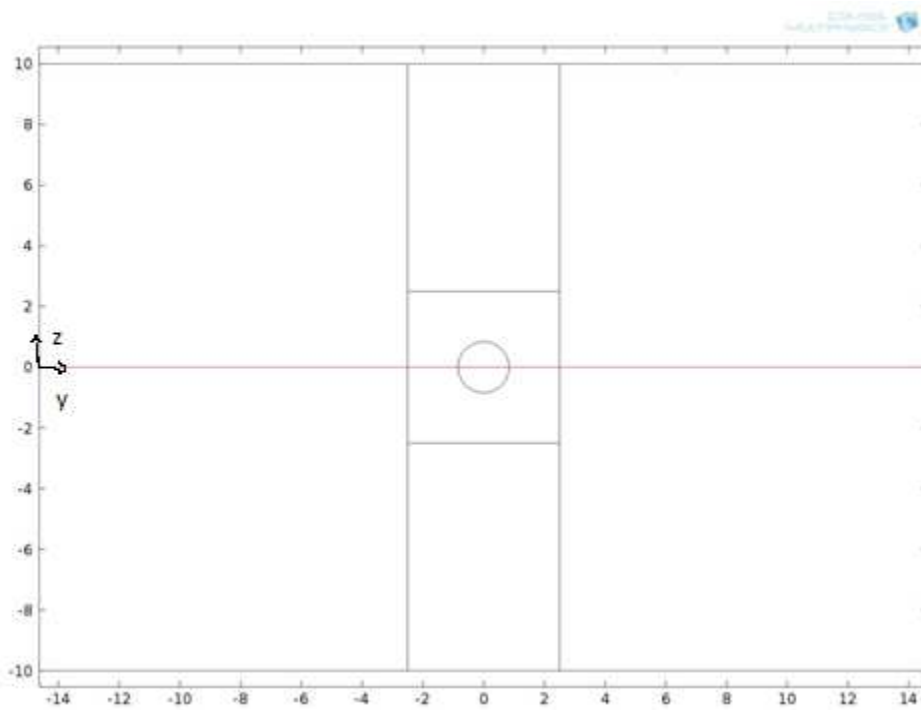


Figure 5.2–9. Geometry and central line for the case with 1 particle

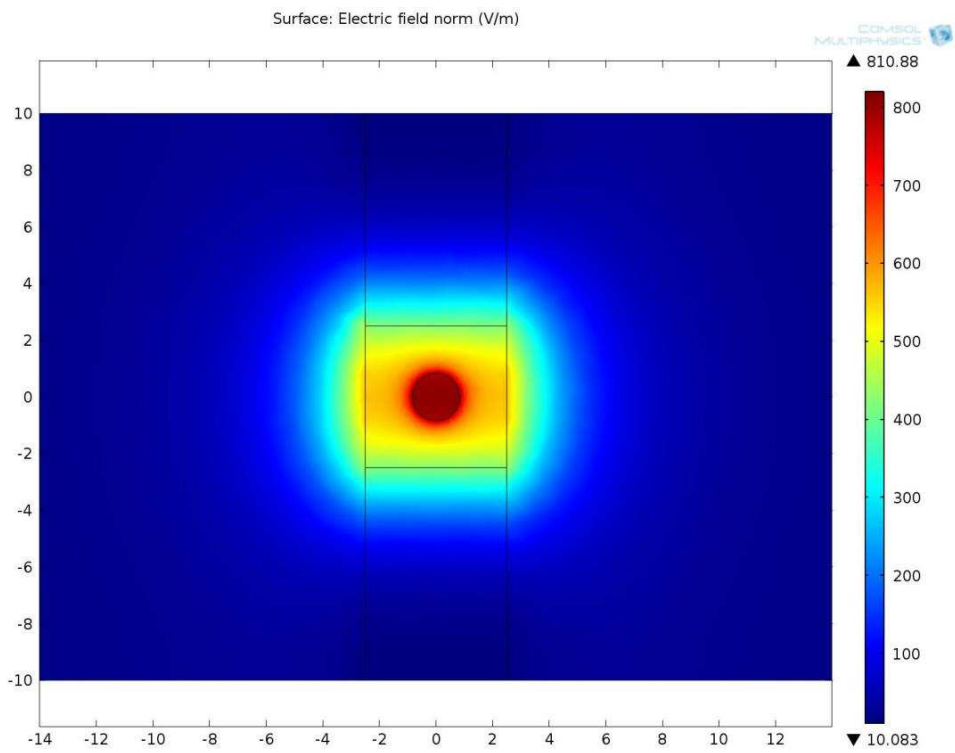


Figure 5.2–10. Electric field distribution for the case with 1 particle

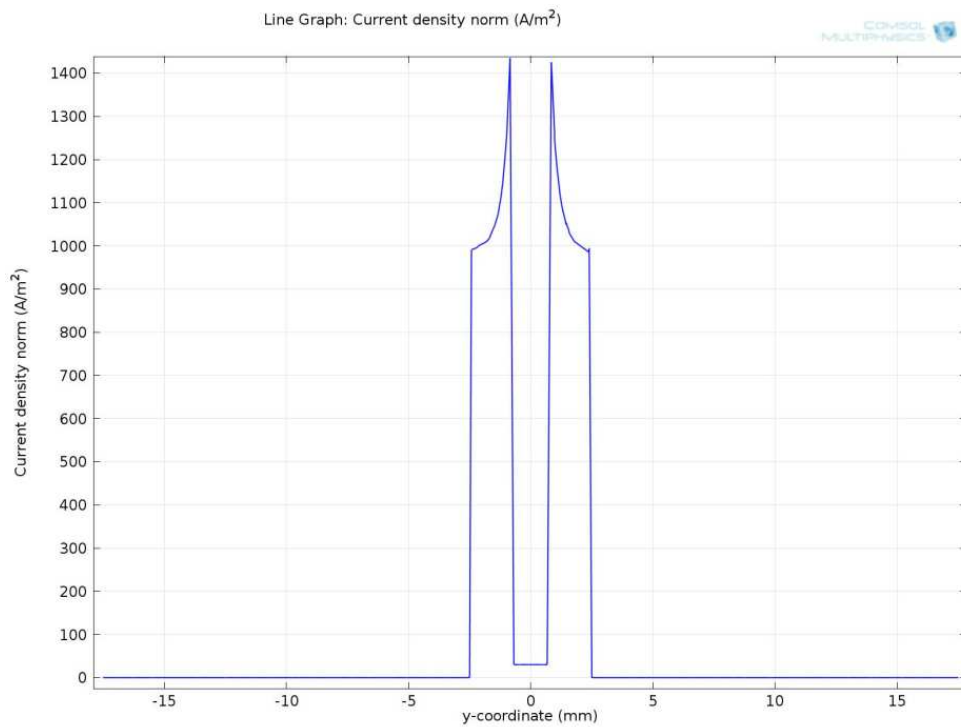


Figure 5.2–11. Current density plot along the central line

Analytical calculations for one particle in the middle can be performed and give the following current density values:

c) For plasma on the edge of particle-plasma system:

$$j = \sigma E = 1425.6 \text{ A/m}^2 \quad (5.2-4)$$

d) For particle:

$$j_b = \sigma_b E = 20 \text{ A/m}^2 \quad (5.2-5)$$

This means that the developed mathematical model works and is in good agreement with theoretical and predicted results.

A fresh look at a fringing shows that it counts for as much as 50 % of total current in our system.

Total current has been calculated in yz-plane that goes through the middle of the volume of interest (Figure 5.2–12). Total current through this plane is computed as a sum of currents through conducting volumes I_1 , I_2 , I_3 . Using COMSOL results the following Table 5.2 has been evaluated. It gives:

$$\frac{I_{tot} - I_2}{I_{tot}} * 100\% \cong 40\% \quad (5.2-6)$$

This together with other obtained results leads to the idea that our model, and hence our system, needs to be redesigned taking into account all the weak points.

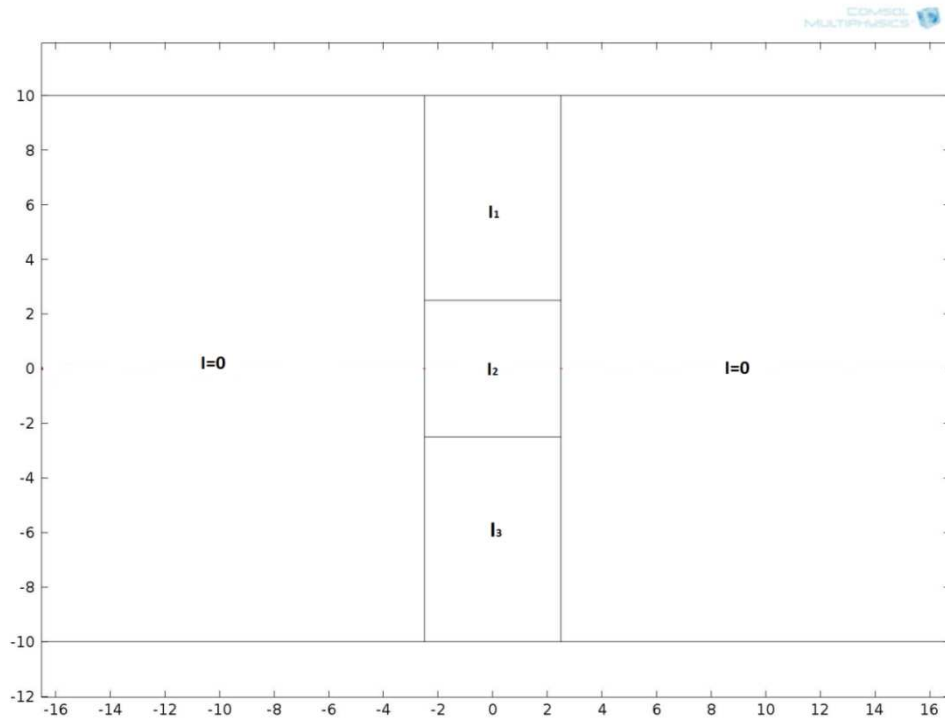


Figure 5.2–12. Cross-section of the volume with yz-plane

Table 5.2. Current through the corresponding conducting volumes and total current through cut-plane

Domain	I, mA
1	7.31
2	22.34
3	7.3
Whole cut –plane	36.95

5.2.3 Comparison of impedances for different cholesterol levels in 3D

Assuming that all necessary validation tests have been done the new set of simulations has been performed. For total cholesterol values equal to 7 mmol/l, 5 mmol/l and 3 mmol/l, a set of curves representing the dependence of the current

density from total cholesterol level and number of cholesterol particles. The upper line is equivalent to total cholesterol of 3 mmol/L, middle one is 5 mmol/L, and the lower represents 7mmol/L case (Figure 5.2–13).

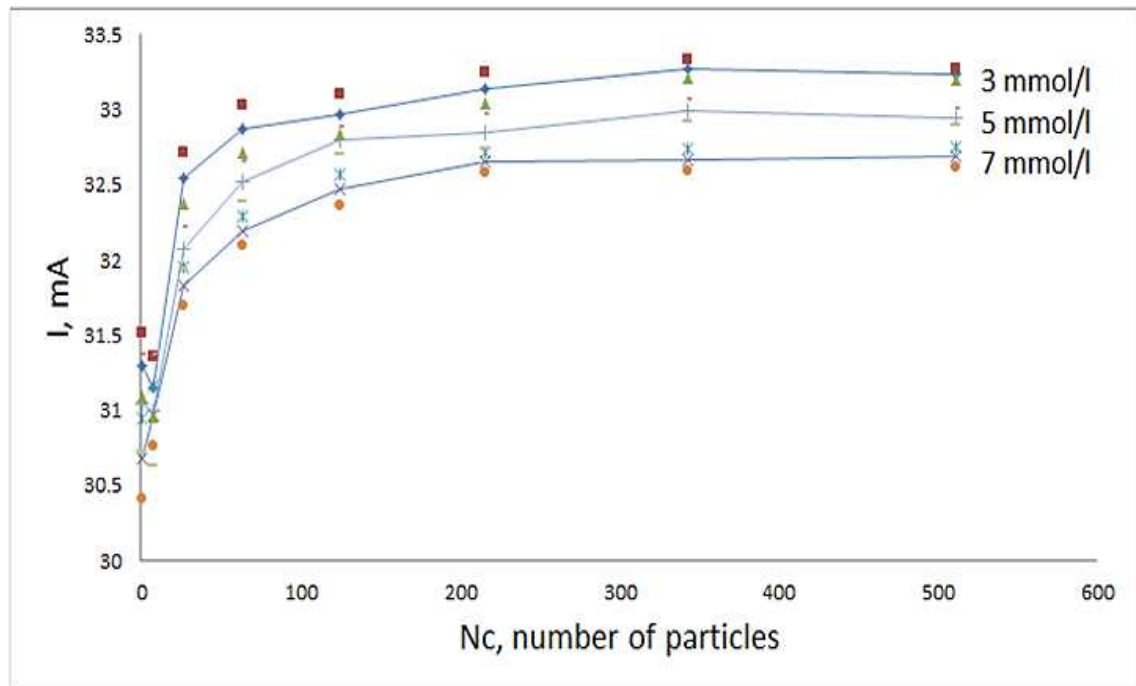


Figure 5.2–13. Current as a function of total cholesterol and number of particles
The difference between the current values is about 1.5 %. Although it is a small value, curves clearly show that for all studied models current values and there standard deviation fall within separate bands.

This set of curves confirms hypothesis that impedance can be used to distinguish two close cholesterol levels in blood.

These encouraging results mean that there is a reason to complicate used model even more by adding different type of blood particles. In next chapter red blood cells are added to add further complexity to COMSOL model.

Chapter 6. Introduction of Red Blood Cells

6.1 Modelling investigations with RBC

6.1.1 RBC and their electrical properties

As mentioned before blood does not only contain plasma and cholesterol. On average, as much as 45% of total blood volume is occupied by blood cells. They can be divided into three main types: red blood cells (RBC or erythrocytes), white blood cells (WBC) and platelets.

RBC represent the major component of blood cells and account for as much as or more than 99% of the blood cells volume [67], [105]. A typical erythrocyte is a disk with diameter of approximately 6.2–8.2 μm [106] and its thickness varies from 2–2.5 μm at the thickest part and to about 0.8–1 μm , which is a minimum thickness in the centre of a cell. They have an average volume of about 90 fl [107] and their surface is about 136 μm^2 , and in solutions of lower osmotic pressure can swell up to a sphere shape containing 150 fl, without membrane distension. If the osmotic pressure falls below 0.5% saline, lysis is complete in 0.35% [91].

The primary function of erythrocytes is carrying haemoglobin, type of protein that delivers oxygen from respiratory organs to the rest of the body and takes away carbon dioxide [108]. Their secondary functions include taking part in vessel wall relaxation process in case of oxygen deficiency [109], [110]; synthesis of nitric oxide, that contributes to regulation of vascular tonus [111]; and release of free radicals, that kills pathogen cells by braking its membrane (immune function) [112], [113].

The other peculiar thing is that erythrocyte width is on average about 25% larger than capillary diameter, and there is a hypotheses that it is due to improvement of the oxygen transfer from erythrocytes to tissues [114]. However, as with the biconcave shape this is not taken into account in the proposed model.

The volume percentage of erythrocytes in human blood is called haematocrit. It varies from 38% to 46% in adult women and form 42% to 54% in adult males [115].

On average adult male has roughly $4.3 - 5.7 \times 10^{12}$ RBC/l and adult woman has about $3.9 - 5.0$ RBC/l at any given time, comprising approximately one quarter of the total human body cell number. For comparison, for white blood counts this number is $4.0 - 10.0 \times 10^9$ WBC/l and for platelets $143 - 400 \times 10^9$ cells/l [108].

Electrical properties of RBC are approximation of results taken from [116] that correlate with values given in [117]. Typical current lines behaviour in biological cells depending on frequency is illustrated in Figure 6.1–1.

At 50 kHz conductivity of RBC is assumed being equal to $\sigma_r = 0.7$ S/m and relative permittivity $\epsilon_{rr} = 79$.

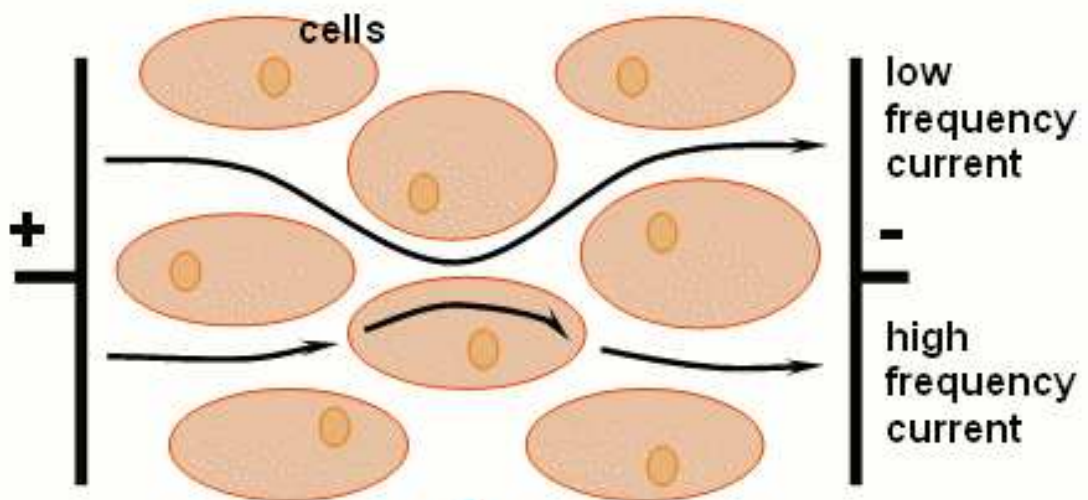


Figure 6.1–1. Frequency dependence of current paths

6.1.2 Maximum percentage of RBC

As dimensions of real RBC vary, there is a need to find the average values of diameter and height for modelling purposes. According to [105] the average diameter is equal to $7.5 \mu\text{m}$. Average height is calculated from values given above using the assumption that erythrocytes are modelled as cylinders and not biconcave disks and is taken as an average between the maximum and minimum thickness, equal to $1.65 \mu\text{m}$.

The particles are distributed randomly within the area of interest, using the same function that was utilized for cholesterol particles (Figure 6.1–2).

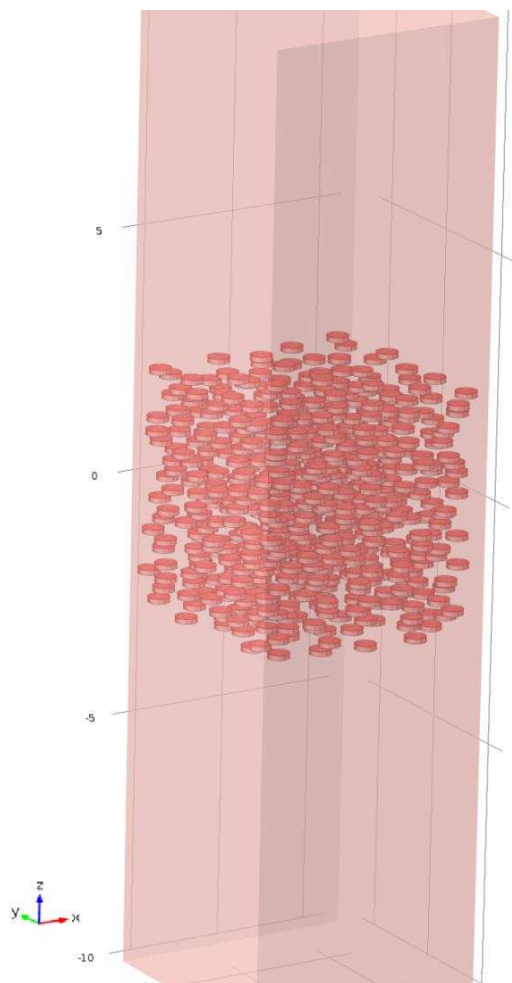


Figure 6.1–2. RBC parallel to xy-plane

The main problem that has been encountered at that point was that it was not physically possible to model the real haematocrit. The highest volume percentage of erythrocytes that was reached did not exceed 40%. More than that, even for that percentage and number of particles above 150, it was not possible to implement truly random distribution, which would include random particle orientation. This partially was attributed to the mathematical method used for calculation of distances between the particles and repair tolerance values within COMSOL model. The main challenge was to create a method that would allow two particles to be in close contact and even touch, but not overlap. In the first models, it was done by introducing the sphere around every RBC, and has been changed to ellipsoid in later script files. Although this method is not ideal, it proved to work and allow reach the number of modelled particles, for which current curve reaches the plateau area, as it will be seen later in the thesis. This led to necessity for implementation of additional assumptions.

6.2 Additional assumptions

As decided, electrodes would be placed on the earlobe. This means further calculations of volume of the blood in an earlobe are required. To do that the total length of capillaries, total volume of blood on capillaries and blood compositions are needed. The density of capillary net in the earlobe is displayed in Figure 6.2–1.

The blood vessels (arteries, capillaries, and veins), laid end-to-end, would measure about 100,000 km (60,000 miles), or approximately 2.5 times the circumference of the earth. Capillaries account for about 80,000 km (50,000 miles) of vasculature in an adult [118].

From [119] the total volume of blood is 7 % of the total body weight or 70 ml/kg. This means that in an average person that weights 63 kg it gives:

$$V_b = m \cdot 0.07 = 4.41 \text{ l} \quad (6.2-1)$$

Although capillaries count for more than 50 % of total blood vessel length the total volume of blood in capillaries in accordance to [120] is equal to only 5 % of total blood volume.

From that the total volume of blood in capillaries is

$$V_{bcap} = V_b \cdot 0.05 = 0.2205 \text{ l} \quad (6.2-2)$$

The total volume of capillaries from capillary radius [91] and total length. The amount of blood per unit of capillaries or the fraction of volume taken by the blood would be a ratio of volume of blood in capillaries to the total volume of capillaries.

$$V_{cap} = l_{capt} \cdot r_{cap} = 1.570 \text{ L} \quad (6.2-3)$$

$$\gamma_{bcap} = \frac{V_{bcap}}{V_{cap}} = 0.14 \quad (6.2-4)$$

The value can be expressed in decimal 0.14/l or as percentage – 14%

To simplify the model we suggest that all of the earlobe volume is filled with capillaries.

Considering this assumption, we can get that an earlobe will contain the amount of blood per unit of capillaries multiplied by the total volume of earlobe (14% of the volume).

If according to [115] on average haematocrit in an adult is about 46%, then only 6.44% of volume will be occupied by RBC in an earlobe.

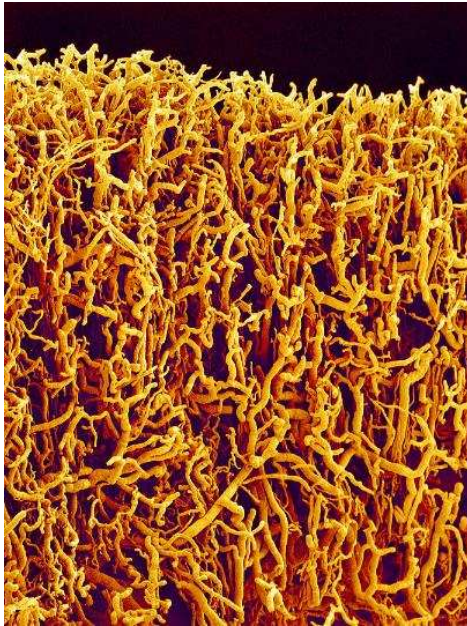


Figure 6.2–1. Capillaries in earlobe
(Susumu Nishinaga)

Although in stationary blood RBC are oriented randomly, they do tend to have predominant orientation due to the blood flow and it changes with each heart contraction. This will have a significant effect on blood impedance [103]. However, this problem would not arise when the measurements are done on the area with domination of capillaries. Due to their geometry, erythrocytes in capillaries are only able to travel in one direction. This domination of orientation can be seen in Figure 6.2–2.



Figure 6.2–2. Alveoli.
Capillary net of an alveola
showing the erythrocytes
within the blood vessels
(Oliver Meckes)

6.3 3D realisation for earlobe proportions

For modelling purposes, the ratio between height and diameter of RBC is kept close to realistic and as it is mentioned above, it is equal to 2.27. As already mentioned geometry is kept simple by RBC being modelled as cylinders, not oval biconcave disks [121]. The central part of the model is shown in Figure 6.3–1.

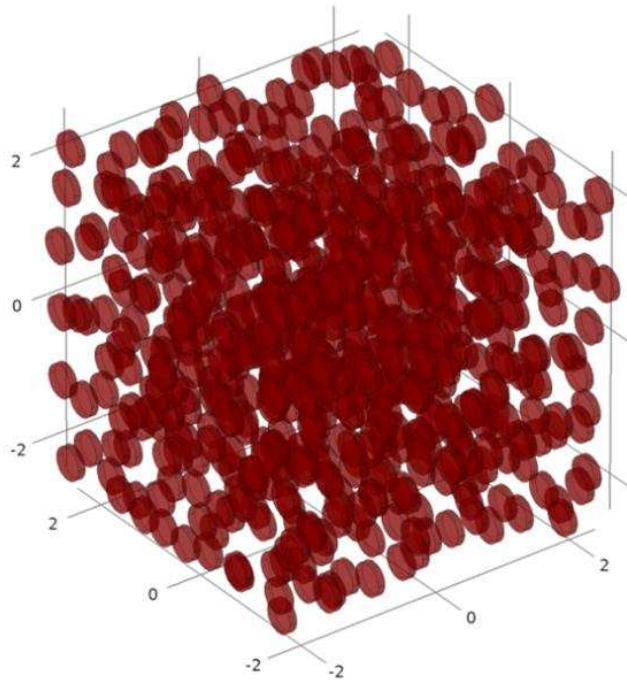


Figure 6.3–1. Distribution of RBC

The plateauing effect is also present for RBC and can be seen in Figure 6.3–2. As expected the much larger number of particles is needed for getting into the plateau area. It is also worth mentioning that for RBC dispersion of the current values is higher than for cholesterol, as there is a higher possibility of them getting accumulated in one spot because of higher concentration.

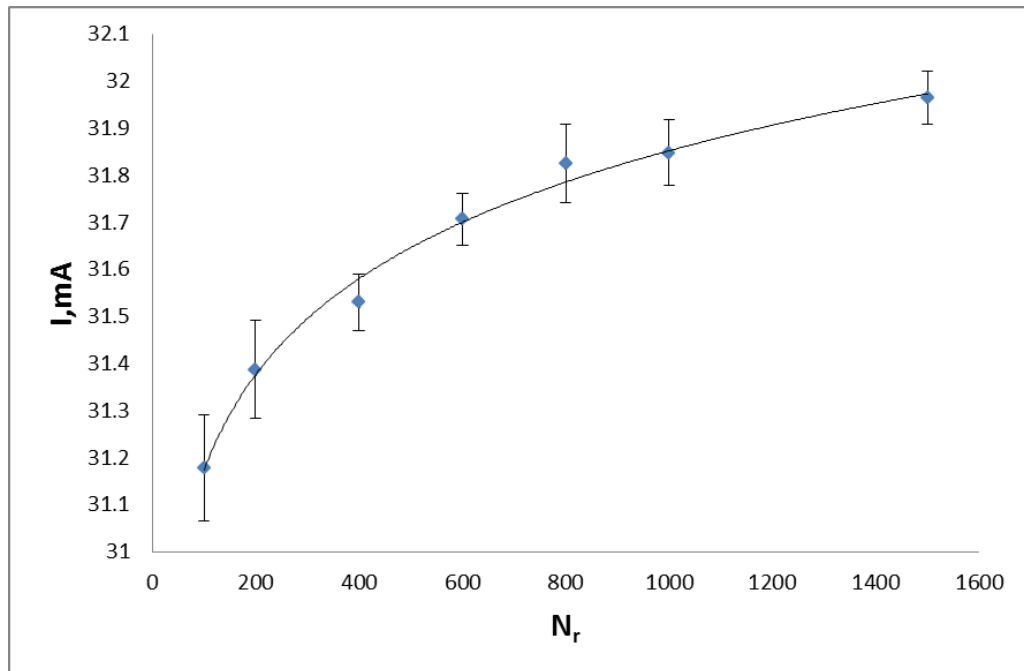


Figure 6.3–2. Variation of current with number of RBC, N_r

Another set of numerical experiments has been performed to determine how particle orientation influences the total impedance of the system. As it also involved cholesterol particles presence/absence, these results would be included below in the 6.4.

6.4 Combination of RBC and cholesterol

The further developed models get more complicated partially due to large fraction of RBC introduced in the area of interest. Although the contrast ratio for electrical properties of erythrocytes is nowhere near as high as of cholesterol, they will still play a key role in impedance change in comparison with pure plasma model. But this is not the only factor complicating the task of new system modelling.

Recalculation of total blood volume would mean recalculation of total volume of cholesterol. For total cholesterol of 5 mmol/l the value will dramatically drop

from 1.87% to just 0.26%. This undoubtedly will cause extra complexity in detection of impedance input for close cholesterol levels.

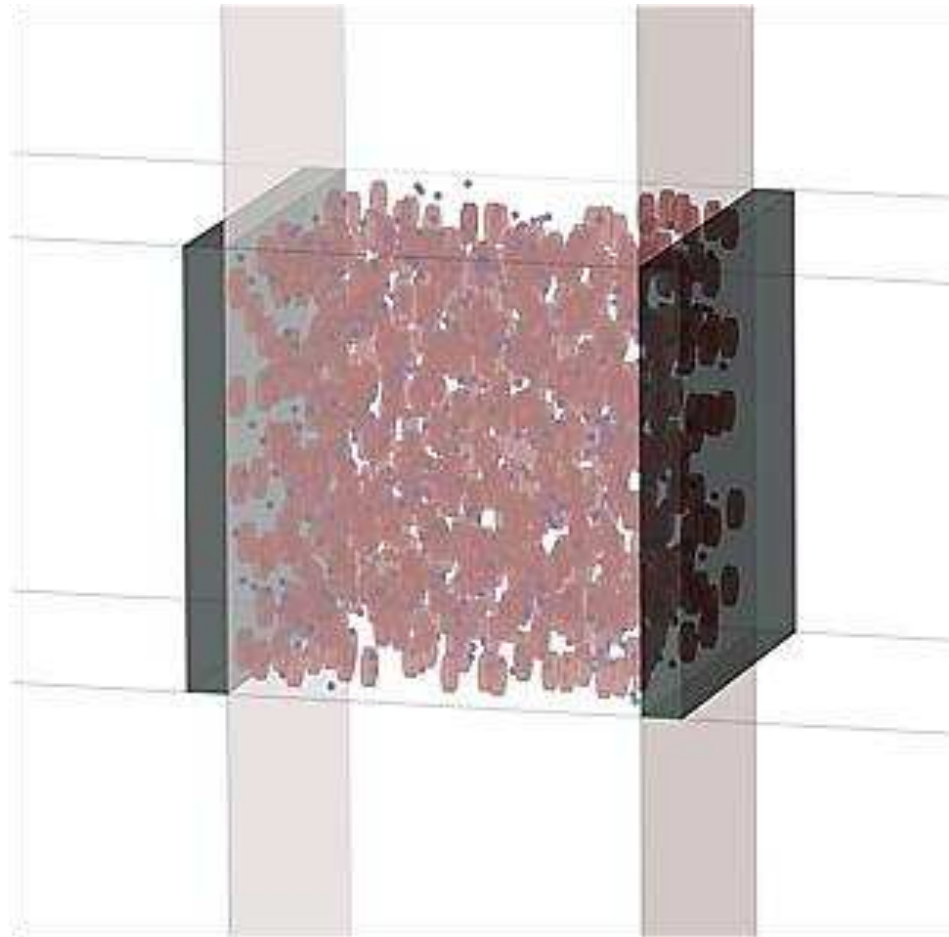


Figure 6.4–1. Distribution of RBC and cholesterol particles

On top of all that, the major difference in sizes between erythrocytes and cholesterol particles makes meshing of the area of interest a challenging task. This is still supposed to be done more or less uniformly with no more than 20% increase in element size in between the two neighbouring elements. MathLab code used for particles placement is present in Appendix 5.

6.4.1 Results showing dependence of current on frequency and the orientation of RBC

Theory suggests that up to 100 kHz RBC properties would not significantly change and there should not be any impact on total current and hence impedance of the system. This has been proven by numerical experiment. The results could be seen in Figure 6.4–2.

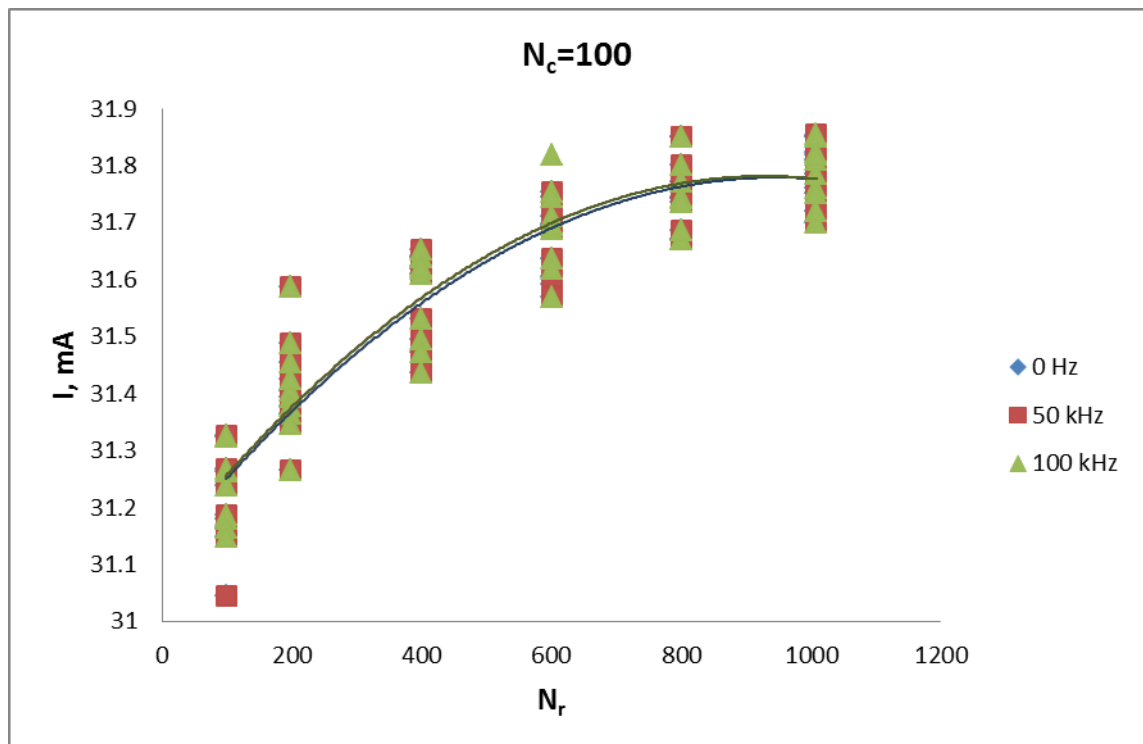


Figure 6.4–2 Dependence of total current on the number of RBC N_r at different frequencies (RBC parallel to the electrode surface).

Again, 10 models for each point on the curve were created to minimize particle distribution influence.

The other question is linked to erythrocytes orientation. As it has been mentioned above, various sources suggest that there will be a change in impedance up to 2 – 4% [103] due to particle inclination in respect to electrode's plane.

It is obvious that resistivity of the system is maximum when cylinder bases are

parallel to the electrode's surface, and is minimum when particles are perpendicular to it.

Two sets of computations have been produced. One for RBC with $\theta = 0^\circ$ (parallel to electrodes) and tilted by $\theta = -45^\circ$ (Figure 6.4–3).

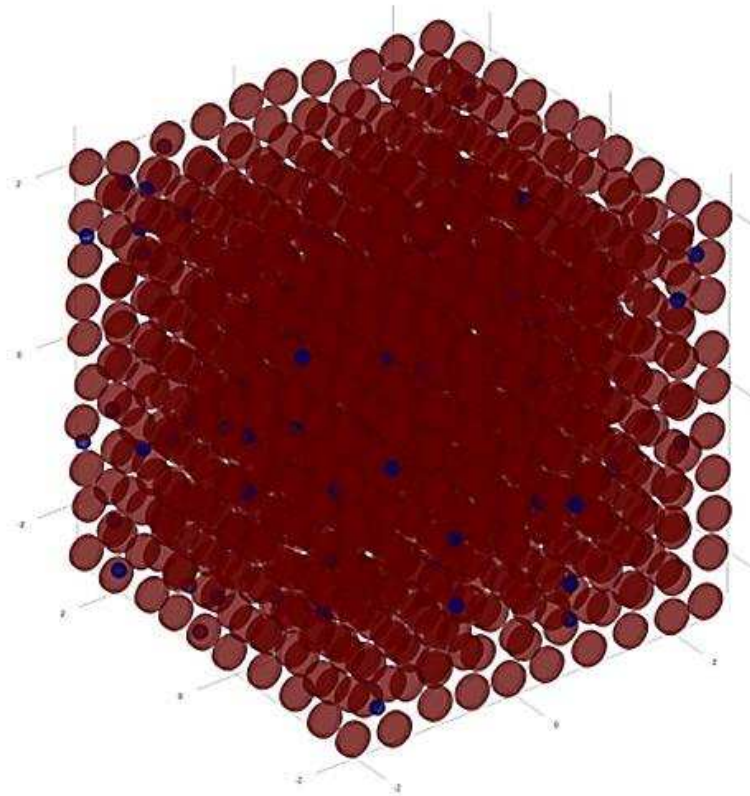


Figure 6.4–3 Distribution of cholesterol and RBC, tilted by $\theta = -45^\circ$.

There was a doubt that dispersion of results for a fixed number of RBC ($N_r < 500$) was due to discretization error. Additional analysis has been performed to give understanding if that was a case. The following results in Figure 6.4–4 and Figure 6.4–5 suggest that meshing quality is stable enough and discretization does not play a key role in case of $\theta = 0^\circ$, however for $\theta = -45^\circ$ coarser mesh seems to have an impact on some of the models. For both cases results more or less simultaneously shift up, that looks like as if they were just moving closer to accurate solution.

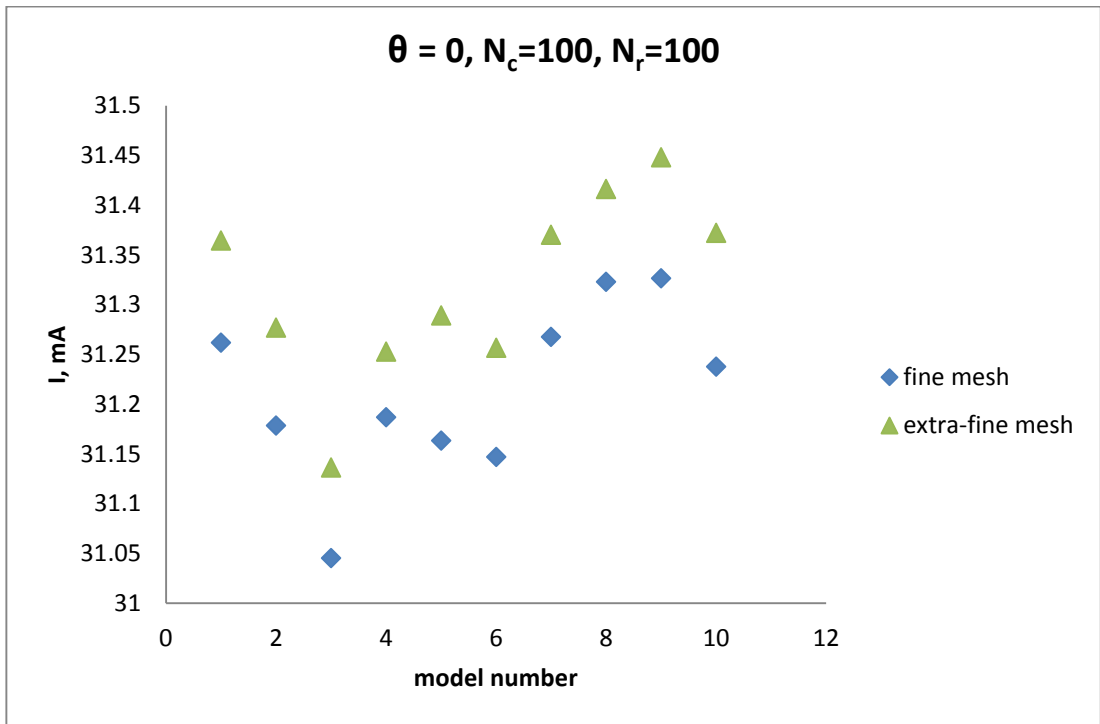


Figure 6.4–4. Dependence of current on mesh for $\theta= 0^0$

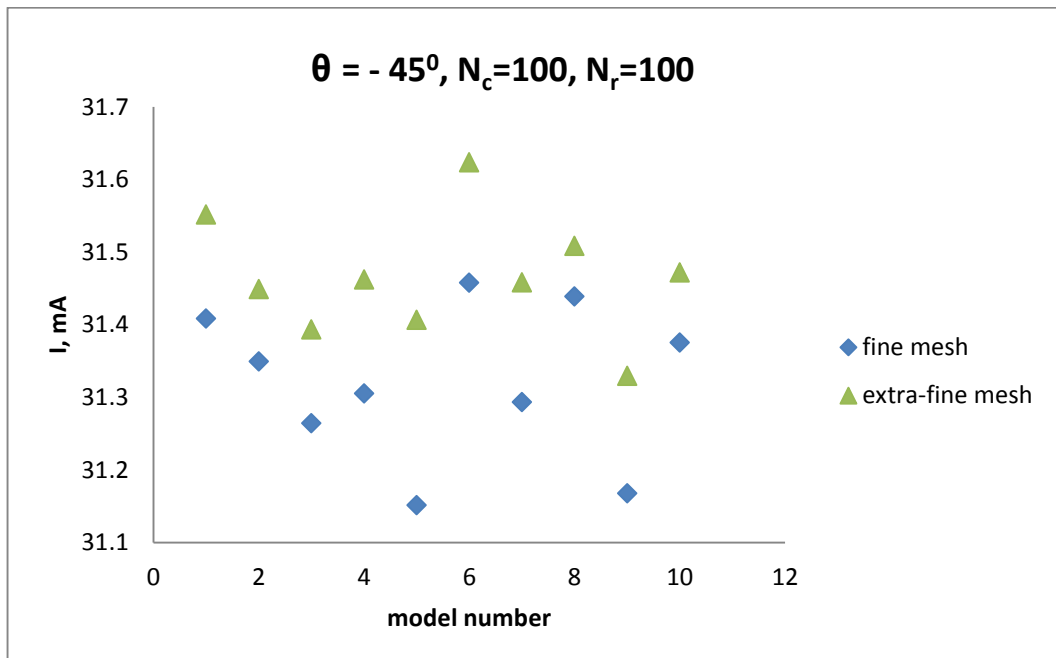


Figure 6.4–5. Dependence of current on mesh for $\theta= -45^0$

This analysis allowed concluding that for RBC orientation has a higher influence on system impedance than particle distribution (dispersion on the graph). Two curves for this study are shown in Figure 6.4–6.

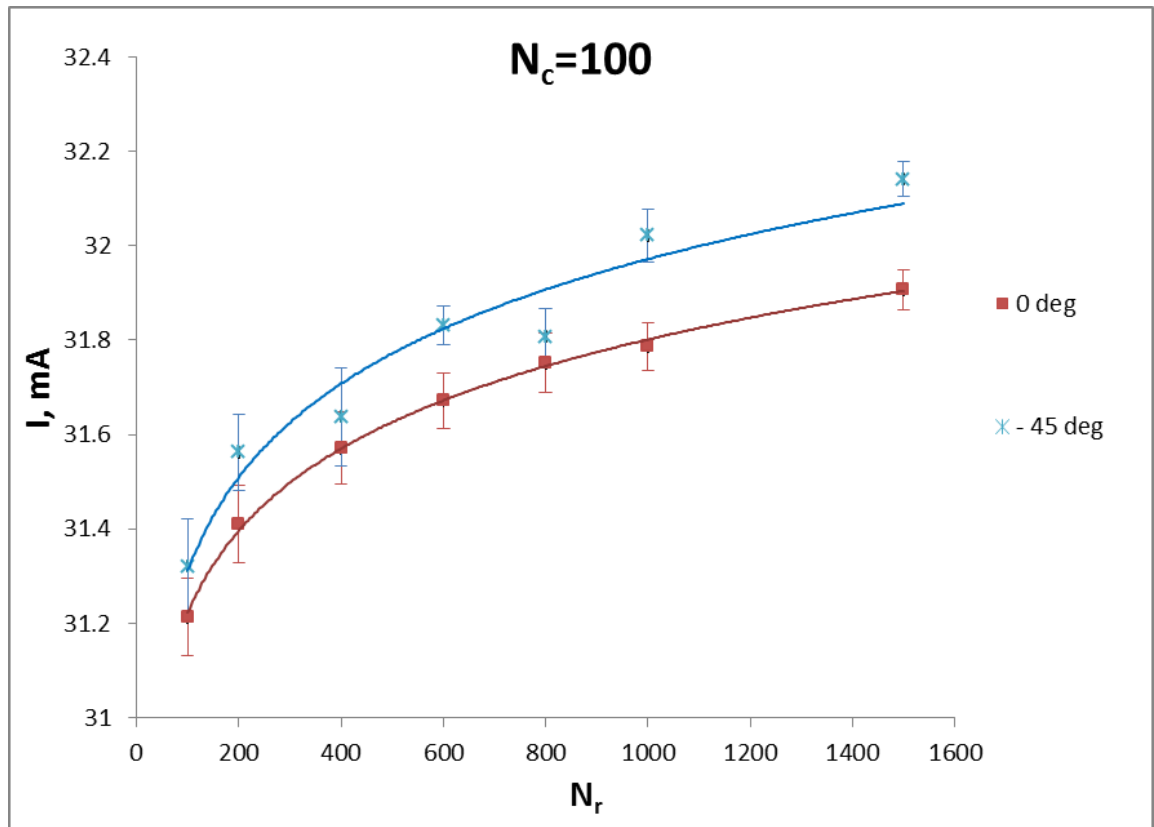


Figure 6.4–6. Dependence of current on the orientation of RBC

Some further analysis gives more details on how RBC orientation influences total current (Table 6.1). This study was aimed at seeing how current on the electrode and, therefore, impedance would change due to RBC being parallel to main planes of the coordinate system. This included 10 models with number of erythrocytes $N_r = 1500$ and number of cholesterol particles $N_c = 500$. This involved performing 4 sets of simulations: with cholesterol particles, with RBC, with mixture of both and with no particles present in the area of interest. To exclude mesh dependence, all of the simulations had the same mesh and instead of exclusion of particles, their properties are changed to those of blood base. Results were put in Table 6.1.

Table 6.1. Current values for different RBC orientation (with and without cholesterol)

mixture type RBC orientation	I, mA			
	RBC+ cholesterol	RBC	cholesterol	Empty
(YZ - plane)	31.85705	31.88651	33.67016	33.72772
o (XZ - plane)	32.21244	32.24641	33.65765	33.71294
- (XY - plane)	32.34572	32.36892	33.69326	33.75665

For presented research impedance change due to inclination varies from 0.7% for $\theta = -45^\circ$ to 1.5% for $\theta = -90^\circ$. For XZ orientation change in current value is in between the two other positioning and is equal to 1.1%.

Due to volume recalculation, cholesterol input in impedance change is getting less and less obvious and gets to the point of being of a same order as methods error (0.1%).

Frequency dependence has been tested for the tilted RBC study as well and it shows no significant influence of frequency change in the band up to 100 kHz, this is presented in Figure 6.4–7. This is expected and it agrees with research and modelling results published by other research groups.

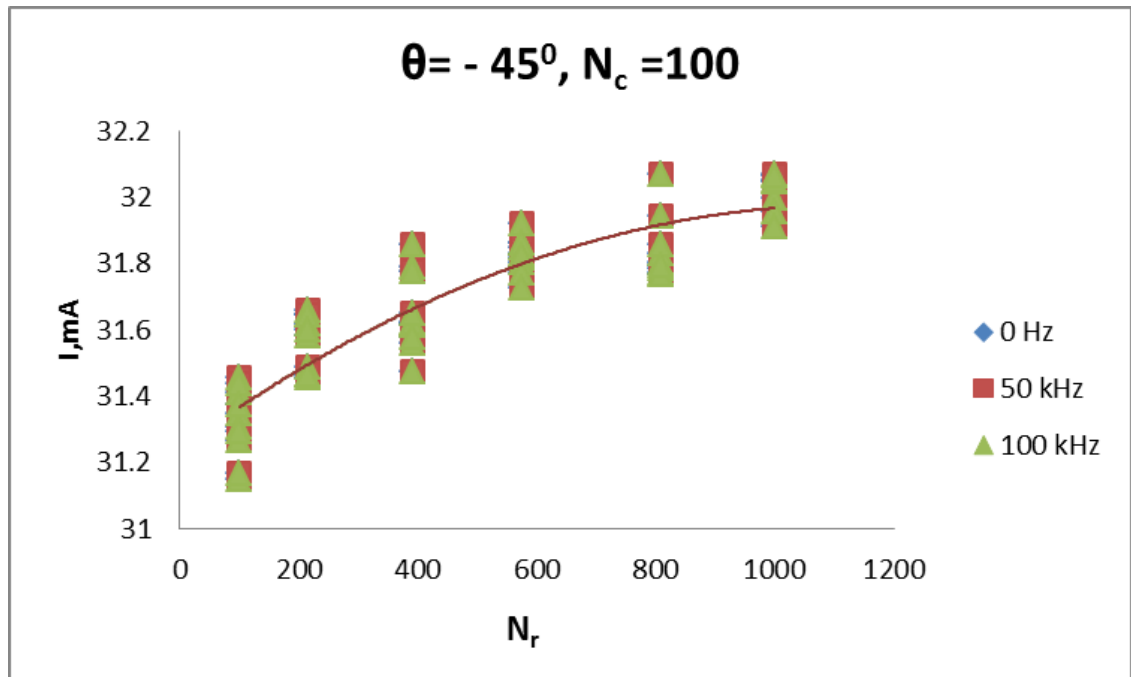


Figure 6.4–7. Dependence of current on frequency for tilted RBC

As expected, in this case RBC input in impedance will be higher, although the contrast ratio for electric properties is smaller. This means that despite of conductivity being of the same order the fact that erythrocytes occupy considerable part of the volume has a significant effect on electrical behaviour of the system.

6.4.2 Dependence of the current curve on the number of cholesterol particles

Although it has been proven in 5.2.3 that for N_c higher than 100 the change in solution is of the same order as global error of simulations, the decision has been made to test the same hypothesis for the mixture of erythrocytes and cholesterol. Results are shown in Figure 6.4–8.

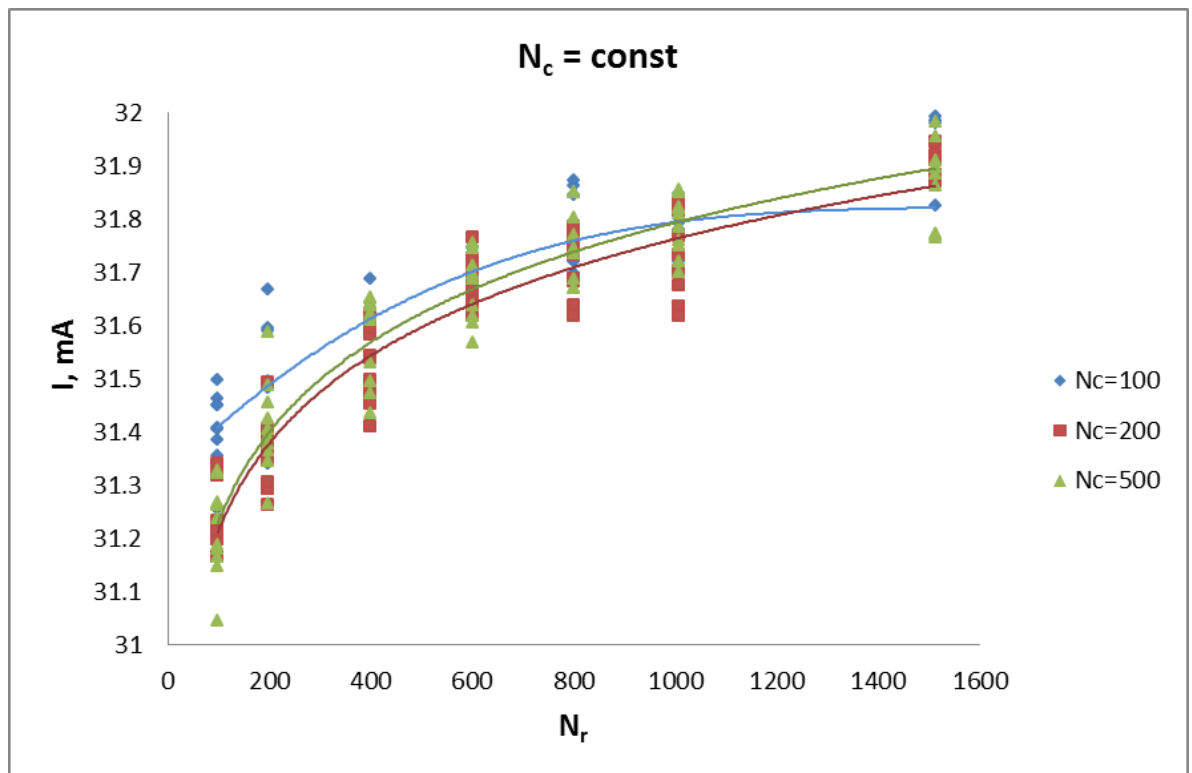


Figure 6.4–8. Dependence of current on number of RBC, N_r ; $N_c = \text{const}$

Although the change in current value is again of the same order as solution tolerance, it is preferable to finish the last set of simulations with N_c equal to 500 particles.

6.4.3 Dependence of the current curve on total cholesterol levels

The final stage of current analysis was to see how total current and hence impedance of the system would change according to different cholesterol levels. Results can be seen in Figure 6.4–9. As predicted, there is a visible difference in current that depends on cholesterol concentration. At the same time, there is a significant overlapping in dispersion for neighbouring TC levels.

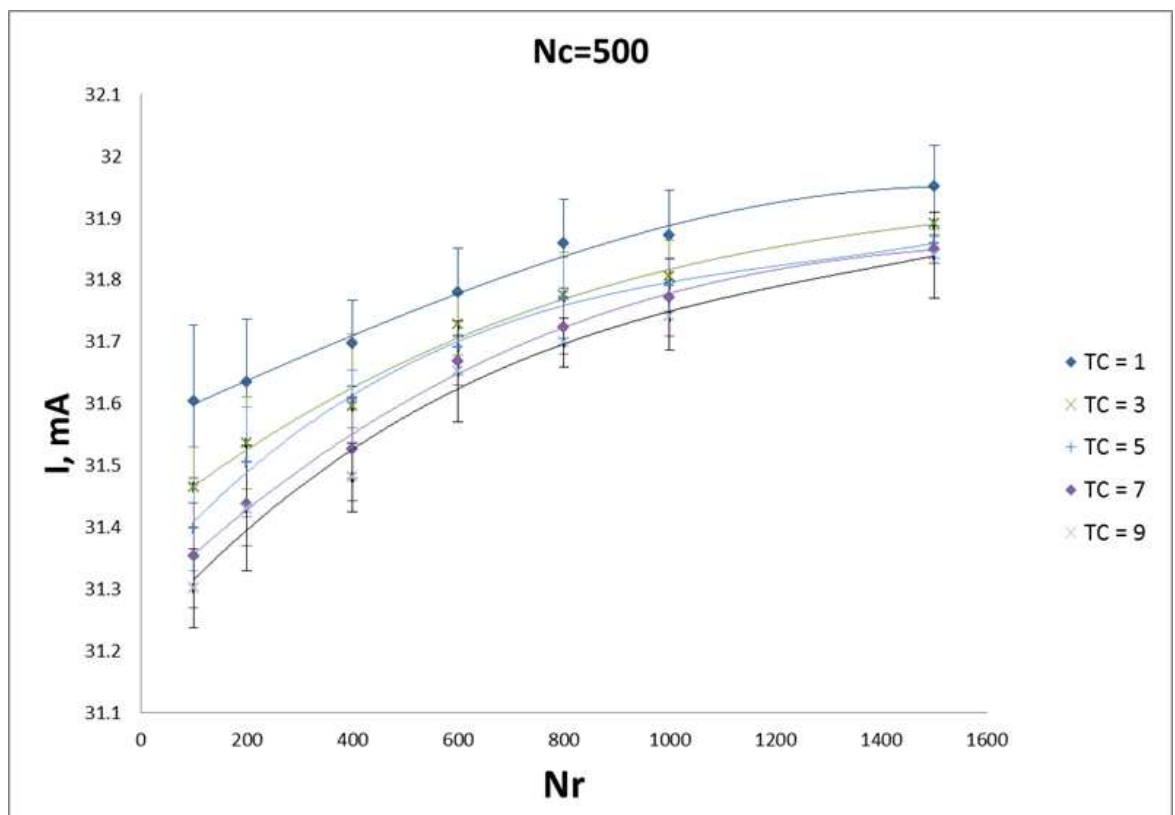


Figure 6.4–9. Dependence of total current for different cholesterol levels

It is very hard to judge if obtained results are what they are supposed to be as the difference between any two close levels is not equal in terms of volume. So more of simulations have been carried out. This has been done for total cholesterol levels of 1, 2, 4 and 8 mmol/l and fixed number of erythrocytes and cholesterol particles, that is equal to 1500 and 500 respectively. In that case

values of current and hence impedance should be equidistant. Figure 6.4–10 illustrates this fact.

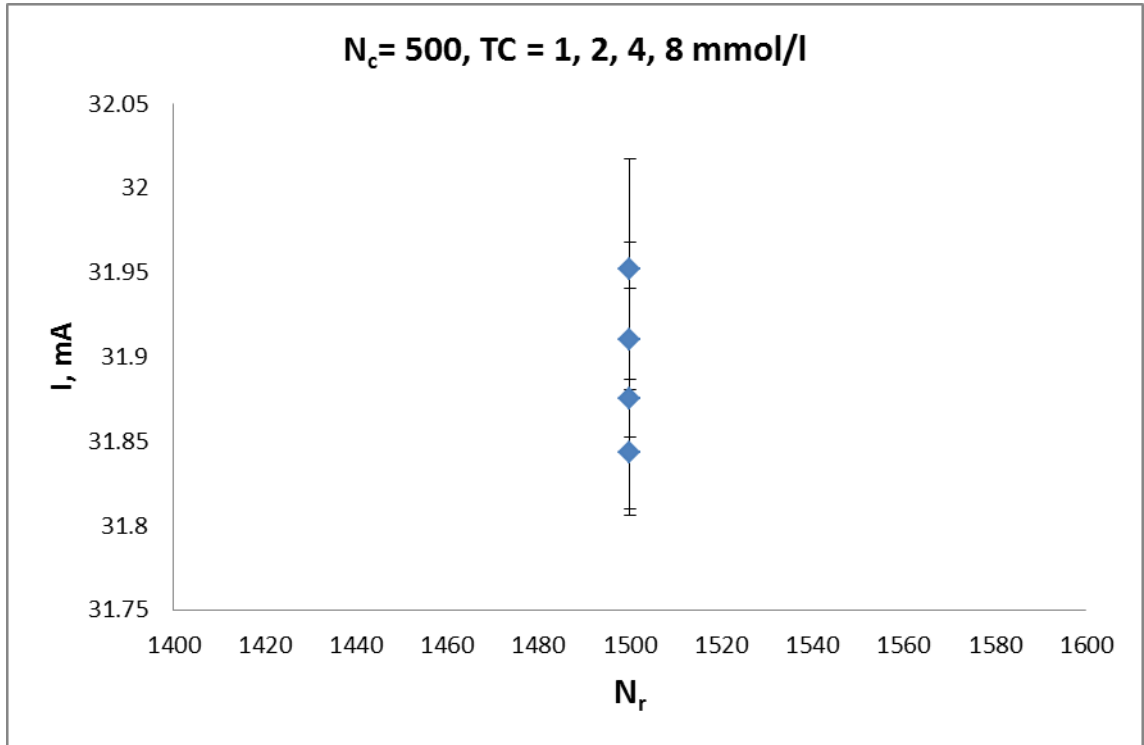


Figure 6.4–10. Values of current for total cholesterol concentrations 1, 2, 4, and 8 mmol/l

Dynamics of mean current value decrease with increase in total cholesterol level is shown in Figure 6.4–11.

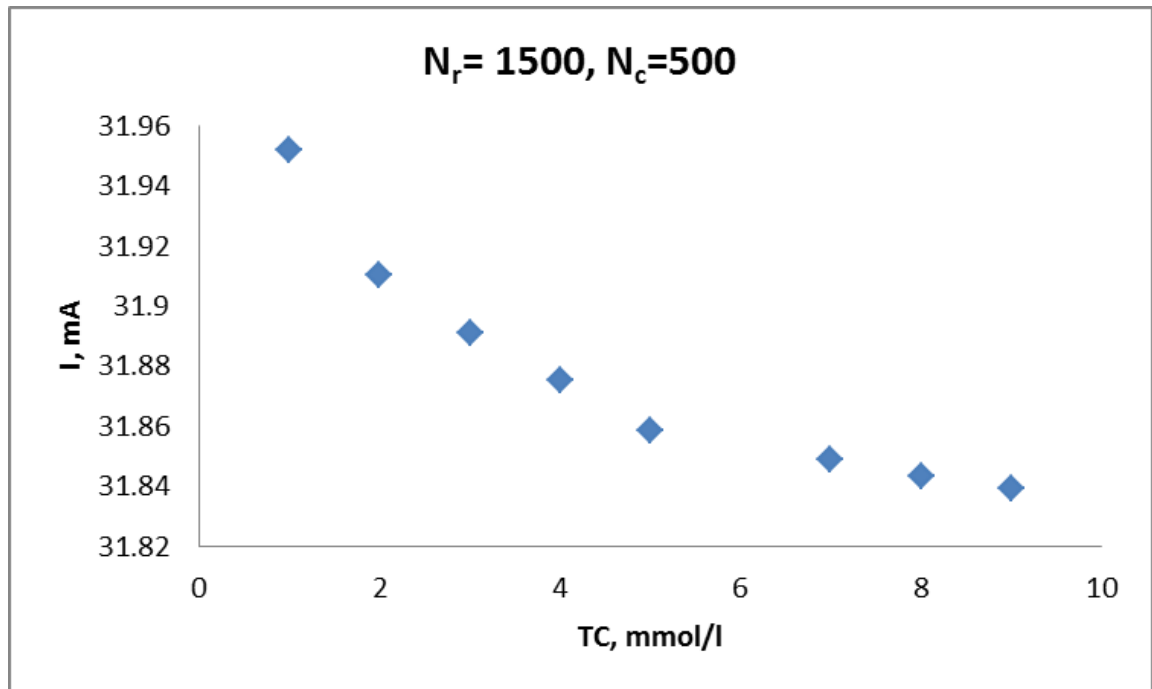


Figure 6.4–11. Average values of current for different cholesterol levels

As expected, there is a steady decrease in current level with increase of total volume, occupied by cholesterol. These results confirm that electrical impedance of blood is a quantity that can be used to determine cholesterol levels in human blood.

There was no experiment set to mimic mathematical model present in this research. And although RBC related results are in good agreement with modelling and experimental results obtained elsewhere (see 6.3), there were still concerns about the way electrodes were modelled.

As explained in Chapter 4 and Chapter 5, electrodes were modelled as hollows to avoid necessity of choosing electrode material at that stage.

Chapter 7. Validation of some of the FE modelling results against simple experimental data

In order to validate the modelling methodology for electrode modelling developed in this work some of the experiments conducted on blood conductivity at City University London were simulated and the results compared. In the experimental study, a 4-electrode system was used in which four electrodes were placed side by side on a non-conducting base plate and immersed in the blood (horse blood) volume to be measured. The two outer acted as the 'driving electrodes' (to which voltage was applied) and the impedance was measured between the two inner electrodes ('measuring electrodes').

Some of the experimental studies conducted using the above set up was simulated using the FE models developed in this work shown in Figure 7–1 (a) and (b). Here the electrodes are positioned 1 mm apart, have a depth, $a = 0.1$ mm, height, $h = 10$ mm and width, $b = 0.5$ mm.

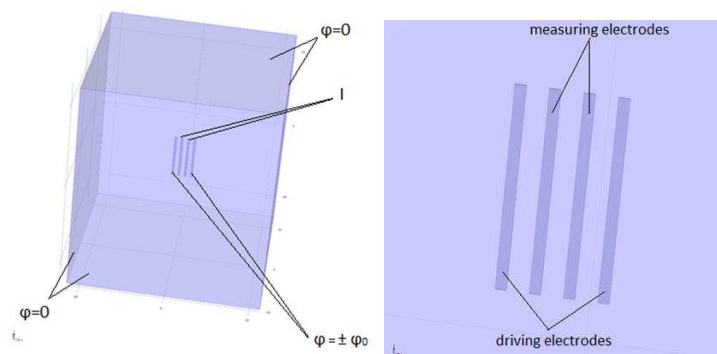


Figure 7–1 (a) computational model of the experimental set-up and (b) details of electrode placement.

Validation of some of the FE modelling results against simple experimental data

All of the outside boundaries are given potential $\phi = 0$, and placed far enough so that they do not affect the field lines nearer to the electrodes. Outer electrodes were set potential $\phi = \pm 5$ V. In addition, inner electrodes are assigned with floating potential.

This is not a trivial problem since it has no straightforward analytical solution.

To simplify the task an additional model was created which was similar to the experimental set up except for the electrodes which, unlike in the experimental set up were placed facing each other (rotated by 90°). This can be seen in Figure 7–1. Here the electrodes are kept 1mm apart.

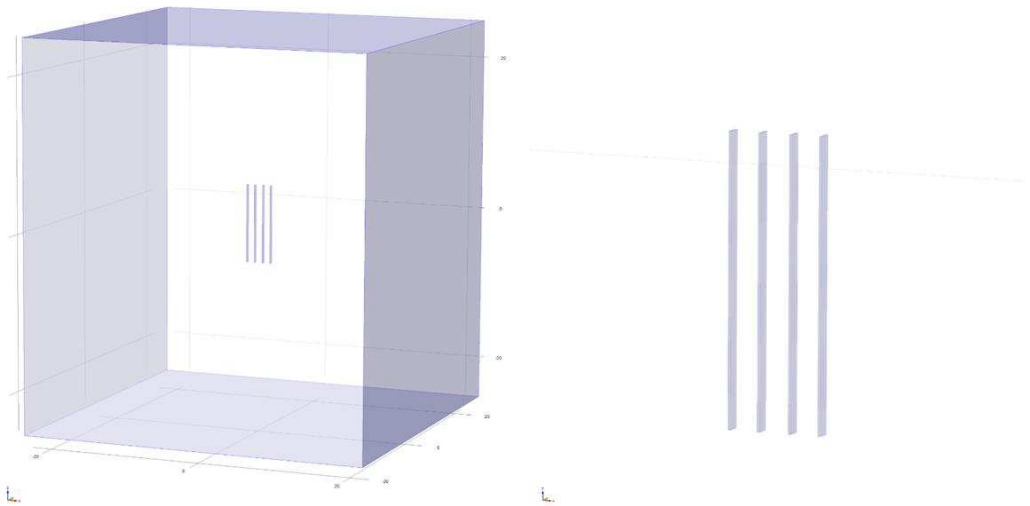


Figure 7–2 (a) additional 3D model and (b) close-up showing details

The first thing that needs to be checked is potential line distribution. As there is no fixed potential on the inner electrodes, care should be taken. Surface of each electrode should be equipotential surface and that can be done by assigning them with appropriate properties. This was done by choosing floating potentials. Resulting potential line distribution can be seen in Figure 7–3.

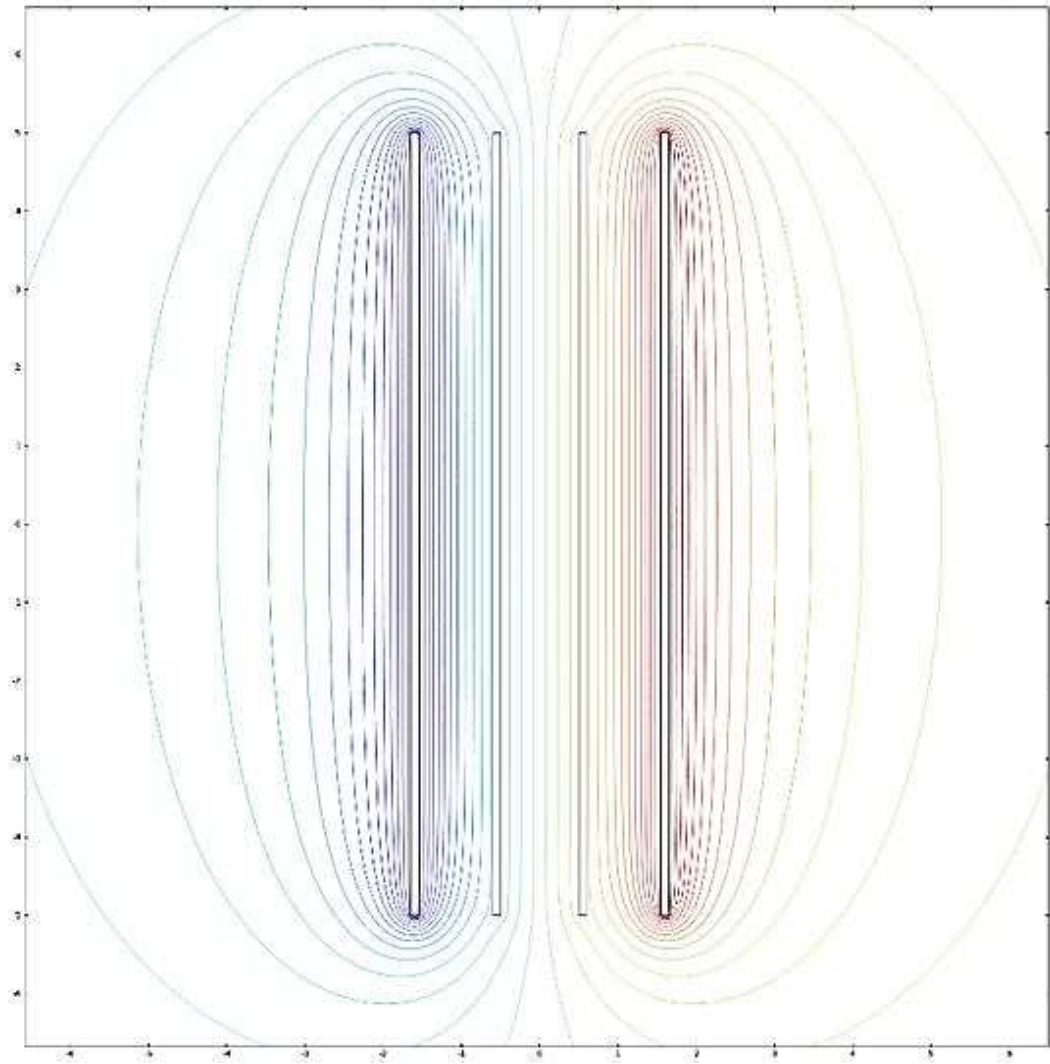


Figure 7–3 Distribution of electric potential lines for electrodes placed facing each other

The condition of equipotential surfaces is satisfied and this can be clearly seen along the cut line going through the centre of xz -plane ($y=0$). This is illustrated below (Figure 7–4).

Validation of some of the FE modelling results against simple experimental data

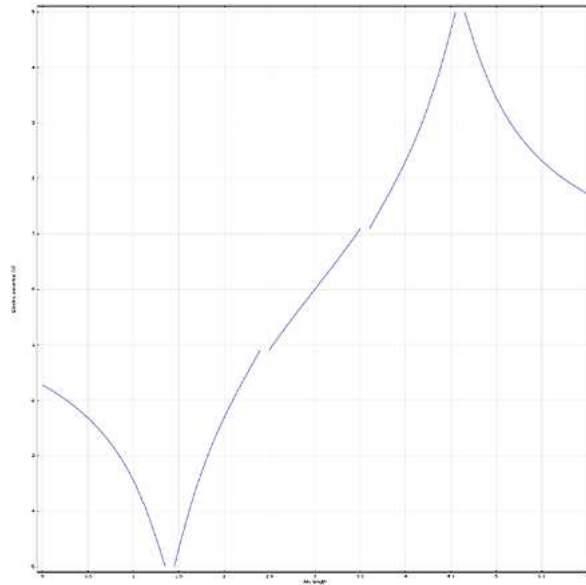


Figure 7–4 Potential distribution along the cut-line ($x=[-5,5]$, $z=0$).

After that, current distribution is checked to see how it flows within the volume of interest ().

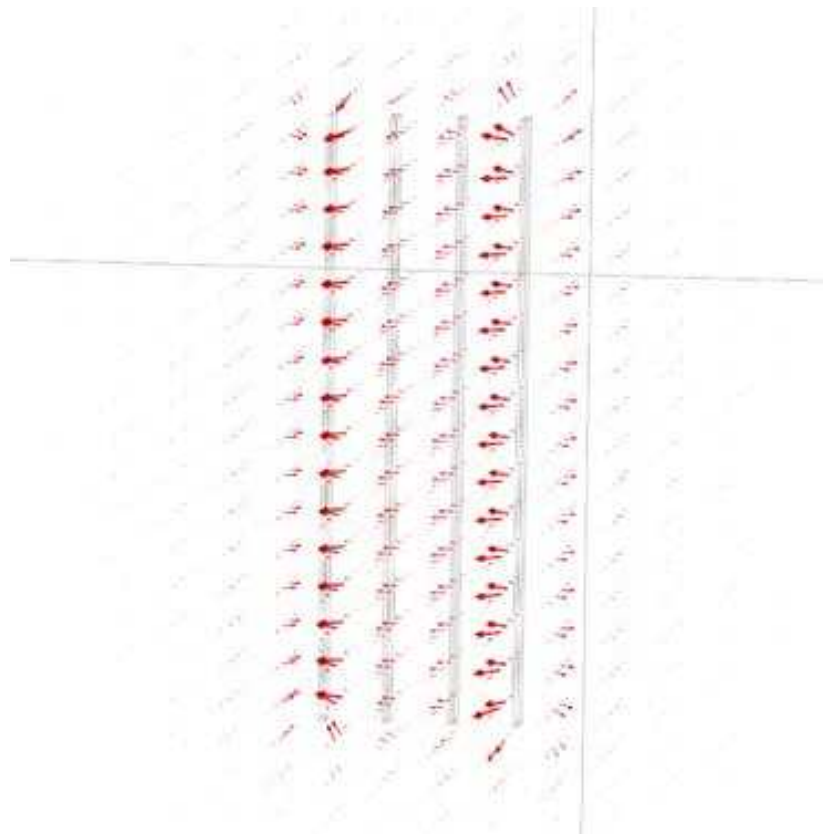


Figure 7–5 Current distribution.

Validation of some of the FE modelling results against simple experimental data

Once this has been done, impedance is calculated using material properties, electrode surface area and distance between the electrodes:

$$Z_{theor} = \frac{d}{\sigma \cdot A} = 285 \text{ Ohm} \quad (7-1)$$

This result is compared with impedance value that can be calculated from potential and current values calculated with COMSOL:

$$Z = \frac{V}{I} = \frac{2.178 \text{ V}}{8.67 \text{ mA}} = 251 \text{ Ohm} \quad (7-2)$$

The theoretical value of impedance exceeds computed by 13.5%. This difference can be attributed to it being a 3D problem.

As results are comparable, the initial model is now considered. Same set of graphs is printed for that model (Figure 7–6, Figure 7–7, Figure 7–8).

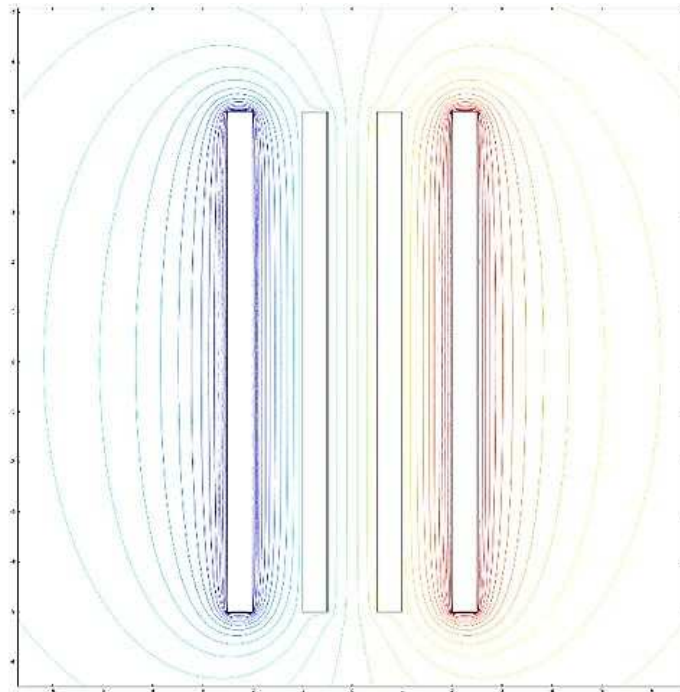


Figure 7–6 Potential distribution between the flat electrodes

Validation of some of the FE modelling results against simple experimental data

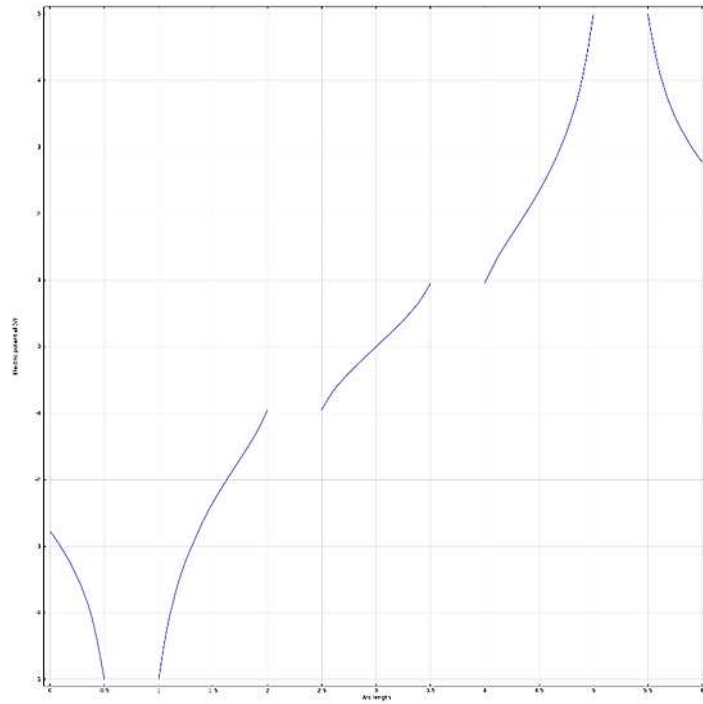


Figure 7–7 Potential distribution along the cut-line for flat electrodes

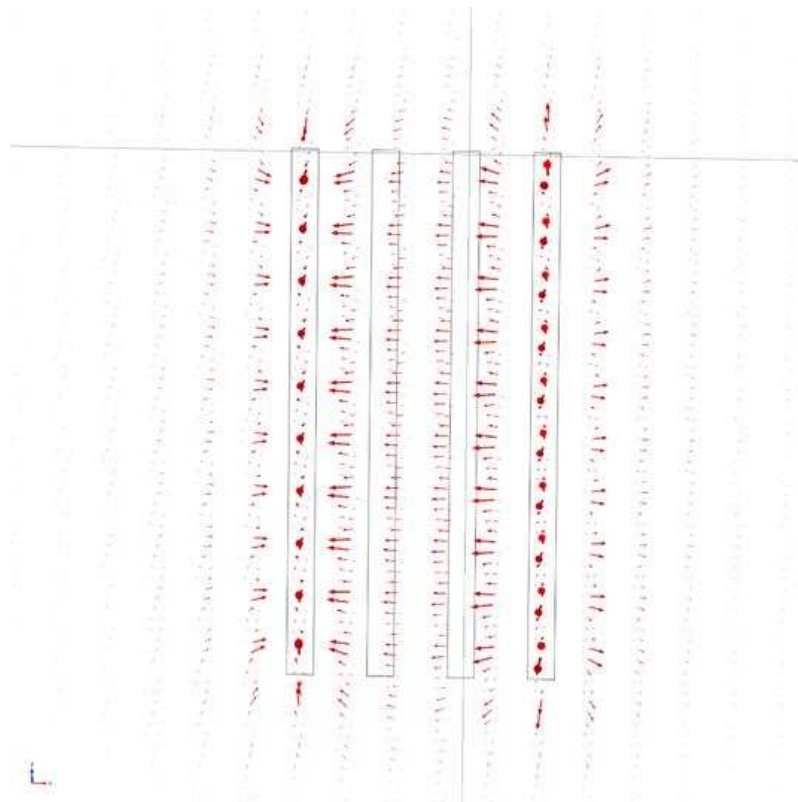


Figure 7–8 Current distribution for flat electrode positioning.

However, calculation of impedance in this study is tricky because potential difference on the driving electrodes will have a significant input into impedance

Validation of some of the FE modelling results against simple experimental data of the system. To measure this contributes a perpendicular plane has been put in the system. It is representing the plane, current flows through (Figure 7–9).

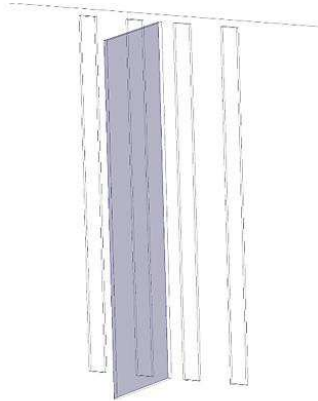


Figure 7–9 Cut plane for flat electrode positioning

When driving electrodes are assigned with potential, resulting current through the cut plane is $I = 11.9 \text{ mA}$. Potential on measuring electrodes is then equal to $\varphi = \pm 0.951 \text{ V}$

When the driving electrodes kept at $\varphi = 0$ (Figure 7–10, Figure 7–11) and driving electrodes are assigned with potential found from previous model, total current through the plane is $I = 7.33 \text{ mA}$.

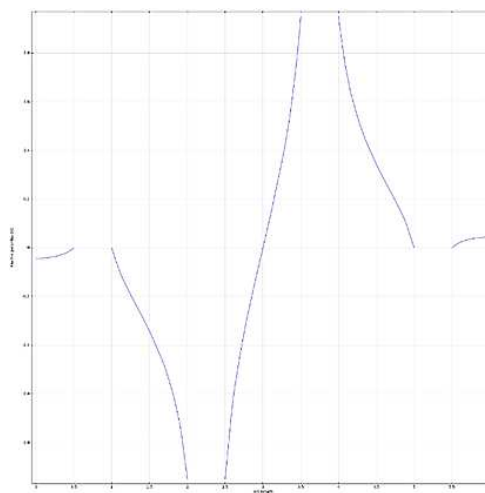


Figure 7–10 Potential distribution for flat electrode positioning, driving electrodes switched off.

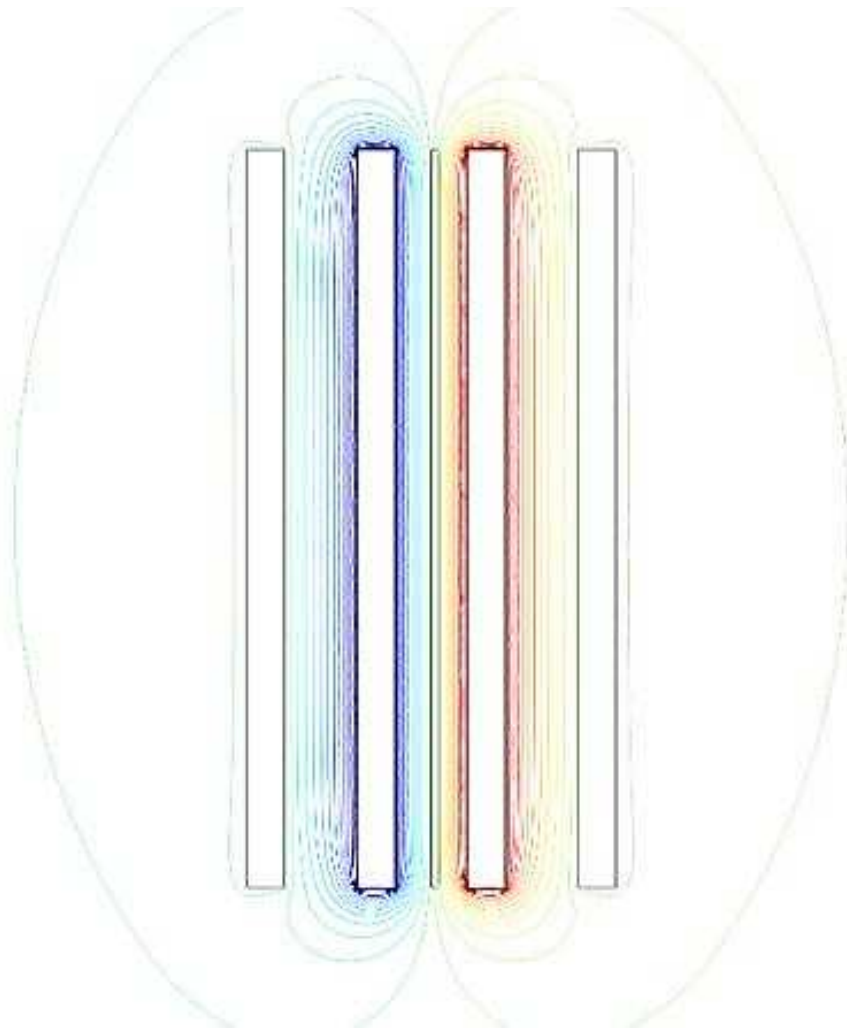


Figure 7–11 Potential lines for flat electrode positioning with switched off electrodes.

This gives resulting impedance $Z = 259 \text{ Ohm}$. This is comparable with experimental results $Z_{\text{exp}} = 250 \text{ Ohm}$. The difference does not exceed 3.6%. This proves that methodology used for electrode modelling gives correct results and can be used for future modelling. This can be done not only within this research, but also in other studies where electrode material is not known.

This completes the set of tests that were undertaken in current research project, which summarizes most important physical and electrical parameters and effects, which determine and influence behaviour of experimental system. At that point, conclusions and further work can be summed up.

Chapter 8. Conclusions and further work

8.1 Conclusions

The possibility and the need for creation of a non-invasive cholesterol measurement device have been discussed. Impedance was taken as a parameter to be measured. As a result of this research, methodologies for human blood modelling and electrode modelling were developed. Tested and validated where possible.

The following aims with corresponding objectives have been achieved.

Aim 1 Justify necessity of new method for cholesterol level measurement. This included:

- a) *Analysis of all existing methods.* It was done in Chapter 1. This included highlighting their advantages and disadvantages.
- b) *In depth understanding of current routine test process.* This included detailed studies of biochemistry books on current blood test methods. It also included visit to biochemistry lab at Whittington Hospital (Whittington Health NHS, London)
- c) *Sought clinician's opinion on proposed method.* Opinion was sought from biochemistry lab staff, medical students, midwife and a GP. All of them concluded that proposed method would ease their work, by minimizing possibility of human error and time needed for obtaining test results.

Aim 2 Development of appropriate methodologies for mathematical modelling and simulation of penetration of electric field and distribution of electric

current and potential in living tissues. This was linked with following objectives:

- a) *Develop 2D realistic finite element (FE) models.* Development of appropriate methodologies for mathematical modelling and simulation of penetration of electric field and distribution of electric current and potential in living tissues has been done.
- b) *Develop 3D realistic finite element (FE) models.* Same methodologies have been used for 3D modelling. For 3D models effect of fringing has been quantified. As it is one of the main issues arising with two electrode system, it needs to be addressed in case experimental prototype will be made.

Aim 3 Investigate the distribution of alternating currents and electric potential in developed FE models. This was achieved through the following objectives:

- a) *Use various physiological properties in FE models developed in Aim1 (a) and Aim1 (b).* 2D simulations have shown that it is possible to distinguish between two close cholesterol levels values and that it is possible to model cholesterol as a set of associations of cholesterol molecules. 3D simulations have shown that although it is still possible to distinguish between two close cholesterol levels values, the difference gets significantly smaller (e.g. for TC 3 and 5 it decreases from 3% to 1.3%)
- b) *Change of material properties.* Further increase in complexity of the model (by introduction of red blood cells) makes differentiation even harder, as multiple effects related to them occur (such as orientation and concentration dependence).
- c) *Change of electrical parameters.* Frequency analysis has shown that for proposed frequencies, changes in current value are not dependant on frequency.

Aim 4 Establish functional relationship between calculated currents on measuring electrodes (hence impedance values) and concentration of cholesterol in the blood. Objective related to this aim is:

- a) *For a given voltage drop, this is done by advanced biomedical signal processing of potential signals calculated by FE modelling.* It has been proven that in all cases current is a quantity to be measured as it gives the impedance of the system because there is a linear relation between voltage, current and impedance

Nevertheless, modelling results conducted in this work have shown that it is possible to discriminate total cholesterol levels in human blood ranging from 1 to 9 mmol/L by impedance technique.

8.2 Contribution to the original work

Methodologies developed in this research can be used in other fields involving electromagnetic simulations.

Particle coagulation technique can successfully replace effective conductivity modelling method. It can be used in electromagnetic simulations of less conductive particles suspended in conductive solvent. It was proven that this methodology works in cases where conductivity ratio $\sigma_{\text{solv}}/\sigma_{\text{part}} > 2$ and simplifies system significantly for ratio >70 . It was also tested on modelling of non-spherical particles and has been proven to work well in case of all particles having the same incline angle.

The other technique that was used in this research allows simplifying electrode modelling. Electrodes were modelled as hollows. This means there is no need to choose specific electrode material. It also helps to overcome problem some of the software faces while modelling metal electrodes.

8.3 Further work

Although blood models at this stage include only two types of particles, nevertheless the methodologies developed in this work can simulate human blood taking into account its major component, the RBC. The analyses reported here represent two extreme cases. One of them is suspension of small quantities of non-conductive particles (cholesterol) with high electric properties contrast ratio. The other one is focused on large quantities of particles with smaller contrast ratio (RBC). There is a need to make it more complicated by adding components that have small contrast ratio and are present in small quantities in the blood (such as WBC, under 1%) and performing further frequency analysis to find out what effect do other components of the realistic blood system have on the impedance of our system (such as other types of blood cells, skin, skin-electrode contact gel).

Despite of the fact that all of the electric parameters for modelling have been taken from experimental data obtained by other research groups, the main problem is that there is no agreement on one set of values and a whole range of values can be found in literature. So to get more realistic results an experimental validation is still needed with parameters of separate components that can be measured in the lab and then put together in a mixture, for which computational modelling is made.

As the field spreads outside of the volume of interest impedance will be influenced not only by cholesterol particles inside but on the outside as well, quantification of this effect needs to be done alongside with experimental validation.

And finally yet importantly, the effect of cholesterol deposited in the skin (used by PreVu diagnostic system) on total impedance of the system needs to be quantified.

Bibliography

- [1] E. T. Bairaktari, K. I. Seferiadis, and M. S. Elisaf, "Evaluation of Methods for the measurement of low-density lipoprotein cholesterol," *J. Cardiovasc. Pharmacol. Ther.*, vol. 10, no. 1, pp. 45–54, 2005.
- [2] L. M. Baudhuina, S. J. Hartmana, J. F. O'Brien, and I. Meissnerb, "Electrophoretic measurement of lipoprotein(a) cholesterol in plasma with and without ultracentrifugation: comparison with an immunoturbidimetric lipoprotein(a) method," *Clin. Biochem.*, vol. 37, no. 6, pp. 481–488, 2004.
- [3] P. N. M. Demacker, M. Hessels, H. Toenhake-Dijkstra, and H. Baadenhuijsen, "Precipitation methods for high-density lipoprotein cholesterol measurement compared, and final evaluation under routine operating conditions of a method with a low sample-to-reagent ratio," *Clin. Chem.*, vol. 43, pp. 663–668, 1997.
- [4] M. S. Mohktar, F. Ibrahim, and N. A. Ismail, "Expert system for non-invasive classification of total cholesterol level using bioelectrical impedance," *F. Ibrahim, N. A. Abu Osman, J. Usman N. A. Kadri Biomed 06, IFMBE Proc.*, vol. 15, pp. 63–66, 2007.
- [5] B. Tender, "In vivo fluid-volume monitoring with impedance technique," 1985.
- [6] H. Scharfetter, P. Brunner, M. Mayer, B. Brandstatter, and H. Hinghofer-Szalkay, "Fat and hydration monitoring by abdominal bioimpedance analysis: data interpretation by hierarchical electrical modeling," *IEEE Trans. Biomed. Eng.*, vol. 52, no. 6, pp. 975–982, Jun. 2005.
- [7] M. Nagai, H. Komiya, Y. Mori, T. Ohta, Y. Kasahara, and Y. Ikeda, "Development of a new method for estimating visceral fat area with multi-

- frequency bioelectrical impedance,” *Tohoku J. Exp. Med.*, vol. 214, no. 2, pp. 105–112, Feb. 2008.
- [8] D. Huber, M. Talary, F. Dewarrat, and A. Caduff, “The compensation of perturbing temperature fluctuation in glucose monitoring technologies based on impedance spectroscopy,” *Med. Biol. Eng. Comput.*, vol. 45, no. 9, pp. 863–876, Sep. 2007.
- [9] A. Caduff, F. Dewarrat, M. Talary, G. Stalder, L. Heinemann, and Y. Feldman, “Non-invasive glucose monitoring in patients with diabetes: a novel system based on impedance spectroscopy,” *Biosens. Bioelectron.*, vol. 22, no. 5, pp. 598–604, Dec. 2006.
- [10] A. Caduff, M. S. Talary, M. Mueller, F. Dewarrat, J. Klisic, M. Donath, L. Heinemann, and W. A. Stahel, “Non-invasive glucose monitoring in patients with Type 1 diabetes: a Multisensor system combining sensors for dielectric and optical characterisation of skin,” *Biosens. Bioelectron.*, vol. 24, no. 9, pp. 2778–2784, May 2009.
- [11] K. N. von Kaulla, P. Ostendorf, and E. von Kaulla, “The impedance machine: a new bedside coagulation recording device,” *J. Med.*, vol. 6, no. 1, pp. 73–88, 1975.
- [12] K. I. Yamakoshi, H. Shimazu, T. Togawa, M. Fukuoka, and H. Ito, “Noninvasive measurement of hematocrit by electrical admittance plethysmography technique,” *IEEE Trans. Biomed. Eng.*, vol. 27, no. 3, pp. 156–161, Mar. 1980.
- [13] L. Mannucci, R. Redaelli, and E. Tremoli, “Effects of aggregating agents and of blood cells on the aggregation of whole blood by impedance technique,” *Thromb. Res.*, vol. 52, no. 2, pp. 143–151, Oct. 1988.
- [14] E. Leah, “Cholesterol,” *Lipidomics Gatew.*, 2009.

- [15] “High cholesterol levels by NHS’ National Health Service,” 2010.
- [16] S. John, A. V Sorokin, and P. D. Thompson, “Phytosterols and vascular disease,” *Curr Opin Lipidol*, vol. 18, no. 1, pp. 35–40, 2007.
- [17] T. H. Haines, “Do sterols reduce proton and sodium leaks through lipid bilayers?,” *Prog Lipid Res*, vol. 40, no. 4, pp. 299–324, 2001.
- [18] M. H. Ross and W. Pawlina, *Histology: a text and atlas: with correlated cell and molecular biology*, 5th ed. Philadelphia, Pa. ; London: Lippincott Williams & Wilkins, 2006, p. xvii, 906 p.
- [19] L. L. Smith, “Another cholesterol hypothesis: cholesterol as antioxidant,” *Free Radic Biol Med*, vol. 11, no. 1, pp. 47–61, 1991.
- [20] D. Weatherby and S. Ferguson, *Blood chemistry and cbc analysis: clinical laboratory testing from a functional perspective*, vol. 1. Jacksonville, OR: Vis Medicatrix Press, 2002.
- [21] W. W. Christie, *Lipid analysis: isolation, separation, identification and structural analysis of lipids*, 3rd ed. Bridgwater: Oily Press, 2003, p. xvi, 416 p.
- [22] “USDA National Nutrient Database for Standard Reference, Release 21,” *United States Dep. Agric.*, 2008.
- [23] R. G. Jensen, M. M. Hagerty, and K. E. McMahon, “Lipids of human milk and infant formulas: a review,” *Am J Clin Nutr*, vol. 31, no. 6, pp. 990–1016, 1978.
- [24] E. J. Behrman and V. Gopalan, “Cholesterol and Plants,” *J. Chem. Educ.*, vol. 82, no. 12, 2005.
- [25] A. Ascherio and W. C. Willett, “Health effects of trans fatty acids,” *Am J Clin Nutr*, vol. 66, no. 4 Suppl, p. 1006S–1010S, 1997.

- [26] J. Le Fanu, *The rise and fall of modern medicine*. London: Little, Brown, 1999, p. xxi, 490p., [16]p. of plates.
- [27] T. C. Campbell and T. M. Campbell II, *The China study: the most comprehensive study of nutrition ever conducted and the startling implications for diet, weight loss and long-term health*, 1st BenBel. Dallas, Tex.: Benbella, 2005, p. xviii, 417 p.
- [28] L. Stryer, *Biochemistry*, 4th ed. New York: W.H. Freeman, 1995, p. xxxiv, 1064 p.
- [29] P. J. Espenshade and A. L. Hughes, "Regulation of sterol synthesis in eukaryotes," *Annu Rev Genet*, vol. 41, pp. 401–427, 2007.
- [30] M. S. Brown and J. L. Goldstein, "The SREBP pathway: regulation of cholesterol metabolism by proteolysis of a membrane-bound transcription factor," *Cell*, vol. 89, no. 3, pp. 331–340, 1997.
- [31] J. M. Berg, J. L. Tymoczko, and L. Stryer, *Biochemistry*, 5th ed. New York: W.H. Freeman, 2002.
- [32] W. H. Elliott and D. C. Elliott, *Biochemistry and molecular biology*, vol. 4th. Oxford ; New York: Oxford University Press, 2009, p. 568.
- [33] O. Weingartner, T. Pinsdorf, K. S. Rogacev, L. Blomer, Y. Grenner, S. Graber, C. Ulrich, M. Girndt, M. Bohm, D. Fliser, U. Laufs, D. Lutjohann, and G. H. Heine, "The relationships of markers of cholesterol homeostasis with carotid intima-media thickness," *PLoS One*, vol. 5, no. 10, p. e13467, 2010.
- [34] G. F. Lewis and D. J. Rader, "New insights into the regulation of HDL metabolism and reverse cholesterol transport," *Circ Res*, vol. 96, no. 12, pp. 1221–1232, 2005.

- [35] D. J. Gordon, J. L. Probstfield, R. J. Garrison, J. D. Neaton, W. P. Castelli, J. D. Knoke, D. R. Jacobs Jr., S. Bangdiwala, and H. A. Tyroler, "High-density lipoprotein cholesterol and cardiovascular disease. Four prospective American studies," *Circulation*, vol. 79, no. 1, pp. 8–15, 1989.
- [36] N. B. Javitt, "Bile acid synthesis from cholesterol: regulatory and auxiliary pathways," *FASEB J*, vol. 8, no. 15, pp. 1308–1311, 1994.
- [37] A. W. Wolkoff and D. E. Cohen, "Bile acid regulation of hepatic physiology: I. Hepatocyte transport of bile acids," *Am J Physiol Gastrointest Liver Physiol*, vol. 284, no. 2, pp. G175–9, 2003.
- [38] H. U. Marschall and C. Einarsson, "Gallstone disease," *J Intern Med*, vol. 261, no. 6, pp. 529–542, 2007.
- [39] P. Gerard, P. Lepercq, M. Leclerc, F. Gavini, P. Raibaud, and C. Juste, "Bacteroides sp. strain D8, the first cholesterol-reducing bacterium isolated from human feces," *Appl Env. Microbiol*, vol. 73, no. 18, pp. 5742–5749, 2007.
- [40] J. D. Brunzell, M. Davidson, C. D. Furberg, R. B. Goldberg, B. V Howard, J. H. Stein, and J. L. Witztum, "Lipoprotein management in patients with cardiometabolic risk: consensus statement from the American Diabetes Association and the American College of Cardiology Foundation," *Diabetes Care*, vol. 31, no. 4, pp. 811–822, 2008.
- [41] P. Durrington, "Dyslipidaemia," *Lancet*, vol. 362, no. 9385, pp. 717–731, 2003.
- [42] "Detection, Evaluation and Treatment of High Blood Cholesterol in Adults (Adult Treatment Panel III) Final Report," *Natl. Institutes Heal. Natl. Hear. Lung Blood Institute.*, 2008.

- [43] W. A. van der Steeg, I. Holme, S. M. Boekholdt, M. L. Larsen, C. Lindahl, E. S. Stroes, M. J. Tikkanen, N. J. Wareham, O. Faergeman, A. G. Olsson, T. R. Pedersen, K. T. Khaw, and J. J. Kastelein, "High-density lipoprotein cholesterol, high-density lipoprotein particle size, and apolipoprotein A-I: significance for cardiovascular risk: the IDEAL and EPIC-Norfolk studies," *J Am Coll Cardiol*, vol. 51, no. 6, pp. 634–642, 2008.
- [44] "How Can I Lower High Cholesterol," *Am. Hear. Assoc.*, 2011.
- [45] "Good Cholesterol Foods," *Good Cholest. Foods*, 2011.
- [46] "National Institute for Health and Clinical Excellence," *Clin. Guidel. 67 Lipid Modif. London*, 2008.
- [47] T. Y. Wang, L. K. Newby, A. Y. Chen, J. Mulgund, M. T. Roe, A. F. Sonel, D. L. Bhatt, E. R. DeLong, E. M. Ohman, W. B. Gibler, and E. D. Peterson, "Hypercholesterolemia paradox in relation to mortality in acute coronary syndrome," *Clin Cardiol*, vol. 32, no. 9, pp. E22–8, 2009.
- [48] S. Lewington, G. Whitlock, R. Clarke, P. Sherliker, J. Emberson, J. Halsey, N. Qizilbash, R. Peto, and R. Collins, "Blood cholesterol and vascular mortality by age, sex, and blood pressure: a meta-analysis of individual data from 61 prospective studies with 55,000 vascular deaths," *Lancet*, vol. 370, no. 9602, pp. 1829–1839, 2007.
- [49] C. A. Burtis, E. R. Ashwood, and D. E. Bruns, *Tietz textbook of clinical chemistry and molecular diagnostics*, vol. 4th. St. Louis, Mo.: Elsevier Saunders, 2006.
- [50] C. M. Smales and D. C. James, *Therapeutic proteins: methods and protocols*, no. 308. Totowa, N.J.: Humana Press, 2005, p. xiv, 482 p.

- [51] P. Roeschlau, E. Bernt, and W. Gruber, "Enzymatic determination of total cholesterol in serum," *Z. Klin. Chem. Klin. Biochem.*, vol. 12, no. 5, p. 226, May 1974.
- [52] H. Sugiuchi, Y. Uji, H. Okabe, T. Irie, K. Uekama, N. Kayahara, and K. Miyauchi, "Direct measurement of high-density lipoprotein cholesterol in serum with polyethylene glycol-modified enzymes and sulfated alpha-cyclodextrin," *Clin. Chem.*, vol. 41, no. 5, pp. 717–723, May 1995.
- [53] H. U. Bergmeyer, *Methods of enzymatic analysis*, vol. 2d English. Weinheim; New York: Verlag Chemie; Academic Press, 1974.
- [54] R. J. Hunter, *Foundations of colloid science*, 2nd ed. New York: Oxford University Press, 2000.
- [55] W. B. Russel, D. A. Saville, and W. R. Schowalter, *Colloidal dispersions*. Cambridge University Press, 1989.
- [56] W. G. Dangerfield and D. Tarlow, "Electrophoresis of plasma lipoproteins," *Proc R Soc Med*, vol. 64, no. 9, pp. 896–899, 1971.
- [57] R. M. Carroll and L. L. Rudel, "Evaluation of a high-performance liquid chromatography method for isolation and quantitation of cholesterol and cholesteryl esters," *J. Lipid Res.*, vol. 22, no. 2, pp. 359–363, 1981.
- [58] J. R. Taylor and L. M. Lopez, "Cholesterol: point-of-care testing," *Ann. Pharmacother.*, vol. 38, no. 7–8, pp. 1252–1257, 2004.
- [59] F. Ibrahim, *3rd Kuala Lumpur International Conference on Biomedical Engineering 2006 : Biomed 2006, 11-14 December 2006, Kuala Lumpur, Malaysia*. Berlin ; [London]: Springer, 2007, p. xvi, 717 p.
- [60] J. H. Stein, W. S. Tzou, J. M. DeCara, A. T. Hirsch, E. R. Mohler 3rd, P. Ouyang, G. L. Pearce, and M. H. Davidson, "Usefulness of increased skin

- cholesterol to identify individuals at increased cardiovascular risk (from the Predictor of Advanced Subclinical Atherosclerosis study),” *Am J Cardiol*, vol. 101, no. 7, pp. 986–991, 2008.
- [61] D. Vaidya, J. Ding, J. G. Hill, J. A. Lima, J. R. Crouse 3rd, R. A. Kronmal, M. Szklo, and P. Ouyang, “Skin tissue cholesterol assay correlates with presence of coronary calcium,” *Atherosclerosis*, vol. 181, no. 1, pp. 167–173, 2005.
- [62] J. D. Kraus, *Electromagnetics*, 4th ed. McGraw-Hill, 1991, p. xix,847p.
- [63] D. K. Cheng, *Field and wave electromagnetics*, 2nd ed. Addison-Wesley, 1989, p. xvi,703p.
- [64] D. Holder, *Electrical impedance tomography: methods, history and applications*. Bristol: Institute of Physics, 2005, p. xiii,456 p.
- [65] S. Grimnes and Ø. G. Martinsen, *Bioimpedance and bioelectricity basics*, 2nd ed. London: Academic, 2008, p. xi, 471 p.
- [66] B. H. Brown, “biological and medical physics , biomedical engineering biological and medical physics , biomedical engineering,” *New York*, vol. 1st, p. 736, 1999.
- [67] G. J. Tortora and B. Derrickson, *Principles of anatomy and physiology*, 12th ed., . Hoboken, N.J.: Wiley ; [Chichester : John Wiley, distributor], 2009, p. 2 v.
- [68] J. Jin, *The finite element method in electromagnetics*, 2nd ed. New York ; [Great Britain]: John Wiley & Sons, 2002, p. xxiv, 753 p.
- [69] S. H. Yungal, *Electrical methods in geophysical exploration of deep sedimentary basins*. London: Chapman & Hall, 1996.

- [70] A. Tura, S. Sbrignadello, S. Barison, S. Conti, and G. Pacini, "Impedance spectroscopy of solutions at physiological glucose concentrations," *Biophys. Chem.*, vol. 129, no. 2–3, pp. 235–241, Sep. 2007.
- [71] A. Tura, S. Sbrignadello, D. Cianciavichia, G. Pacini, and P. Ravazzani, "A low frequency electromagnetic sensor for indirect measurement of glucose concentration: in vitro experiments in different conductive solutions," *Sensors (Basel)*, vol. 10, no. 6, pp. 5346–5358, 2010.
- [72] A. Tura, S. Sbrignadello, E. Mambelli, P. Ravazzani, A. Santoro, and G. Pacini, "Sodium concentration measurement during hemodialysis through ion-exchange resin and conductivity measure approach: in vitro experiments," *PLoS One*, vol. 8, no. 7, p. e69227, Jul. 2013.
- [73] Y. Oshima and T. Shiga, "Within-day variability of whole-body and segmental bioelectrical impedance in a standing position," *Eur. J. Clin. Nutr.*, vol. 60, no. 8, pp. 938–941, Aug. 2006.
- [74] Y. Oshima, T. Shiga, H. Namba, and S. Kuno, "Estimation of whole-body skeletal muscle mass by bioelectrical impedance analysis in the standing position," *Obes. Res. Clin. Pract.*, vol. 4, no. 1, pp. e1–e82, 2010.
- [75] M. Grossi, M. Lanzoni, A. Pompei, R. Lazzarini, D. Matteuzzi, and B. Ricco, "An embedded portable biosensor system for bacterial concentration detection," *Biosens. Bioelectron.*, vol. 26, no. 3, pp. 983–990, Nov. 2010.
- [76] M. Grossi, M. Lanzoni, A. Pompei, R. Lazzarini, D. Matteuzzi, and B. Ricco, "Detection of microbial concentration in ice-cream using the impedance technique," *Biosens. Bioelectron.*, vol. 23, no. 11, pp. 1616–1623, Jun. 2008.
- [77] M. A. Oliver, I. Gobantes, J. Arnau, J. Elvira, P. Riu, N. Grebol, and J. M. Monfort, "Evaluation of the electrical impedance spectroscopy (EIS)

- equipment for ham meat quality selection,” *Meat Sci.*, vol. 58, no. 3, pp. 305–312, Jul. 2001.
- [78] L. Guerrero, I. Gobantes, M. A. Oliver, J. Arnau, M. Dolors Guardia, J. Elvira, P. Riu, N. Grebol, and J. M. Monfort, “Green hams electrical impedance spectroscopy (EIS) measures and pastiness prediction of dry cured hams,” *Meat Sci.*, vol. 66, no. 2, pp. 289–294, Feb. 2004.
- [79] H. P. Schwan and K. R. Foster, “RF-field interactions with biological systems: Electrical properties and biophysical mechanisms,” *Proc. IEEE*, vol. 68, no. 1, pp. 104–113, Jan. 1980.
- [80] K. R. Visser, R. Lamberts, and W. G. Zijlstra, “Origin of the impedance cardiogram,” in *Proceedings of the Annual International Conference of the IEEE Engineering in Medicine and Biology Society*, 1988, pp. 763–765 vol.2.
- [81] S. S. Rao, *The finite element method in engineering*, 4th ed. Oxford: Butterworth-Heinemann, 2005, p. 688 p.
- [82] O. C. Zienkiewicz, R. L. Taylor, and J. Z. Zhu, *The finite element method : its basis and fundamentals*, vol. 6th ed. Amsterdam London: Elsevier Butterworth-Heinemann, 2005.
- [83] “Online: www.comsol.com,” 2013.
- [84] Y. Saad and M. H. Schultz, “GMRES: a generalized minimal residual algorithm for solving nonsymmetric linear systems,” *SIAM J. Sci. Stat. Comput.*, vol. 7, no. 3, pp. 856–869, 1986.
- [85] T. Fahey and R. Rolph, “Venous and capillary blood hematocrit at rest and following submaximal exercise,” *Eur. J. Appl. Physiol. Occup. Physiol.*, vol. 34, no. 1, pp. 109–112, 1975.

- [86] P. S. Bachorik, R. Rock, T. Cloey, E. Treciak, D. Becker, and W. Sigmund, "Cholesterol screening: comparative evaluation of on-site and laboratory-based measurements," *Clin Chem*, vol. 36, no. 2, pp. 255–260, 1990.
- [87] Z. Y. Chang, G. M. Pop, and G. M. Meijer, "A comparison of two- and four-electrode techniques to characterize blood impedance for the frequency range of 100 Hz to 100 MHz," *IEEE Trans Biomed Eng*, vol. 55, no. 3, pp. 1247–1249, 2008.
- [88] S. H. Khan and F. Abdullah, "Finite element modelling of multielectrode capacitive systems for flow imaging," *Iee Proc. G Circuits, Devices Syst.*, vol. 140, no. 3.
- [89] E. C. Texter, F. G. Hirsch, F. E. Horan, L. A. Wood, C. Ballard, I. S. Wright, D. Starr, and B. P. Blandin, "The electrical conductivity of blood: II. relation to red cell count," *Am. Soc. Hematol. Blood*, pp. 1036–1048, 2010.
- [90] F. G. Hirsch, E. C. Texter, L. A. Wood, W. C. Ballard, F. E. Horan, I. S. Wright, C. Frey, D. Starr, and D. Ph, "The electrical conductivity of blood: I. relationship to erythrocyte concentration," *Am. Soc. Hematol. Blood*, pp. 1017–1035, 2010.
- [91] W. Ganong, *Review of medical physiology*, vol. 17th. London: Prentice-Hall International, 1995.
- [92] J. C. Maxwell and J. J. Thomson, *A treatise on electricity and magnetism*, 3d ed. Oxford,: Clarendon, 1892.
- [93] B. He, "Modeling & Imaging of Bioelectrical Activity - Principles and Applications."
<http://www.springer.com/engineering/biomedical+engineering/book/978-0-306-48112-3>.

- [94] R. W. Sillars, "The properties of a dielectric containing semiconducting particles of various shapes," *Inst. Electr. Eng. - Proc.*, vol. 12, no. 35, pp. 139–155, 1937.
- [95] M. H. Boyle, "The electrical properties of heterogeneous mixtures containing an oriented spheroidal dispersed phase," *Colloid Polym. Sci.*, vol. 263, no. 1, pp. 51–57, 1985.
- [96] H. Fricke, "The Maxwell-Wagner Dispersion in a Suspension of Ellipsoids," *J. Phys. Chem.*, vol. 57, no. 9, pp. 934–937, 1953.
- [97] D. K. Stiles and B. Oakley, "Simulated characterization of atherosclerotic lesions in the coronary arteries by measurement of bioimpedance," *IEEE Trans Biomed Eng.*, vol. 50, no. 7, pp. 916–921, 2003.
- [98] G. Lee, *Advances in Automation and Robotics, Vol.1: Selected papers from the 2011 International Conference on Automation and Robotics (ICAR 2011), Dubai, December 1-2, 2011 (Google eBook)*, vol. 2011. Springer, 2011, p. 684.
- [99] K. W. Horch and G. S. Dhillon, "Neuroprosthetics: Theory and Practice -," 1988.
<https://www.google.co.uk/search?q=Neuroprosthetics:+Theory+and+Practice&btnG=Search+Books&tbn=bks&tbo=1>.
- [100] M. Akay, Ed., *Wiley Encyclopedia of Biomedical Engineering*. Hoboken, NJ, USA: John Wiley & Sons, Inc., 2006.
- [101] A. J. Fenn, *Breast Cancer Treatment by Focused Microwave Thermotherapy*. Jones & Bartlett Learning, 2006, p. 216.
- [102] E. Aristovich and S. H. Khan, "Non-invasive measurement of cholesterol in human blood by impedance technique: an investigation by 2D finite

- element field modelling,” *J. Phys. Conf. Ser.*, vol. 459, p. 012030, Sep. 2013.
- [103] R. Gaw, “The Effect of Red Blood Cell Orientation on the Electrical Impedance of Pulsatile Blood with Implications for Impedance Cardiography,” 2010.
http://eprints.qut.edu.au/39448/1/Richelle_Gaw_Thesis.pdf.
- [104] L. A. H. Critchley, “Impedance cardiographyThe impact of new technology,” *Anaesthesia*, vol. 53, no. 7, pp. 677–684, Jul. 1998.
- [105] E. N. Marieb and K. Hoehn, *Anatomy and Physiology*. Pearson Benjamin Cummings, 2008, p. 1048.
- [106] M. L. Turgeon, *Clinical Hematology: Theory and Procedures, Volume 936*. Lippincott Williams & Wilkins, 2005, p. 570.
- [107] C. E. McLaren, G. M. Brittenham, and V. Hasselblad, “Statistical and graphical evaluation of erythrocyte volume distributions.,” *Am. J. Physiol.*, vol. 252, no. 4 Pt 2, pp. H857–66, Apr. 1987.
- [108] G. Knight and A. Blann, *Haematology*. Oxford University Press, 2010, p. 384.
- [109] J. Wan, W. D. Ristenpart, and H. A. Stone, “Dynamics of shear-induced ATP release from red blood cells.,” *Proc. Natl. Acad. Sci. U. S. A.*, vol. 105, no. 43, pp. 16432–7, Oct. 2008.
- [110] D. L. Diesen, D. T. Hess, and J. S. Stamler, “Hypoxic vasodilation by red blood cells: evidence for an s-nitrosothiol-based signal.,” *Circ. Res.*, vol. 103, no. 5, pp. 545–53, Aug. 2008.

- [111] P. Ulker, L. Sati, C. Celik-Ozenci, H. J. Meiselman, and O. K. Baskurt, "Mechanical stimulation of nitric oxide synthesizing mechanisms in erythrocytes.," *Biorheology*, vol. 46, no. 2, pp. 121–32, Jan. 2009.
- [112] S. Kesava, "Red blood cells do more than just carry oxygen New findings by NUS team show they aggressively attack bacteria too," 2007. <http://www.dbs.nus.edu.sg/events/media/info/2007/dingSTsep07.pdf>.
- [113] N. Jiang, N. S. Tan, B. Ho, and J. L. Ding, "Respiratory protein-generated reactive oxygen species as an antimicrobial strategy.," *Nat. Immunol.*, vol. 8, no. 10, pp. 1114–22, Oct. 2007.
- [114] G. K. SNYDER and B. A. SHEAFOR, "Red Blood Cells: Centerpiece in the Evolution of the Vertebrate Circulatory System," *Integr. Comp. Biol.*, vol. 39, no. 2, pp. 189–198, Apr. 1999.
- [115] A. Fauci, E. Braunwald, D. Kasper, S. Hauser, D. Longo, J. Jameson, and J. Loscalzo, *Harrison's Principles of Internal Medicine, 17th Edition*. Mcgraw-hill, 2008, p. 2958.
- [116] B. Bianco, G. P. Drago, M. Marchesi, C. Martini, G. S. Mela, and S. Ridella, "Measurements of Complex Dielectric Constant of Human Sera and Erythrocytes," *IEEE Trans. Instrum. Meas.*, vol. 28, no. 4, pp. 290–295, Dec. 1979.
- [117] *Encyclopedia of Surface and Colloid Science, Volume 3*. CRC Press, 2006, p. 6675.
- [118] M. J. Loe and W. D. Edwards, "A light-hearted look at a lion-hearted organ (or, a perspective from three standard deviations beyond the norm). Part 1 (of two parts).," *Cardiovasc. Pathol.*, vol. 13, no. 5, pp. 282–92, Jan. 2004.

- [119] J. R. Cameron, J. G. Skofronick, and R. M. Grant, *Physics of the Body*. Medical Physics Publishing Corporation, 1999, p. 394.
- [120] L. Sherwood, *Human Physiology: From Cells to Systems*. Cengage Learning, 2008, p. 928.
- [121] E. Aristovich and S. Khan, "Non-invasive measurement of cholesterol in human blood by impedance technique: an investigation by 3D finite element field modelling," *J. Phys. Conf. Ser.*, vol. 450, p. 012057, Jun. 2013.
- [122] G. Steiner and E. Shafir, *Primary hyperlipoproteinemias*. New York: McGraw-Hill, Health Professions Division, 1991.

Appendix 1. Calculation of total volume of cholesterol in a given volume of blood for given total cholesterol level

The simplest way to calculate the volume of cholesterol in 1 mm³ is by using the density of cholesterol ($\rho_{chol} = 1.03 \frac{g}{cm^3}$) and its molar weight ($MW_{chol} = 3.87 * 10^2 \frac{g}{mol}$) [122]. The volume of 1 mole of cholesterol will then be:

$$V_{mol\ of\ chol} = \frac{MW}{\rho} = \frac{3.87 * 10^2 \frac{g}{mol}}{1.03 \frac{g}{cm^3}} = 3.757 * 10^5 \text{ mm}^3/mol \quad (A1-1)$$

From the definition of molar weight then volume of one cholesterol particle is:

$$V_{chol\ part} = \frac{V_{mol\ of\ chol}}{N_A} = \frac{3.75 * 10^5 \frac{mm^3}{mol}}{6.022 * 10^{23} \frac{part}{mol}} = 0.622 * 10^{-18} \text{ mm}^3 \quad (A1-1)$$

Knowing the quantity of total cholesterol ($v_{Totchol} = 5 \text{ mmol/L}$) can find the volume of cholesterol in 1 mm³:

$$\begin{aligned} V_{chol\ in\ 1\ mm^3} &= V_{mol\ of\ chol} * v_{Totchol} = \\ &= \left(3.75 * \frac{10^5 \text{ mm}^3}{mol} \right) * \left(5 * 10^{-8} \frac{mol}{mm^3} \right) = \\ &= 1.87 * 10^{-2} \text{ mm}^3 \end{aligned} \quad (A1-3)$$

Appendix 2. Software procedures for building 2D finite element models

In 2D model building looks as following

GEOMETRY1

In the **Model Builder** window, select **Model 1>Geometry 1** and change length unit to mm.

Block 1

Right-click on **Geometry 1** and select **Square**, modify **Side length** to 5, **Position>Centre** (x, y as 0).

Rectangle 1

In the **Model Builder** window, right-click **Geometry** and choose **Rectangle**. Choose rectangle settings. Locate the **Size** section. In the **Width** edit field, type 14.5. In the **Height** field, type 5. Locate the **Position** section. Select **Base** corner. In the **x** edit field, type -17.5. And in the **y** field put -2.5. Click the **Build Selected** button.

Rectangle 2

In the **Model Builder** window, right-click **Geometry** and choose **Rectangle**. Choose rectangle settings. Locate the **Size** section. In the **Width** edit field, type 15. In the **Height** field, type 7.5. Locate the **Position** section. Select **Base** corner. In the **x** edit field, type -17.5. And in the **y** field put -10. Click the **Build Selected** button.

Rectangle 3

In the **Model Builder** window, right-click **Geometry** and choose **Rectangle**. Choose rectangle settings. Locate the **Size** section. In the **Width** edit field, type 15. In the **Height** field, type 7. 5. Locate the **Position** section. Select **Base** corner. In the **x** edit field, type -17.5. And in the **y** field put -2.5. Click the **Build Selected** button.

Rectangle 4

In the **Model Builder** window, right-click **Geometry** and choose **Rectangle**. Choose rectangle settings. Locate the **Size** section. In the **Width** edit field, type 5. In the **Height** field, type 7. 5. Locate the **Position** section. Select **Base** corner. In the **x** edit field, type -2.5. And in the **y** field put -2.5. Click the **Build Selected** button.

Rectangle 5

In the **Model Builder** window, right-click **Geometry** and choose **Rectangle**. Choose rectangle settings. Locate the **Size** section. In the **Width** edit field, type 5. In the **Height** field, type 7. 5. Locate the **Position** section. Select **Base** corner. In the **x** edit field, type -2.5. And in the **y** field put -10. Click the **Build Selected** button.

Mirror 1

In the **Model Builder** window, right-click **Geometry > Transforms** and choose **Mirror**. Choose mirror settings. Tick the **Keep input objects** and put into **Point on Line of Reflection** zeros. Click the **Build Selected** button.

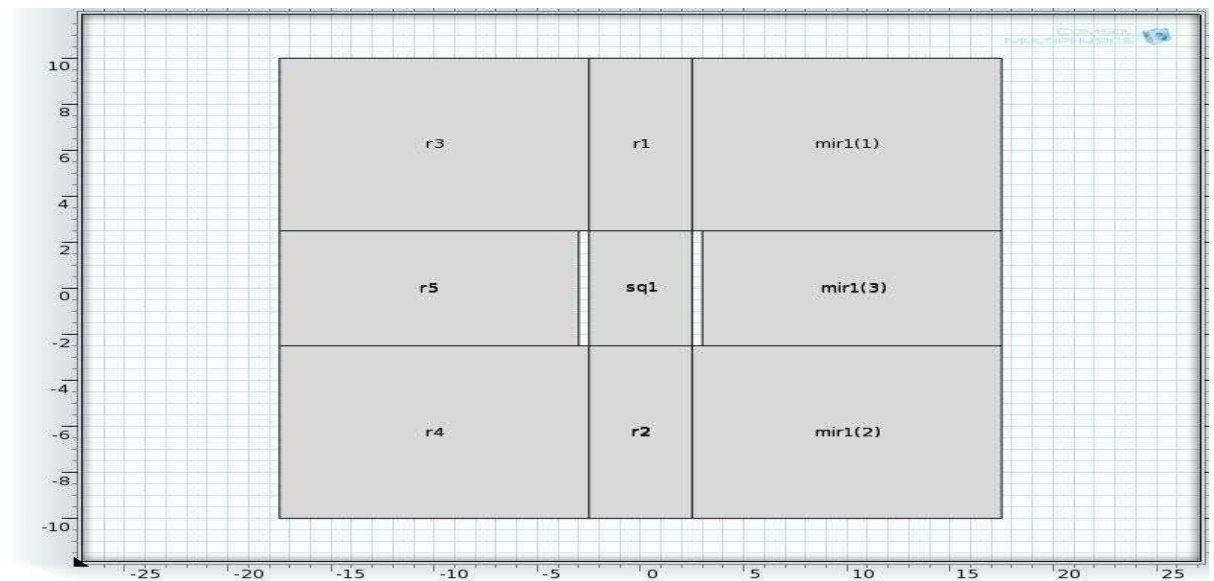


Figure A2-8.3–1 Basic model in 2D.

MAGNETIC AND ELECTRIC FIELDS

Ground1

In the **Model Builder** window, right-click **Magnetic and Electric Fields** > **Magnetic Insulation 1** and choose **Ground 1**. Select all outside boundaries.

Electric potential 1

In the **Model Builder** window, right-click **Magnetic and Electric Fields** > **Magnetic Insulation 1** and choose **Electric Potential**. Select boundaries 8, 9, 10, 13 and put **Electric potential1** value $V_0 - 1.428$. In this model electrodes are modelled as hollows, so that is why potential is applied on all four boundaries.

Electric potential 2

In the **Model Builder** window, right-click **Magnetic and Electric Fields** > **Magnetic Insulation 1** and choose **Electric Potential**. Select boundaries 20,21,23,25 and put **Electric potential2** value $V_0 1.428$.

MESH1

In the **Model Builder** window, click **Model 1>Mesh 1**. Go to the **Settings** window for Mesh. Locate the **Mesh Settings** section. Select User-controlled mesh in **Sequence type**. Right-click on **Mesh 1**, change **Element size** to custom, **Element size parameters** set as 0.5 for **Maximum element size** and 0,05 for **Minimum element size**.

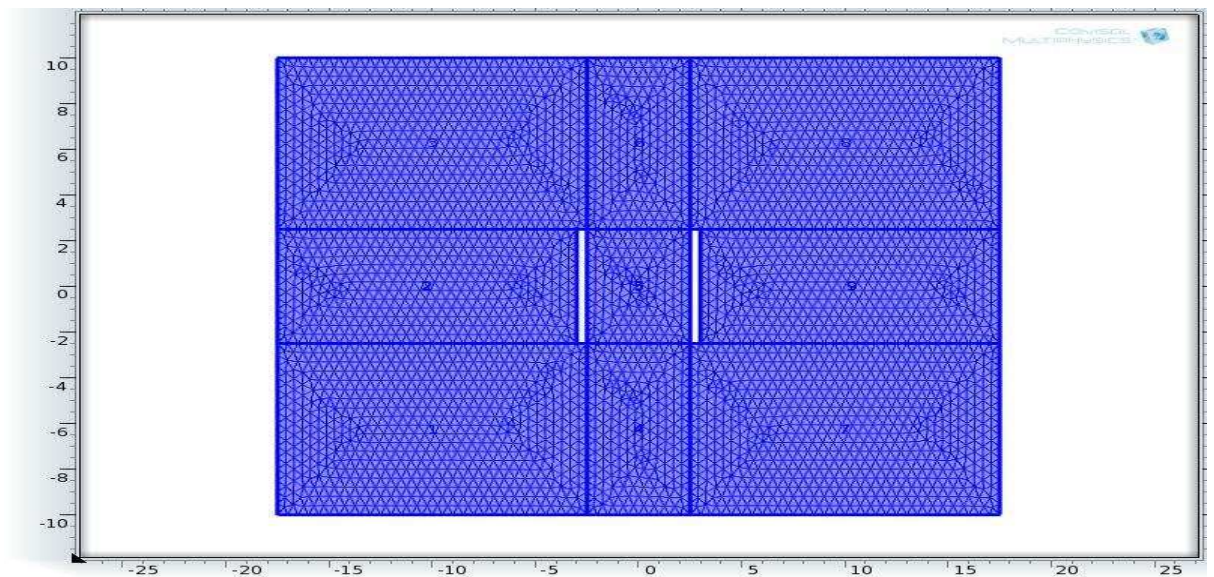


Figure A2-8.3–2 Mesh for 2D geometry.

STUDY 1

In the **Model Builder** window, select **Study 1 > Step 1: Frequency Domain**. In frequency domain settings put 50000 in **Frequencies** field. Right-click **Study 1** and choose **Compute**.

RESULTS

Right-click on **Results** and select **2D Plot Group**. Right-click on **2D Plot Group 1**, select **Surface 1** and choose electric potential (V) in **Expression**.

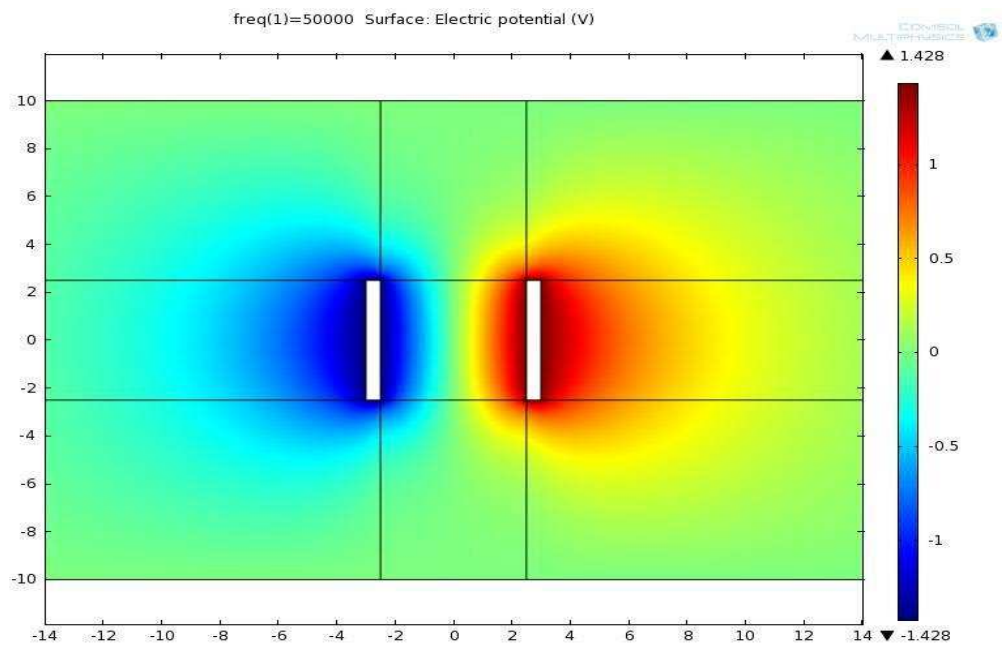


Figure A2-8.3-3 Electric potential in 2D basic model.

Appendix 3. Software procedures for building 3D finite element models

In 3D geometry building looks as following

GEOMETRY1

In the **Model Builder** window, select **Model 1>Geometry 1** and change length unit to mm.

Block 1

Right-click on **Geometry 1** and select **Block**, modify **Width**, **Depth** and **Height** changing to 5, **Position>Centre** (x, y, z as 0).

Work Plane 1

In the **Model Builder** window, right-click **Model 1>Geometry 1** and choose **Work Plane**. Go to **Settings**, locate plane as xz-plane and put **y-coordinate** as -2.5. Click the **Build Selected** button.

Rectangle 1

In the **Model Builder** window, right-click **Geometry** and choose **Rectangle**. Choose rectangle settings. Locate the **Size** section. In the **Width** edit field, type 14.5. In the **Height** field, type 5. Locate the **Position** section. Select **Base** corner. In the **x** edit field, type -17.5. And in the **y** field put -2.5. Click the **Build Selected** button.

Rectangle 2

In the **Model Builder** window, right-click **Geometry** and choose **Rectangle**. Choose rectangle settings. Locate the **Size** section. In the **Width** edit field, type

15. In the **Height** field, type 7.5. Locate the **Position** section. Select **Base** corner. In the **x** edit field, type -17.5. And in the **y** field put -10. Click the **Build Selected** button.

Rectangle 3

In the **Model Builder** window, right-click **Geometry** and choose **Rectangle**. Choose rectangle settings. Locate the **Size** section. In the **Width** edit field, type 15. In the **Height** field, type 7. 5. Locate the **Position** section. Select **Base** corner. In the **x** edit field, type -17.5. And in the **y** field put -2.5. Click the **Build Selected** button.

Rectangle 4

In the **Model Builder** window, right-click **Geometry** and choose **Rectangle**. Choose rectangle settings. Locate the **Size** section. In the **Width** edit field, type 5. In the **Height** field, type 7. 5. Locate the **Position** section. Select **Base** corner. In the **x** edit field, type -2.5. And in the **y** field put -2.5. Click the **Build Selected** button.

Rectangle 5

In the **Model Builder** window, right-click **Geometry** and choose **Rectangle**. Choose rectangle settings. Locate the **Size** section. In the **Width** edit field, type 5. In the **Height** field, type 7. 5. Locate the **Position** section. Select **Base** corner. In the **x** edit field, type -2.5. And in the **y** field put -10. Click the **Build Selected** button.

Mirror 1

In the **Model Builder** window, right-click **Geometry > Transforms** and choose **Mirror**. Choose mirror settings. Tick the **Keep input objects** and put into **Point on Line of Reflection** zeros. Click the **Build Selected** button.

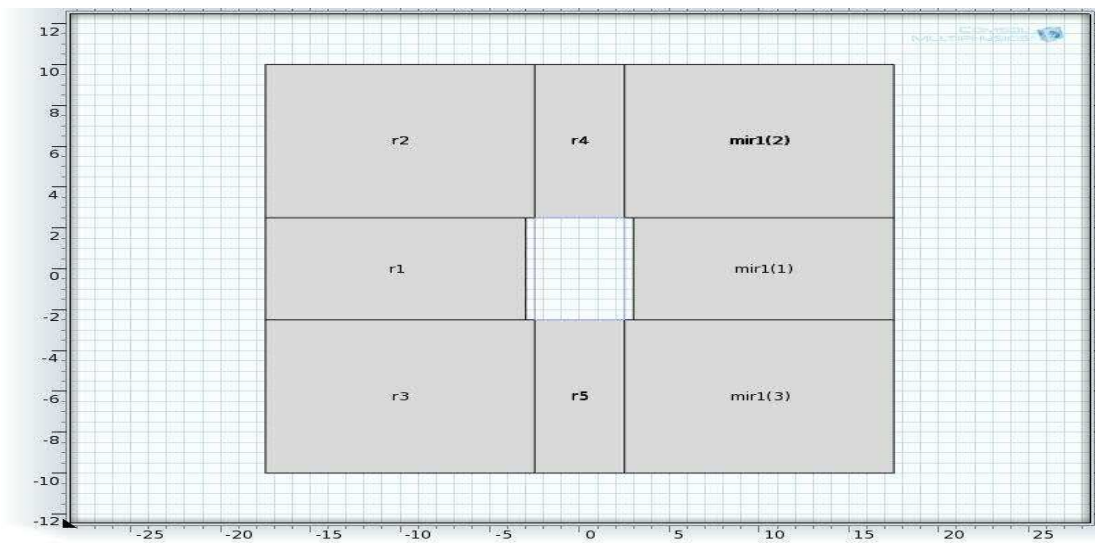


Figure A3-8.3–1 Work plane 1.

Extrude 1

Right-click on the **Work Plane 1** and select **Extrude**. In extrude settings tick the **Keep cross-sectional faces** and **Reverse directions** and put 5 into **Distances** field. Click the **Build Selected** button.

Work Plane 2

In the **Model Builder** window, right-click **Model 1>Geometry 1** and choose **Work Plane**. Go to **Settings**, locate plane as xz-plane and put **y-coordinate** as -17.5. Click the **Build Selected** button.

Rectangle 1

In the **Model Builder** window, right-click **Geometry** and choose **Rectangle**. Choose rectangle settings. Locate the **Size** section. In the **Width** edit field, type 35. In the **Height** field, type 20. Locate the **Position** section. Select **Base** corner. In the **x** edit field, type -17.5. And in the **y** field put -10. Click the **Build Selected** button.

Extrude 2

Right-click on the **Work Plane 1** and select **Extrude**. In extrude settings tick the **Keep cross-sectional faces** and **Reverse directions** and put 15 into **Distances** field. Click the **Build Selected** button.

Work Plane 3

In the **Model Builder** window, right-click **Model 1>Geometry 1** and choose **Work Plane**. Go to **Settings**, locate plane as xz-plane and put **y-coordinate** as 17.5. Click the **Build Selected** button.

Rectangle 1

In the **Model Builder** window, right-click **Geometry** and choose **Rectangle**. Choose rectangle settings. Locate the **Size** section. In the **Width** edit field, type 35. In the **Height** field, type 20. Locate the **Position** section. Select **Base** corner. In the **x** edit field, type -17.5. And in the **y** field put -10. Click the **Build Selected** button.

Extrude 2

Right-click on the **Work Plane 1** and select **Extrude**. In extrude settings tick the **Keep cross-sectional faces** and put 15 into **Distances** field. Click the **Build Selected** button.

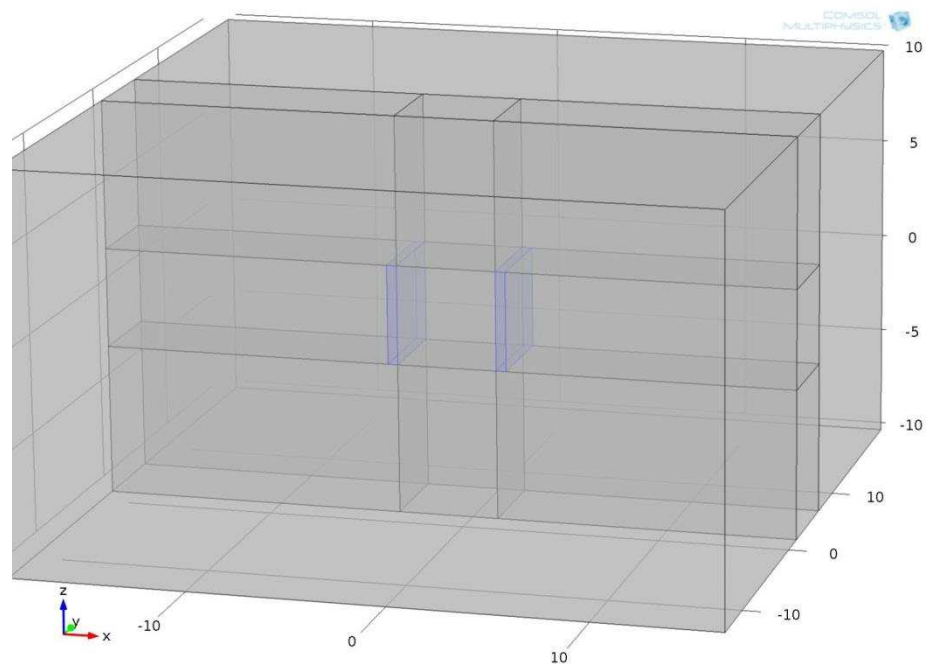


Figure A3-8.3–2 Geometry.

MAGNETIC AND ELECTRIC FIELDS

Electric potential 1

In the **Model Builder** window, right-click **Magnetic and Electric Fields > Magnetic Insulation 1** and choose **Electric Potential**. Select boundaries 22-26, 30 and put **Electric potential** value V_0 1.428. In this model electrodes are modelled as hollows, so that is why potential is applied on all six boundaries.

Electric potential 2

In the **Model Builder** window, right-click **Magnetic and Electric Fields > Magnetic Insulation 1** and choose **Electric Potential**. Select boundaries 43, 44, 45, 48, 51, 53 and put **Electric potential** value V_0 -1.428.

MESH1

In the **Model Builder** window, click **Model 1>Mesh 1**. Go to the **Settings** window for Mesh. Locate the **Mesh Settings** section. From the **Element size** list, select **Extra Fine**. Click the **Build All** button.

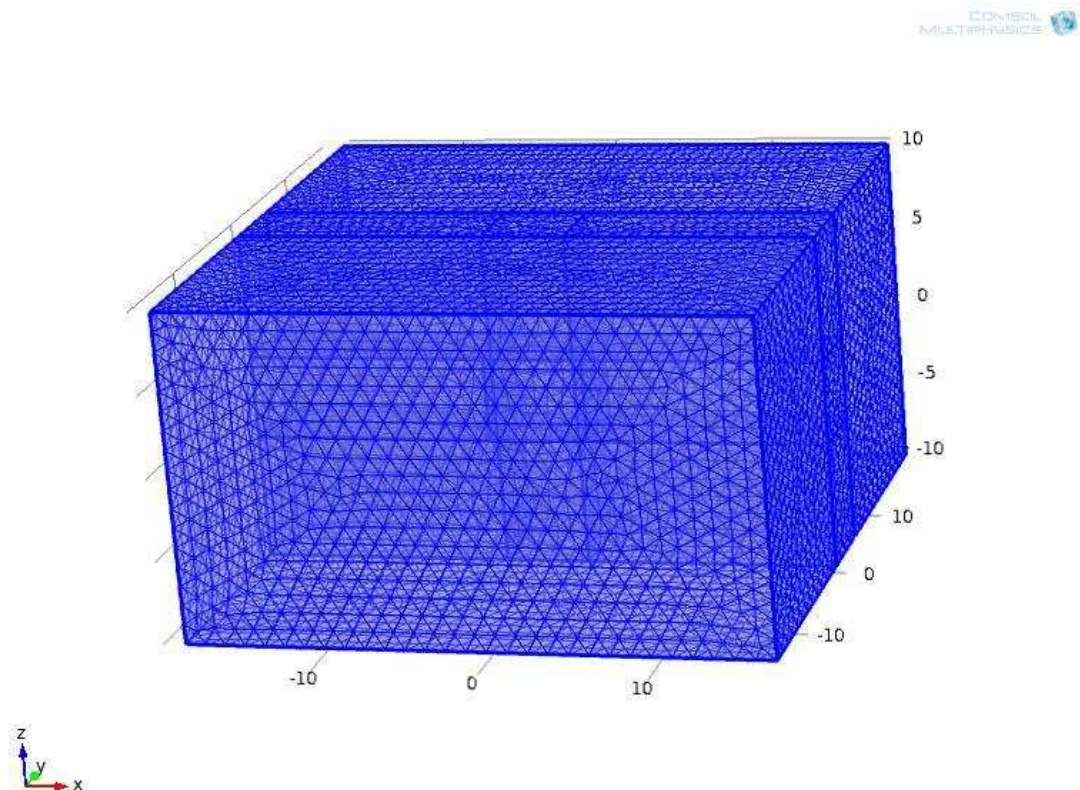


Figure A3-8.3–3. Mesh of main geometry.

STUDY 1

In the **Model Builder** window, select **Study 1 > Step 1: Frequency Domain**. In frequency domain settings put 50000 in **Frequencies** field. Right-click **Study 1** and choose **Compute**.

RESULTS

To display electric field distribution in the middle of geometry it is necessary to build a cut-plane. For that go to **Results > Data Sets** and select **Cut Plane**. In settings put yz-plane and 0 in **x-coordinate**.

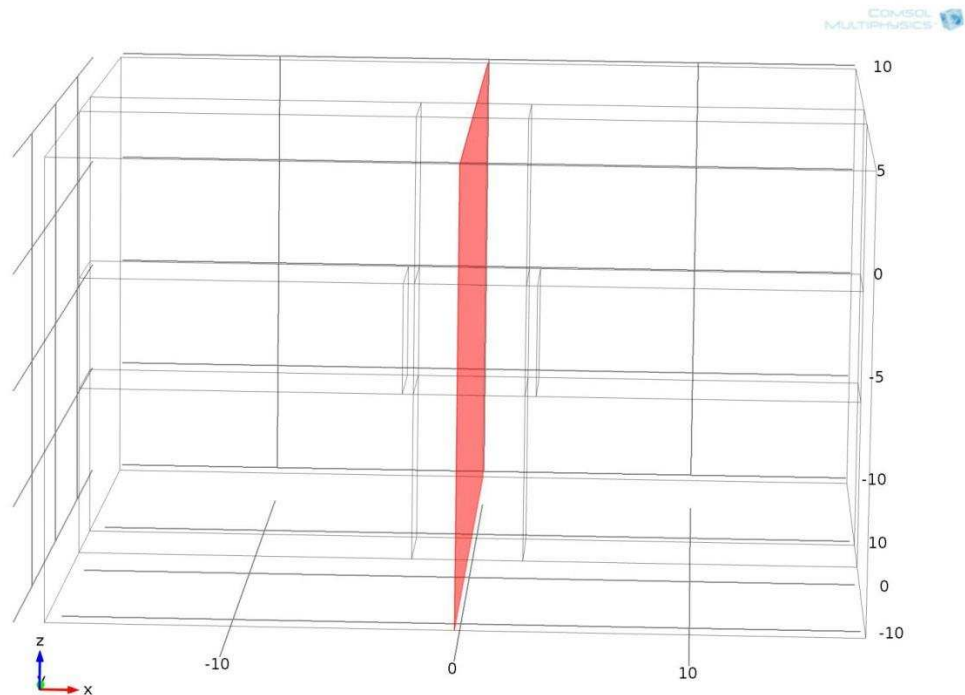


Figure A3-8.3–4 Cut-plane 1, $x=0$.

Right-click **Results** and select **2D Plot Group**. In settings put **Data set** Cut Plane 1. Right-click on **2D Plot Group 1**, select **Surface** and choose **mef. normE** in **Expression**.

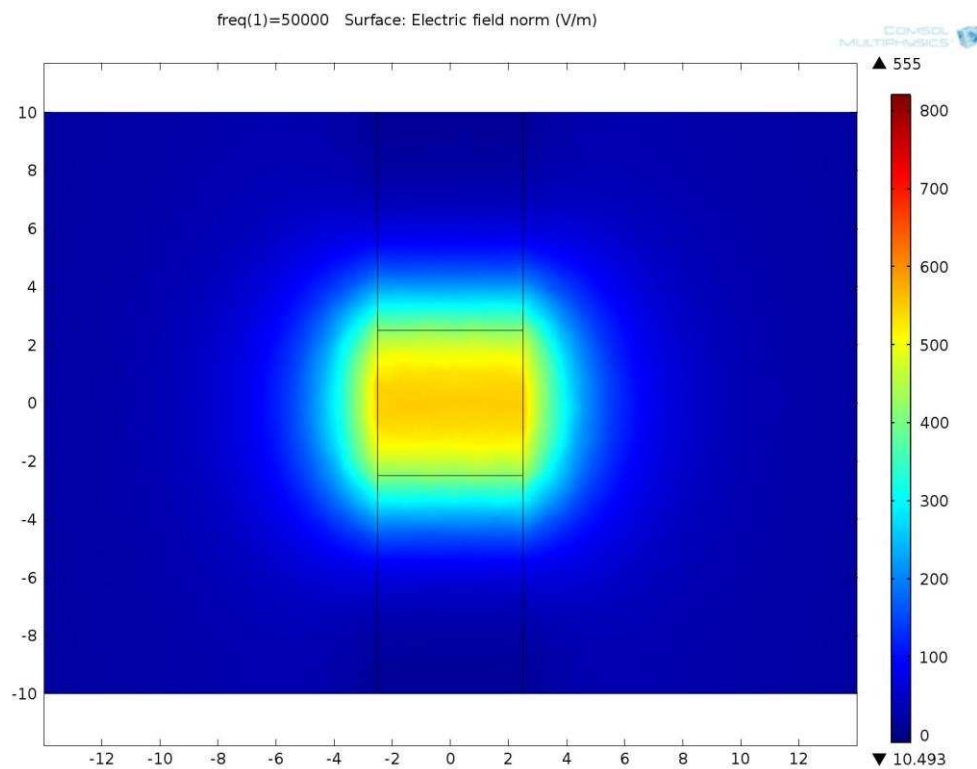


Figure A3-8.3–5 2D Plot of electric field (cut-plane1).

To display current density along the line, do **Results > Data Sets** and select **Cut Line 3D**. In settings put y-coordinate for **Point 1** -17.5 and 17.5 for **Point 2**, leaving all the others as 0. Plot it by pressing **Plot** button.

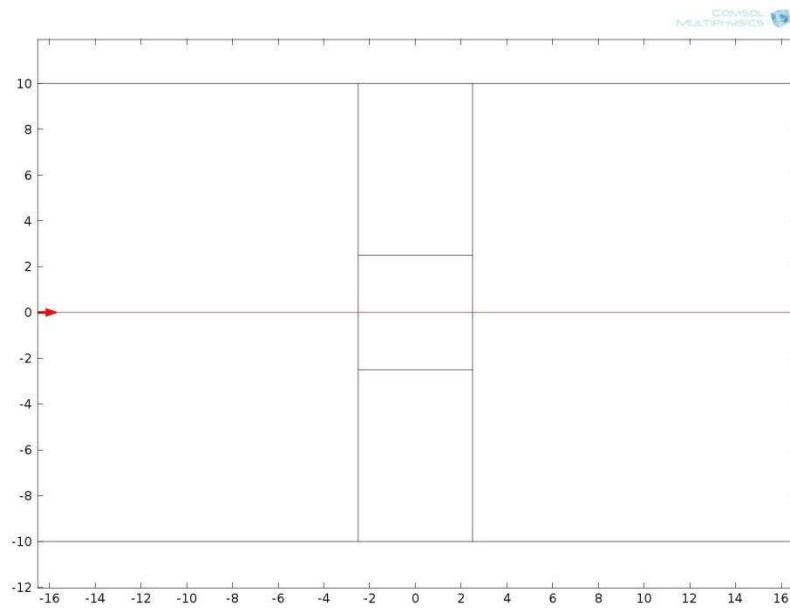


Figure A3-8.3–6 Cut Line 3D 1

Right-click **Results** and select **1D Plot Group**. In settings put **Data set** Cut Line3D 1. Right-click on **1D Plot Group 1**, select **Line Graph** and choose **mef. normJ** in **Expression**.

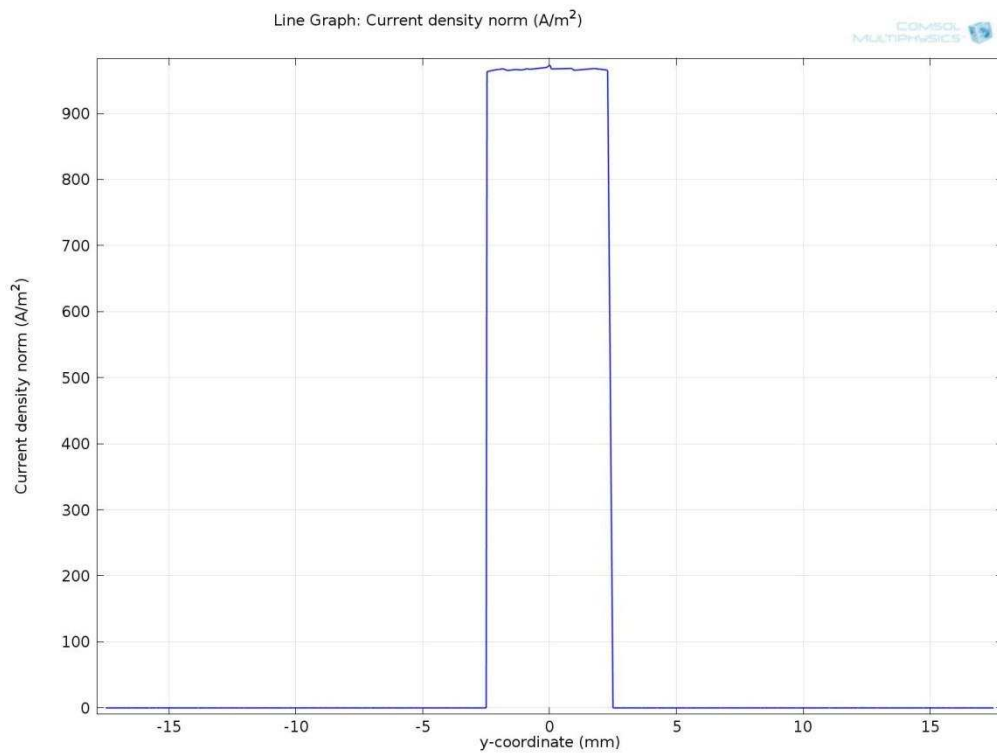


Figure A3-8.3-7 Current density along cut line.

Appendix 4. MatLab scripts for random distribution of cholesterol particles in 3D finite element models

```

function out = one_3D
%
% katia_init.m
%
% ==== COPYRIGHT EKATERINA ARISTOVICH ====
%
% Model exported on Jan 31 2011, 22:35 by COMSOL 4.0.0.982.
RandStream.setDefaultStream ...
    (RandStream('mt19937ar','seed',sum(100*clock)));

Volume = 125;
length = Volume^(1/3);
TC=5;
n_of_c= 125;

CVIB=TC*3.75*0.001*Volume;
R_of_one=(3*CVIB/(4*pi))^(1/3);
% DS2=pi*R_of_one^2;

import com.comsol.model.*
import com.comsol.model.util.*
File = fopen('C:\\Users\\taesche\\My
Documents\\modelling\\3D64\\currentvalues125.txt','w');

```



```

    model.geom('geom1').feature('blk1').setIndex('size',
'5', 2);
    model.geom('geom1').run('blk1');

    model.geom('geom1').feature.create('wp1', 'WorkPlane');

model.geom('geom1').feature('wp1').geom.feature.create('r1'
, 'Rectangle');

model.geom('geom1').feature('wp1').geom.feature('r1').set('
base', 'corner');

model.geom('geom1').feature('wp1').geom.feature('r1').set('
pos',
                                {'-6'
                                '-2'}
);

model.geom('geom1').feature('wp1').geom.feature('r1').set('
lx', '3.5');

model.geom('geom1').feature('wp1').geom.feature('r1').set('
ly', '4.5');
    model.geom('geom1').feature('wp1').geom.run('r1');
    model.geom('geom1').feature('wp1').set('quickplane',
'zx');

model.geom('geom1').feature('wp1').geom.feature('r1').setIn
dex('size', '.5', 0);

model.geom('geom1').feature('wp1').geom.feature('r1').setIn
dex('size', '14.5', 0);

model.geom('geom1').feature('wp1').geom.feature('r1').setIn
dex('size', '7.5', 1);

model.geom('geom1').feature('wp1').geom.feature('r1').setIn
dex('pos', '-17.5', 0);

model.geom('geom1').feature('wp1').geom.feature('r1').setIn
dex('pos', '-2.5', 1);

```

```
model.geom('geom1').feature('wp1').geom.feature('r1').setIn  
dex('size', '5', 1);
```

```
    model.geom('geom1').feature('wp1').set('quickplane',  
'xz');
```

```
model.geom('geom1').feature('wp1').geom.feature.create('r2'  
, 'Rectangle');
```

```
model.geom('geom1').feature('wp1').geom.feature('r2').set('  
base', 'corner');
```

```
model.geom('geom1').feature('wp1').geom.feature('r2').set('  
pos', {'-17.5' '2.5'});
```

```
model.geom('geom1').feature('wp1').geom.feature('r2').set('  
lx', '12.5');
```

```
model.geom('geom1').feature('wp1').geom.feature('r2').set('  
ly', '7.5');
```

```
    model.geom('geom1').feature('wp1').geom.run('r2');
```

```
model.geom('geom1').feature('wp1').geom.feature('r2').setIn  
dex('size', '15', 0);
```

```
    model.geom('geom1').feature('wp1').geom.run('r2');
```

```
model.geom('geom1').feature('wp1').geom.feature.create('r3'  
, 'Rectangle');
```

```
model.geom('geom1').feature('wp1').geom.feature('r3').set('  
base', 'corner');
```

```
model.geom('geom1').feature('wp1').geom.feature('r3').set('  
pos', {'-20' '-10'});
```



```
model.geom('geom1').feature('wp1').geom.feature('r3').set('
lx', '17');

model.geom('geom1').feature('wp1').geom.feature('r3').set('
ly', '7.5');
    model.geom('geom1').feature('wp1').geom.run('r3');

model.geom('geom1').feature('wp1').geom.feature('r3').setIn
dex('pos', '-17.5', 0);
    model.geom('geom1').feature('wp1').geom.run('r3');

model.geom('geom1').feature('wp1').geom.feature('r3').setIn
dex('size', '15', 0);
    model.geom('geom1').feature('wp1').geom.run('r3');

model.geom('geom1').feature('wp1').geom.feature.create('r4'
, 'Rectangle');

model.geom('geom1').feature('wp1').geom.feature('r4').set('
base', 'corner');

model.geom('geom1').feature('wp1').geom.feature('r4').set('
pos', {'-2.5' '2.5'});

model.geom('geom1').feature('wp1').geom.feature('r4').set('
lx', '7.5');

model.geom('geom1').feature('wp1').geom.feature('r4').set('
ly', '7.5');
    model.geom('geom1').feature('wp1').geom.run('r4');

model.geom('geom1').feature('wp1').geom.feature('r4').setIn
dex('size', '5', 0);
    model.geom('geom1').feature('wp1').geom.run('r4');

model.geom('geom1').feature('wp1').geom.feature.create('r5'
, 'Rectangle');
```

```

model.geom('geom1').feature('wp1').geom.feature('r5').set('
base', 'corner');

model.geom('geom1').feature('wp1').geom.feature('r5').set('
pos', {'-2.5' '-10'});

model.geom('geom1').feature('wp1').geom.feature('r5').set('
lx', '5');

model.geom('geom1').feature('wp1').geom.feature('r5').set('
ly', '7.5');
    model.geom('geom1').feature('wp1').geom.run('r5');
    model.geom('geom1').feature('wp1').geom.run('r5');

model.geom('geom1').feature('wp1').geom.feature.create('mir
1', 'Mirror');

model.geom('geom1').feature('wp1').geom.feature('mir1').sel
ection('input').set({'r1' 'r2' 'r3'});

model.geom('geom1').feature('wp1').geom.feature('mir1').set
('keep', 'on');
    model.geom('geom1').feature('wp1').geom.run('mir1');
    model.geom('geom1').run('wp1');
    model.geom('geom1').run('wp1');
    model.geom('geom1').feature.create('ext1', 'Extrude');

model.geom('geom1').feature('ext1').setIndex('distance',
'5', 0);

model.geom('geom1').feature('ext1').setIndex('distance',
'2.5', 0);
    model.geom('geom1').run('ext1');
    model.geom('geom1').feature('ext1').set('reverse',
'on');
    model.geom('geom1').run('ext1');

```

```

    model.geom('geom1').feature('wp1').set('quicky',      '-
2.5');
    model.geom('geom1').feature('ext1').set('reverse',
'off');

model.geom('geom1').feature('ext1').setIndex('distance',
'5', 0);
    model.geom('geom1').run('ext1');
    model.geom('geom1').feature('ext1').set('reverse',
'on');
    model.geom('geom1').run('ext1');
    model.geom('geom1').run('ext1');
    model.geom('geom1').feature.create('wp2', 'WorkPlane');
    model.geom('geom1').feature('wp2').set('quickplane',
'xz');
    model.geom('geom1').feature('wp2').set('quicky', '-5');
    model.geom('geom1').run('wp2');

model.geom('geom1').feature('wp2').geom.feature.create('r1'
, 'Rectangle');

model.geom('geom1').feature('wp2').geom.feature('r1').set('
base', 'corner');

model.geom('geom1').feature('wp2').geom.feature('r1').set('
pos', {'-17.5' '-10'});

model.geom('geom1').feature('wp2').geom.feature('r1').set('
lx', '35');

model.geom('geom1').feature('wp2').geom.feature('r1').set('
ly', '20');
    model.geom('geom1').feature('wp2').geom.run('r1');
    model.geom('geom1').run('wp2');
    model.geom('geom1').feature.create('ext2', 'Extrude');
    model.geom('geom1').feature('wp2').set('quicky',      '-
17.5');
    model.geom('geom1').run('wp2');

```

```

model.geom('geom1').feature('ext2').setIndex('distance',
'15', 0);
    model.geom('geom1').run('ext2');
    model.geom('geom1').feature('ext2').set('reverse',
'on');
    model.geom('geom1').run('ext2');
    model.geom('geom1').run('ext2');
    model.geom('geom1').feature.create('wp3', 'WorkPlane');
    model.geom('geom1').feature('wp3').set('quickplane',
'xz');
    model.geom('geom1').feature('wp3').set('quicky',
'17.5');
    model.geom('geom1').run('wp3');
    model.geom('geom1').run('wp3');
    model.geom('geom1').feature.create('ext3', 'Extrude');

model.geom('geom1').feature('ext3').setIndex('distance',
'15', 0);
    model.geom('geom1').feature.remove('ext3');

model.geom('geom1').feature('wp3').geom.feature.create('r1'
, 'Rectangle');

model.geom('geom1').feature('wp3').geom.feature('r1').set('
base', 'corner');

model.geom('geom1').feature('wp3').geom.feature('r1').set('
pos', {'-17.5' '-10'});

model.geom('geom1').feature('wp3').geom.feature('r1').set('
lx', '35');

model.geom('geom1').feature('wp3').geom.feature('r1').set('
ly', '20');
    model.geom('geom1').feature('wp3').geom.run('r1');
    model.geom('geom1').run('wp3');
    model.geom('geom1').feature.create('ext3', 'Extrude');

```

```

model.geom('geom1').feature('ext3').setIndex('distance',
'15', 0);
    model.geom('geom1').run('ext3');

a=-length/2;
b=length/2;

k_x=round(n_of_c^(1/3));
k_y=k_x;
k_z=round(n_of_c/(k_x*k_y));
n_of_c=k_x*k_y*k_z;

h_x=(b-a)/k_x;
h_y=(b-a)/k_y;
h_z=(b-a)/k_z;

radius= (3*CVIB/(4*n_of_c*pi))^(1/3)

num=0;
%geometrical_iterations
for i=1:k_x;
    for j=1:k_y;
        for k=1:k_z;
            num=num+1;

            name1=sprintf('c%d', num);
            ebx=a+radius+(i-1)*h_x;
            eex=ebx+h_x-2*radius;
            x=ebx+(eex-ebx).*rand;

```

```

        eby=a+radius+(j-1)*h_y;
        eey=eby+h_y-2*radius;
        y=eby+(eey-eby).*rand;
        ebz=a+radius+(k-1)*h_z;
        eez=ebz+h_z-2*radius;
        z=ebz+(eez-ebz).*rand;

        model.geom('geom1').feature.create(name1,
'Sphere');
        model.geom('geom1').feature(name1).set('r',
sprintf('%f',radius));

model.geom('geom1').feature(name1).setIndex('pos',
sprintf('%f',x), 0);

model.geom('geom1').feature(name1).setIndex('pos',
sprintf('%f',y), 1);

model.geom('geom1').feature(name1).setIndex('pos',
sprintf('%f',z), 2);

        model.geom('geom1').run(name1);

        c=sprintf('sphere %d is ok \n',num)
    end
end
end

model.geom('geom1').run;

model.material.create('mat1');
model.material('mat1').name('blood_base');
model.material('mat1').selection.set([1]);

model.material('mat1').materialModel('def').set('electricco
nductivity', {'1.76'});

```

```
model.material('mat1').materialModel('def').set('relpermittivity', {'79'});

model.material('mat1').materialModel('def').set('relpermeability', {'1'});

    model.material.create('mat2');
    model.material('mat2').name('cholesterol');

model.material('mat2').materialModel('def').set('electricconductivity', {'0.025'});

model.material('mat2').materialModel('def').set('relpermeability', {'1'});

model.material('mat2').materialModel('def').set('relpermittivity', {'10000'});

    model.material.create('mat3');
    model.material('mat3').name('Air');

model.material('mat3').materialModel('def').set('relpermeability', '1');

model.material('mat3').materialModel('def').set('relpermittivity', '1');

model.material('mat3').materialModel('def').set('electricconductivity', '0');

    mat_n=n_of_c+8;
    mat_n1=n_of_c+9;
    mat_m=n_of_c+11;
    model.material('mat2').selection.set([9:mat_n]);
    model.material('mat1').selection.set([6 7 8])
```

```
    model.material('mat3').selection.set([1:5,
mat_n1:mat_m]);

    c='materials ok'

    model.mesh('mesh1').feature.create('ftet1', 'FreeTet');
    model.mesh('mesh1').run;

    model.physics('mef').feature.create('pot1',
'ElectricPotential', 2);

model.physics('mef').feature('pot1').selection.set([1043
1044 1045 1048 1051 1053]);
    model.physics('mef').feature('pot1').set('V0', 1, '-
1.428');

    model.physics('mef').feature.create('pot2',
'ElectricPotential', 2);
    model.physics('mef').feature('pot2').selection.set([22
23 24 25 26 30]);
    model.physics('mef').feature('pot2').set('V0', 1,
'1.428');

    model.study('std1').feature('freq').set('plist',
'50000');

    model.name('twelve_spheres.mph');

    model.view('view1').set('transparency', 'on');

    model.sol.create('sol1');
    model.sol('sol1').feature.create('st1', 'StudyStep');
    model.sol('sol1').feature('st1').set('study', 'std1');
    model.sol('sol1').feature('st1').set('studystep',
'freq');
```



```

    model.sol('sol1').feature.create('v1', 'Variables');
    model.sol('sol1').feature.create('s1', 'Stationary');
    model.sol('sol1').feature('s1').set('nonlin',
'linearized');
    model.sol('sol1').feature('s1').feature.create('p1',
'Parametric');

model.sol('sol1').feature('s1').feature('p1').set('pname',
'freq');

model.sol('sol1').feature('s1').feature('p1').set('plist',
'50000');

model.sol('sol1').feature('s1').feature('p1').set('plot',
'off');

model.sol('sol1').feature('s1').feature('p1').set('probesel
', 'all');

model.sol('sol1').feature('s1').feature('p1').set('probes',
{});
    model.sol('sol1').feature('s1').feature.create('fc1',
'FullyCoupled');
    model.sol('sol1').feature('s1').feature.create('il',
'Iterative');

model.sol('sol1').feature('s1').feature('il').set('linsolve
r', 'gmres');

model.sol('sol1').feature('s1').feature('fc1').set('linsolv
er', 'il');

model.sol('sol1').feature('s1').feature('il').feature.creat
e('mg1', 'Multigrid');

model.sol('sol1').feature('s1').feature('il').feature('mg1'
).feature('pr').feature.create('sv1', 'SORVector');

model.sol('sol1').feature('s1').feature('il').feature('mg1'
).feature('pr').feature('sv1').set('prefun', 'sorvec');

```

```

model.sol('sol1').feature('s1').feature('i1').feature('mg1')
).feature('po').feature.create('sv1', 'SORVector');

model.sol('sol1').feature('s1').feature('i1').feature('mg1')
).feature('po').feature('sv1').set('prefun', 'soruvec');

model.sol('sol1').feature('s1').feature.remove('fcDef');
    model.sol('sol1').attach('std1');
    model.sol('sol1').feature('v1').set('initmethod',
'sol');
    model.sol('sol1').feature('v1').set('initsol', 'sol1');
    model.sol('sol1').feature('v1').set('initmethod',
'init');
    model.sol('sol1').feature('v1').set('initsol', 'zero');

model.sol('sol1').feature('v1').feature('mod1_A').set('solv
efor', 'off');

model.sol('sol1').feature('v1').feature('mod1_A').set('out'
, 'off');
    model.sol('sol1').feature('s1').set('linpsol', 'sol1');

    model.result.create('pg1', 3);
    model.result('pg1').set('data', 'dset1');
    model.result('pg1').feature.create('surf1', 'Surface');
    model.result.create('pg2', 3);
    model.result('pg2').set('data', 'dset1');
    model.result('pg2').feature.create('slc1', 'Slice');

model.sol('sol1').runAll;

model.result('pg1').run;

model.result.numerical.create('int1', 'IntSurface');
model.result.numerical('int1').selection.set([30]);

```

```

    model.result.numerical('int1').set('expr',
'mef.normJ');
    model.result.numerical('int1').set('descr',      'Current
density norm');
    model.result.table.create('tbl1', 'Table');
    model.result.table('tbl1').comments('Surface
Integration 1 (mef.normJ)');
    model.result.numerical('int1').set('table', 'tbl1');
    model.result.numerical('int1').setResult;

    model.result.numerical.create('int2', 'IntSurface');
    model.result.numerical('int2').selection.set([1043]);
    model.result.numerical('int2').set('expr',
'mef.normJ');
    model.result.numerical('int2').set('descr',      'Current
density norm');
    model.result('pg1').run;

    name_f=sprintf('C:\\Users\\taesche\\My
Documents\\modelling\\3D64\\125_spheres%d.mph',g);
    model.save(name_f);

    J1 = model.result.numerical('int1').getReal();
    J2 = model.result.numerical('int2').getReal();
    File          =          fopen('C:\\Users\\taesche\\My
Documents\\modelling\\3D64\\currentvalues125.txt','a');
    fprintf(File,'%d\t\t%f\t\t%f\t\t| \n', g, J1, J2);
    fclose(File);

end
out = model;

```

Appendix 5. MatLab scripts for random distribution of RBC and cholesterol particles in 3D finite element models

Main file:

```
function out = one_3D

% katia_init.m
%
% ==== COPYRIGHT EKATERINA ARISTOVICH ====
%
% Model exported on Jan 31 2011, 22:35 by COMSOL 4.0.0.982.
RandStream.setDefaultStream ...
    (RandStream('mt19937ar', 'seed', sum(100*clock)));

%Total volume of domain
Volume = 125;
%length of the domain - we consider it to be a cube
length = Volume^(1/3);

% TC - total cholesterol
TC=5;

%Volume of all RBC in the domain
CVIB=Volume*0.000525*TC;
Volume_RBC=Volume*0.0644;

%Number of RBC
N_RBC=1000;

%Number of cholesterol particles
N_CHOL=100;

import com.comsol.model.*
import com.comsol.model.util.*
File =
fopen('C:\Users\Katia\Documents\Katya\modelling\3D64\ext_fi
ne\RBC\currentvaluescholrbc.txt','w');
fprintf (File, 'Model Number\t Current left side (A/m)\t
Current right side (A/m) \n' );
fclose(File);
```

```

for g=1:20;
% g=0;
    model = ModelUtil.create('Model');

    model.modelPath('D:\\Red_Blood_cells');

    model.modelNode.create('mod1');

    model.geom.create('geom1', 3);

    model.mesh.create('mesh1', 'geom1');

    model.physics.create('mef',
'ElectricInductionCurrents', 'geom1');

    model.study.create('std1');
    model.study('std1').feature.create('freq',
'Frequency');

    model.geom('geom1').lengthUnit('mm');

    model.name('katia_3D_one.mph');

    model.geom('geom1').feature.create('blk1', 'Block');
    model.geom('geom1').feature('blk1').set('base',
'center');
    model.geom('geom1').feature('blk1').setIndex('size',
'5', 0);
    model.geom('geom1').feature('blk1').setIndex('size',
'5', 1);
    model.geom('geom1').feature('blk1').setIndex('size',
'5', 2);
    model.geom('geom1').run('blk1');

    model.geom('geom1').feature.create('wp1', 'WorkPlane');

model.geom('geom1').feature('wp1').geom.feature.create('r1',
, 'Rectangle');

model.geom('geom1').feature('wp1').geom.feature('r1').set('
base', 'corner');

model.geom('geom1').feature('wp1').geom.feature('r1').set('
pos', {'-6' '-2'});

```

```

model.geom('geom1').feature('wp1').geom.feature('r1').set('
lx', '3.5');

model.geom('geom1').feature('wp1').geom.feature('r1').set('
ly', '4.5');
    model.geom('geom1').feature('wp1').geom.run('r1');
    model.geom('geom1').feature('wp1').set('quickplane',
'zx');

model.geom('geom1').feature('wp1').geom.feature('r1').setIn
dex('size', '.5', 0);

model.geom('geom1').feature('wp1').geom.feature('r1').setIn
dex('size', '14.5', 0);

model.geom('geom1').feature('wp1').geom.feature('r1').setIn
dex('size', '7.5', 1);

model.geom('geom1').feature('wp1').geom.feature('r1').setIn
dex('pos', '-17.5', 0);

model.geom('geom1').feature('wp1').geom.feature('r1').setIn
dex('pos', '-2.5', 1);

model.geom('geom1').feature('wp1').geom.feature('r1').setIn
dex('size', '5', 1);

    model.geom('geom1').feature('wp1').set('quickplane',
'xz');

model.geom('geom1').feature('wp1').geom.feature.create('r2'
, 'Rectangle');

model.geom('geom1').feature('wp1').geom.feature('r2').set('
base', 'corner');

model.geom('geom1').feature('wp1').geom.feature('r2').set('
pos', {'-17.5' '2.5'});

model.geom('geom1').feature('wp1').geom.feature('r2').set('
lx', '12.5');

```

```

model.geom('geom1').feature('wp1').geom.feature('r2').set('
ly', '7.5');
    model.geom('geom1').feature('wp1').geom.run('r2');

model.geom('geom1').feature('wp1').geom.feature('r2').setIn
dex('size', '15', 0);
    model.geom('geom1').feature('wp1').geom.run('r2');

model.geom('geom1').feature('wp1').geom.feature.create('r3'
, 'Rectangle');

model.geom('geom1').feature('wp1').geom.feature('r3').set('
base', 'corner');

model.geom('geom1').feature('wp1').geom.feature('r3').set('
pos', {'-20' '-10'});

model.geom('geom1').feature('wp1').geom.feature('r3').set('
lx', '17');

model.geom('geom1').feature('wp1').geom.feature('r3').set('
ly', '7.5');
    model.geom('geom1').feature('wp1').geom.run('r3');

model.geom('geom1').feature('wp1').geom.feature('r3').setIn
dex('pos', '-17.5', 0);
    model.geom('geom1').feature('wp1').geom.run('r3');

model.geom('geom1').feature('wp1').geom.feature('r3').setIn
dex('size', '15', 0);
    model.geom('geom1').feature('wp1').geom.run('r3');

model.geom('geom1').feature('wp1').geom.feature.create('r4'
, 'Rectangle');

model.geom('geom1').feature('wp1').geom.feature('r4').set('
base', 'corner');

model.geom('geom1').feature('wp1').geom.feature('r4').set('
pos', {'-2.5' '2.5'});

model.geom('geom1').feature('wp1').geom.feature('r4').set('
lx', '7.5');

model.geom('geom1').feature('wp1').geom.feature('r4').set('
ly', '7.5');

```

```

    model.geom('geom1').feature('wp1').geom.run('r4');

model.geom('geom1').feature('wp1').geom.feature('r4').setIndex('size', '5', 0);
    model.geom('geom1').feature('wp1').geom.run('r4');

model.geom('geom1').feature('wp1').geom.feature.create('r5', 'Rectangle');

model.geom('geom1').feature('wp1').geom.feature('r5').set('base', 'corner');

model.geom('geom1').feature('wp1').geom.feature('r5').set('pos', {'-2.5' '-10'});

model.geom('geom1').feature('wp1').geom.feature('r5').set('lx', '5');

model.geom('geom1').feature('wp1').geom.feature('r5').set('ly', '7.5');
    model.geom('geom1').feature('wp1').geom.run('r5');
    model.geom('geom1').feature('wp1').geom.run('r5');

model.geom('geom1').feature('wp1').geom.feature.create('mir1', 'Mirror');

model.geom('geom1').feature('wp1').geom.feature('mir1').selection('input').set({'r1' 'r2' 'r3'});

model.geom('geom1').feature('wp1').geom.feature('mir1').set('keep', 'on');
    model.geom('geom1').feature('wp1').geom.run('mir1');
    model.geom('geom1').run('wp1');
%    model.geom('geom1').run('wp1');
    model.geom('geom1').feature.create('ext1', 'Extrude');

model.geom('geom1').feature('ext1').setIndex('distance', '5', 0);

model.geom('geom1').feature('ext1').setIndex('distance', '2.5', 0);
    model.geom('geom1').run('ext1');
    model.geom('geom1').feature('ext1').set('reverse', 'on');
    model.geom('geom1').run('ext1');

```



```

    model.geom('geom1').feature('wp1').set('quicky', '-
2.5');
    model.geom('geom1').feature('ext1').set('reverse',
'off');

model.geom('geom1').feature('ext1').setIndex('distance',
'5', 0);
    model.geom('geom1').run('ext1');
    model.geom('geom1').feature('ext1').set('reverse',
'on');
    model.geom('geom1').run('ext1');
    model.geom('geom1').run('ext1');
    model.geom('geom1').feature.create('wp2', 'WorkPlane');
    model.geom('geom1').feature('wp2').set('quickplane',
'xz');
    model.geom('geom1').feature('wp2').set('quicky', '-5');
    model.geom('geom1').run('wp2');

model.geom('geom1').feature('wp2').geom.feature.create('r1'
, 'Rectangle');

model.geom('geom1').feature('wp2').geom.feature('r1').set('
base', 'corner');

model.geom('geom1').feature('wp2').geom.feature('r1').set('
pos', {'-17.5' '-10'});

model.geom('geom1').feature('wp2').geom.feature('r1').set('
lx', '35');

model.geom('geom1').feature('wp2').geom.feature('r1').set('
ly', '20');
    model.geom('geom1').feature('wp2').geom.run('r1');
    model.geom('geom1').run('wp2');
    model.geom('geom1').feature.create('ext2', 'Extrude');
    model.geom('geom1').feature('wp2').set('quicky', '-
17.5');
    model.geom('geom1').run('wp2');

model.geom('geom1').feature('ext2').setIndex('distance',
'15', 0);
    model.geom('geom1').run('ext2');
    model.geom('geom1').feature('ext2').set('reverse',
'on');
    model.geom('geom1').run('ext2');
    model.geom('geom1').run('ext2');
    model.geom('geom1').feature.create('wp3', 'WorkPlane');

```

```

    model.geom('geom1').feature('wp3').set('quickplane',
'xz');
    model.geom('geom1').feature('wp3').set('quicky',
'17.5');
    model.geom('geom1').run('wp3');
    model.geom('geom1').run('wp3');
    model.geom('geom1').feature.create('ext3', 'Extrude');

model.geom('geom1').feature('ext3').setIndex('distance',
'15', 0);
    model.geom('geom1').feature.remove('ext3');

model.geom('geom1').feature('wp3').geom.feature.create('r1'
, 'Rectangle');

model.geom('geom1').feature('wp3').geom.feature('r1').set('
base', 'corner');

model.geom('geom1').feature('wp3').geom.feature('r1').set('
pos', {'-17.5' '-10'});

model.geom('geom1').feature('wp3').geom.feature('r1').set('
lx', '35');

model.geom('geom1').feature('wp3').geom.feature('r1').set('
ly', '20');
    model.geom('geom1').feature('wp3').geom.run('r1');
    model.geom('geom1').run('wp3');
    model.geom('geom1').feature.create('ext3', 'Extrude');

model.geom('geom1').feature('ext3').setIndex('distance',
'15', 0);
    model.geom('geom1').run('ext3');
%    model.geom('geom1').runAll;

%    model.geom('geom1').run;
%-----
%-----
% RED BLOOD CELLS
% recalculate volume

    k_y_r=round(N_RBC^(1/3)/1.8);
    k_z_r=k_y_r;
    k_x_r=round(N_RBC/(k_y_r*k_z_r));
    N_RBC=k_x_r*k_y_r*k_z_r;
    R_RBC=(Volume_RBC*2.27/(N_RBC*pi))^(1/3);
    h_RBC=R_RBC/2.27;

```

```

eps=R_RBC/40;
a=eps-length/2;
b=-eps+length/2;

h_x_r=(b-a)/k_x_r ;
h_y_r=(b-a)/k_y_r ;
h_z_r=(b-a)/k_z_r ;

clear coord_rbc;
num=0;
for i=1:k_x_r;
    for j=1:k_y_r;
        for k=1:k_z_r;
            num=num+1;

% for rand RBC orientation

%         p=rand;
%         for ll=1:3
%             if p<0.5
%                 t(ll)=-1;
%             else t(ll)=1;
%             end
%         end
dir_x=1;%t(1)*rand;
dir_y=0;%t(2)*rand;
dir_z=0;%t(3)*rand;

name1=sprintf('rbc%d',num);
ebx=a+(i-1)*h_x_r+eps;
x=ebx;
eby=a+R_RBC+(j-1)*h_y_r+eps;
eey=eby+h_y_r-2*R_RBC-2*eps;%*abs(dir_y);
y=eby+(eey-eby).*rand;
ebz=a+R_RBC+(k-1)*h_z_r+eps;
eez=ebz+h_z_r-2*R_RBC-2*eps;%*abs(dir_y);
z=ebz+(eez-ebz).*rand;

coord_rbc(num,1)=x;
coord_rbc(num,2)=y;
coord_rbc(num,3)=z;

model.geom('geom1').feature.create(name1, 'Cylinder');

model.geom('geom1').feature(name1).set('r',sprintf('%f',R_R
BC) );

```

```

model.geom('geom1').feature(name1).set('h',sprintf('%f',h_R
BC) );

model.geom('geom1').feature(name1).setIndex('pos',
sprintf('%f',x), 0);

model.geom('geom1').feature(name1).setIndex('pos',
sprintf('%f',y), 1);

model.geom('geom1').feature(name1).setIndex('pos',
sprintf('%f',z), 2);

model.geom('geom1').feature(name1).setIndex('ax3',
sprintf('%f',dir_x), 0);

model.geom('geom1').feature(name1).setIndex('ax3',
sprintf('%f',dir_y), 1);

model.geom('geom1').feature(name1).setIndex('ax3',
sprintf('%f',dir_z), 2);

model.geom('geom1').feature(name1).set('rot', '0');
    % model.geom('geom1').run(name1);
    end
    end
    end
end

% for cholesterol

radius= (3*CVIB/(4*N_CHOL*pi))^(1/3);

coord_chol=[];

for i=1:N_CHOL
    is_on=1;
    while(is_on)
        x=a+radius+(b-a-2*radius)*rand;
        y=a+radius+(b-a-2*radius)*rand;
        z=a+radius+(b-a-2*radius)*rand;

        is_on=0;
        for j=1:N_RBC
            if (1.6*(x-coord_rbc(j,1))^2+0.9*(y-
coord_rbc(j,2))^2+0.9*(z-
coord_rbc(j,3))^2<=(R_RBC+radius)^2)

```

```

                is_on=1;
                break;
            end
        end
    end

    if(i>1)
    for j=1:i-1
        if ((x-coord_chol(j,1))^2+(y-
coord_chol(j,2))^2+(z-coord_chol(j,3))^2<=(2*radius)^2)
            is_on=1;
            break;
        end
    end
    end
end

coord_chol(i,1)=x;
coord_chol(i,2)=y;
coord_chol(i,3)=z;

    name1=sprintf('colest%d',i);
%       c=sprintf('making %d',k)
        model.geom('geom1').feature.create(name1,
'Sphere');
        model.geom('geom1').feature(name1).set('r',
sprintf('%f',radius));

model.geom('geom1').feature(name1).setIndex('pos',
sprintf('%f',x), 0);

model.geom('geom1').feature(name1).setIndex('pos',
sprintf('%f',y), 1);

model.geom('geom1').feature(name1).setIndex('pos',
sprintf('%f',z), 2);
    end
    %model.geom('geom1').runAll;
    model.geom('geom1').run;

name_f=sprintf('C:\\Users\\Katia\\Documents\\Katya\\modelli
ng\\3D64\\ext_fine\\RBC\\Parallel_RBCyz_%d_%d_%d.mph',N_RBC
,N_CHOL,g);
    model.save(name_f);

try

```

```
model.geom('geom1').run;

model.material.create('mat1');
model.material('mat1').name('blood_base');

model.material('mat1').materialModel('def').set('electricco
nductivity', {'1.76'});

model.material('mat1').materialModel('def').set('relpermitt
ivity', {'79'});

model.material('mat1').materialModel('def').set('relpermeab
ility', {'1'});

    model.material.create('mat2');
    model.material('mat2').name('cholesterol');

model.material('mat2').materialModel('def').set('electricco
nductivity', {'0.025'});

model.material('mat2').materialModel('def').set('relpermeab
ility', {'1'});

model.material('mat2').materialModel('def').set('relpermitt
ivity', {'10000'});

    model.material.create('mat3');
    model.material('mat3').name('Air');

model.material('mat3').materialModel('def').set('relpermeab
ility', '1');

model.material('mat3').materialModel('def').set('relpermitt
ivity', '1');

model.material('mat3').materialModel('def').set('electricco
nductivity', '0');

    model.material.create('mat4');
    model.material('mat4').name('RBC');

model.material('mat4').materialModel('def').set('electricco
nductivity', {'0.7'});

model.material('mat4').materialModel('def').set('relpermitt
ivity', {'79'});
```

```

model.material('mat4').materialModel('def').set('relpermeability', {'1'});

%!!!!!!!!!!!!!!!!!!!!!!!!!!!!!!!!!!!!!!!!!!!!!!!!!!!!!!!!!!!!!!!!!!!!

        domains = Get_Domains(model.geom('geom1'));
% domains = model.geom('geom1').objectNames();
        domains = char(domains);

        ind_colest=find (domains(:,1)=='c' &
domains(:,2)=='o');
        ind_RBC = find (domains(:,1)=='r' &
domains(:,2)=='b');
        ind_air = [1:5, (size(domains,1)-
2):size(domains,1)];
        not_BB = [ind_colest,ind_RBC,ind_air];
        BB= find(~ismember([1:size(domains)],not_BB));

        model.material('mat4').selection.set(ind_RBC);

model.material('mat2').selection.set(ind_colest);
model.material('mat3').selection.set(ind_air);
model.material('mat1').selection.set(BB);

        c='materials ok'

        model.save(name_f);

        model.physics('mef').feature.create('pot1',
'ElectricPotential', 2);
        sel=mphselectbox(model,'geom1', [-3.0001,-2.5,-
2.5 ; -2.4999,2.5,2.5]','boundary');

model.physics('mef').feature('pot1').selection.set(sel);
        model.physics('mef').feature('pot1').set('V0',
1, '-1.428');

        model.physics('mef').feature.create('pot2',
'ElectricPotential', 2);
        sel=mphselectbox(model,'geom1', [3.0001,-2.5,-
2.5 ; 2.4999,2.5,2.5]','boundary');

model.physics('mef').feature('pot2').selection.set(sel);

```

```

        model.physics('mef').feature('pot2').set('V0',
1, '1.428');
        model.save(name_f);
        c='boundaries ok'
% %!!!!!!!!!!!!!!!!!!!!!!!!!!!!!!!!!!!!!!!!!!!!!!!!!!!!!!!!!!!!!!!!!!!!
        model.mesh('mesh1').feature.create('ftet1',
'FreeTet');

model.mesh('mesh1').feature('size').set('hauto', '2');
        model.mesh('mesh1').run;
        c='mesh ok'
        model.save(name_f);

model.study('std1').feature('freq').set('plist', '50000');

        model.name('twelve_spheres.mph');

        model.view('view1').set('transparency', 'on');

        model.sol.create('sol1');
        model.sol('sol1').feature.create('st1',
'StudyStep');
        model.sol('sol1').feature('st1').set('study',
'std1');

model.sol('sol1').feature('st1').set('studystep', 'freq');
        model.sol('sol1').feature.create('v1',
'Variables');
        model.sol('sol1').feature.create('s1',
'Stationary');
        model.sol('sol1').feature('s1').set('nonlin',
'linearized');

model.sol('sol1').feature('s1').feature.create('p1',
'Parametric');

model.sol('sol1').feature('s1').feature('p1').set('pname',
'freq');

model.sol('sol1').feature('s1').feature('p1').set('plist',
'50000');

```



```

model.sol('sol1').feature('s1').feature('p1').set('plot',
'off');

model.sol('sol1').feature('s1').feature('p1').set('probesel
', 'all');

model.sol('sol1').feature('s1').feature('p1').set('probes',
{});

model.sol('sol1').feature('s1').feature.create('fc1',
'FullyCoupled');

model.sol('sol1').feature('s1').feature.create('i1',
'Iterative');

model.sol('sol1').feature('s1').feature('i1').set('linsolve
r', 'gmres');

model.sol('sol1').feature('s1').feature('fc1').set('linsolv
er', 'i1');

model.sol('sol1').feature('s1').feature('i1').feature.creat
e('mg1', 'Multigrid');

model.sol('sol1').feature('s1').feature('i1').feature('mg1'
).feature('pr').feature.create('sv1', 'SORVector');

model.sol('sol1').feature('s1').feature('i1').feature('mg1'
).feature('pr').feature('sv1').set('prefun', 'sorvec');

model.sol('sol1').feature('s1').feature('i1').feature('mg1'
).feature('po').feature.create('sv1', 'SORVector');

model.sol('sol1').feature('s1').feature('i1').feature('mg1'
).feature('po').feature('sv1').set('prefun', 'soruvec');

model.sol('sol1').feature('s1').feature.remove('fcDef');
        model.sol('sol1').attach('std1');

model.sol('sol1').feature('v1').set('initmethod', 'sol');
        model.sol('sol1').feature('v1').set('initsol',
'sol1');

model.sol('sol1').feature('v1').set('initmethod', 'init');
        model.sol('sol1').feature('v1').set('initsol',
'zero');

```

```

model.sol('sol1').feature('v1').feature('mod1_A').set('solvefor', 'off');

model.sol('sol1').feature('v1').feature('mod1_A').set('out', 'off');
                                model.sol('sol1').feature('s1').set('linpsol',
                                'sol1');

                                model.result.create('pg1', 3);
                                model.result('pg1').set('data', 'dset1');
                                model.result('pg1').feature.create('surfl',
                                'Surface');

                                model.result.create('pg2', 3);
                                model.result('pg2').set('data', 'dset1');
                                model.result('pg2').feature.create('slc1',
                                'Slice');

                                model.sol('sol1').runAll;

                                model.result('pg1').run;

                                model.result.numerical.create('int1',
                                'IntSurface');

model.result.numerical('int1').selection.set([30]);
                                model.result.numerical('int1').set('expr',
                                'mef.normJ');
                                model.result.numerical('int1').set('descr',
                                'Current density norm');
                                model.result.table.create('tbl1', 'Table');
                                model.result.table('tbl1').comments('Surface
                                Integration 1 (mef.normJ)');
                                model.result.numerical('int1').set('table',
                                'tbl1');

                                model.result.numerical('int1').setResult;

                                model.result.numerical.create('int2',
                                'IntSurface');

model.result.numerical('int2').selection.set([2787]);
                                model.result.numerical('int2').set('expr',
                                'mef.normJ');
                                model.result.numerical('int2').set('descr',
                                'Current density norm');
                                model.result('pg1').run;

```

```

%name_f=sprintf('C:\\Users\\Katia\\Documents\\Katya\\modelling\\3D64\\ext_fine\\RBC\\Parallel_RBCyz_%d_%d_%d.mph',N_RBC,N_CHOL,g);
    model.save(name_f);

    J1 = model.result.numerical('int1').getReal();
    J2 = model.result.numerical('int2').getReal();
    File =
fopen('C:\\Users\\Katia\\Documents\\Katya\\modelling\\3D64\\ext_fine\\RBC\\currentvalues343.txt','a');
    fprintf(File,'%d\t\t%f\t\t%f\t\t| \n', g, J1,
J2);
    fclose(File);

    catch exception
        c=sprintf('file %d is failed to compute! \n',g)
    end
end
out = model;

```